FINAL REPORT (Confidential)

PROJECT TITLE:

Drying Fuel Alcohols and Natural Gas with Biosorbents Based on Agricultural By-products

ADF Project No. 20130220

Submitted to

Saskatchewan Ministry of Agriculture
Saskatchewan Canola Development Commission
Western Grains Research Foundation

August 31, 2018

Principal Investigator:
Dr. Catherine Hui Niu
Department of Chemical and Biological Engineering
University of Saskatchewan
Saskatoon, SK, S7N 5A9
Email: catherine.niu@usask.ca
Tel. (306) 966 2174

Co-Investigator:
Dr. Ajay Dalai
Department of Chemical and Biological Engineering
University of Saskatchewan
Saskatoon, SK, S7N 5A9
Email: ajay.dalai@usask.ca
Tel. (306) 966 4771

ABSTRACT

Drying natural gas is crucial in the industry. Current methods have concerns of high energy consumption, and environmental pollution. In addition, there is current interest in using biofuel alcohols, and alternative energy efficient separation technologies are in demand.

To address the above mentioned issues, **the overall objective of this research project was proposed to formulate high performance biosorbents from agricultural by-products for drying natural gas, and fuel alcohols in a pressure swing adsorption (PSA) process**. By successfully completing this project, we have achieved the following significant results:

1. High performance biosorbents were developed from canola meal after protein extraction, flax shives and oat hulls, and characterized in composition, surface area, pore size distribution, functional groups, and thermal stability.
2. The flax shives based biosorbent successfully dried natural gas (methane) at room temperature in a pressure swing adsorption process, and was regenerated inline at vacuum and 30-50^{o}C. The biosorbent has been reused for 70 adsorption-desorption cycles without deterioration. The water selectivity is high because adsorption of methane was negligible.
3. The biosorbents made from the canola meal, and oat hulls successfully dried lower grade butanol, and achieved 99% fuel grade butanol. The fraction of the biosorbents such as cellulose and protein demonstrated their capability for selective water adsorption, however, their adsorption capacities are not as high as that of the raw material such as canola meal.
4. Economic analysis was done for drying natural gas, and butanol vapor using the biosorbents. The estimates based on the achieved experimental data demonstrated reduced energy consumption and costs in comparison with a number of methods used in the respective industry. More in-depth analysis is needed in the regards.

The results achieved from this project demonstrated that the agriculture by-products have a great potential for industrial application of drying gases and fuel alcohol vapors.

TABLE OF CONTENTS

CHAPTER 1. INTRODUCTION

The overall objective of this research project is to formulate high performance biosorbents from agricultural by-products for drying natural gas, and fuel alcohols in a pressure swing adsorption (PSA) process.

Research into this process is important, as natural gas is an important energy source for industry, transportation, and homes. It is also used as a chemical feedstock in the manufacture of plastics and other commercially important organic chemicals. Natural gas primarily contains methane, however it is commonly together with various amounts of water, carbon dioxide, hydrocarbons, etc. It must be dried before entering distribution pipelines to control corrosion and prevent formation of solid hydrocarbon/water hydrates. The methods including glycol dehydrators, condensation, etc. have issues such as pollution, high energy consumption and processing costs. Adsorption process has been used widely in new installations for natural gas dehydration using molecular sieves (MS) as the adsorbent. MS removes water vapor from the mixed gas stream selectively. However, the process is also energy intensive and costly mainly because the water saturated MS is regenerated at a temperature up to above 200^{o}C (Kidnay, et al., 2011; Netusil and Ditl 2011; Mokhatab and Poe 2012). Thus there is an incentive to develop an alternative process for drying (dehydrating) natural gas (both terms are used in this report.).

In addition, there is a greatly increasing interest in using bio-alcohols such as methanol, ethanol, propanol and butanol as a sustainable energy source. Biobutanol is preferred to bioethanol and other alcohols, mainly because of its superior fuel properties that are very similar to gasoline. It is less corrosive and can be easily transported through existing pipelines. Butanol also has higher combustion value, and octane rating with less ignition problems (Visioli et al., 2014). Biobutanol is often produced through acetone-butanol-ethanol (ABE) fermentation. However, as butanol is toxic to microorganisms when above 2 v/v% butanol in the fermentation broth (Moreira et al., 1981), it is difficult to obtain its high concentration. Thus, it is imperative to purify butanol from diluted aqueous media. Unless concentrated to over 99 v/v%, biofuels can neither be mixed with gasoline nor be used as a stand-alone fuel. Conventionally, for purification of butanol from ABE process, distillation is first carried out which produces azeotropic vapor of about 55 v/v% butanol

and 45 v/v% water followed by multiple decantation and distillation. However, it is a costly and energy intensive process (Gupta Kumar et al., 2013).

Previous results showed that canola meal in its raw form or after protein extraction exhibited capabilities to dry ethanol ((Baylak et al., 2012; and Ranjbar et al., 2013). As alcohols share similar characteristic features in terms of polarity with respect to their hydroxyl functional group, canola meal material after protein extraction, and similar agriculture by-products may also dehydrate other commercially significant alcohols such as butanol. In addition, natural gas (methane) is a non-polar gas, and water is polar, the polar groups of the agriculture by-products may also have a potential to interact with water molecules so as to selectively adsorb water from methane. However, such work was not done yet prior to this project.

Saskatchewan is one of the key provinces in Canada to produce canola, flax, oat, barley, wheat, and other agricultural products. Abundant by-products are generated such as canola meal, flax shives, oat hulls, barley and wheat straw and so on in the industry. To develop novel technologies for effective uses of the agriculture by-products, research of these materials on drying application need to be investigated.

The aim of this research project is to formulate high performance bio-adsorbents from the agricultural by-products for drying bio-alcohols and natural gas at low costs. These biosorbents are re-usable for dehydration and regeneration cycles. The exhausted biomaterials may be used for fuel bio-alcohols production through gasification or fermentation in the future. The technology generated from this research will make it possible to dehydrate water containing bio-alcohols and natural gas to achieve fuels of high purity. Use of the biosorbents for this purpose will not require any new facility other than that in molecular sieves process for drying bio-alcohols or natural gas in industry but at a reduced temperature for water saturated adsorbent regeneration.

In addition, in this research project were biosorbents characterized. Investigation of adsorption kinetics and equilibrium contributed to the knowledge of adsorption using biomaterials. The results obtained from this project provide important information on developing novel uses of agricultural by-products and improving the performance of dehydration of bio-alcohols and natural gas in the current industry.

1.1 HYPOTHESIS

Natural gas (methane) is a non-polar gas, and water is polar, it is hypothesized that flax shives, a representative of cellulosic agriculture by-products, can selectively adsorb water through polar attraction between the polar groups in their structures and water molecules so as to dry methane. It was also hypothesized that canola meal after protein extraction, and oat hulls which contain polar groups and porous structure can dry the commercially significant alcohol butanol because water molecules have higher polarity and smaller size than butanol molecules which favor water adsorption.

1.2. OBJECTIVE

To test the hypotheses, the overall objective was formed in this research project to formulate high performance biosorbents from agricultural by-products for drying natural gas, and fuel alcohols in a pressure swing adsorption (PSA) process.

To achieve that, the following specific work plan was proposed in the original proposal which was approved by the Saskatchewan Ministry of Agriculture, Saskatchewan Canola Development Commission, and Western Grains Research Foundation.

- Formulate and characterize novel biosorbents

- Optimize dehydration process in a pressure swing adsorption process

- Investigate the adsorption kinetics and equilibrium

- Regenerate water saturated biosorbents for reuse

- Economic analysis

According to the above mentioned work plan, the project was completed successfully. Natural gas (methane), and butanol was successfully dried by flax shives, oat hulls, and canola meal after protein extraction. Significant results were achieved in the following areas:

- Drying natural gas using flax shives,

- Drying butanol using canola meal after protein extraction,

- Drying butanol using oat hulls

- Economic analysis of methane, and butanol using the biosorbents

The details of the results are presented in the following chapters.

1.3. REFERENCES

Baylak, T.; Kumar, P.; Niu, C. H.; Dalai, A. Ethanol Dehydration in a Fixed Bed using Canola Meal. Energy and Fuels 2012, 26(8), 5226-31.

Gupta Kumar, V.; Schmoll, M.; Makki, M.; Tuohy, M.; Antonio, M. M. Applications of Microbial Engineering; first ed., CRC Press: Austria, 2013; 282-296.

Kidnay, A. J., W. R. Parrish and D. G. McCartney (2011). Fundamentals of natural gas processing, CRC Press.

Mokhatab, S. and W. A. Poe (2012). Handbook of natural gas transmission and processing, Gulf Professional Publishing.

Moreira, A.R., Ulmer, D.C., and Linden, J.C. (1981). Butanol toxicity in the butylic fermentation. Biotechnol. Bioeng. Symp. 11, 567–579.

Netusil, M. and P. Ditl (2011). "Comparison of three methods for natural gas dehydration." Journal of Natural Gas Chemistry 20(5): 471-476.

Ranjbar, Z.; Tajallipour, M.; Niu, C.H.*, and Dalai, A. Water Removal from Ethanol Vapor by Adsorption on Canola Meal after Protein Extraction. Ind. Eng. Chem. Eng. 2013, in press.

Visioli, J. L.; Enzweiler, H.; Kuhn, C. R.; Schwaab, M.; Mazutti, A. M. Sustainable Chem. Processes. 2014, 2, 1-9.

ACCOMPLISHED WORK

CHAPTER 2. DRYING NATURAL GAS USING FLAX SHIVES

2.1 ABSTRACT

Dehydration of gases is crucial in industry. Current dehydration methods have concerns of high energy consumption, and environmental pollution. In this work, natural gas, an important energy source, was selected as a model gas to investigate dehydration using a cost effective biosorbent in a pressure swing adsorption process. The biosorbent was developed from flax shives, a byproduct from the flax industry and a representative of renewable cellulose materials. The morphology, surface functional groups and thermal stability of the biosorbent were investigated by Field Emission Scanning Electron Microscope (FE-SEM), X-ray photoelectron spectroscopy (XPS), and thermal gravimetric analysis (TGA). The biosorbent has higher water adsorption capacity (up to 0.9 g/g) and higher water selectivity compared to conventional adsorbents. Adsorption of the main component of natural gas, i.e. non-polar methane, was negligible. In addition, the most significant operation factors and interaction among them were determined in regards to their effects on water adsorption capacity. The water adsorption equilibrium data were well simulated by the Redhead, and Fowler-Guggenhein (F-G) models. Based on the Redhead modeling results, the surface area was determined for water adsorption. The F-G modelling results indicated that the adsorbed water molecules on the surface of the biosorbent were attracted with one another, however, the interaction is weak. The length of mass transfer zone was also calculated at various operation factors. Furthermore, the water saturated biosorbent was regenerated at room temperature at a fast rate. The biosorbent has been used for seventy adsorption-desorption cycles without deterioration. Though the dehydration process was effectively operated at room temperature in this work, the TGA results showed that biosorbent was stable at temperatures up to 200°C. The results indicate that the biosorbent or like can be used in a pressure swing adsorption process for dehydration of natural gas and other non-polar gases in the industry.

2.2 INTRODUCTION

Natural gas is an important energy source for industry, transportation, and homes. It is also used as a chemical feedstock in the manufacturing of plastics and other commercially important organic chemicals. Natural gas contains primarily methane; however, it also commonly contains varied amounts of water, carbon dioxide, and hydrocarbons, among other components. The presence of water in natural gas substantially decreases the heating value of natural gas (Mokhatab and Poe 2012). In addition, natural gas must be dried before entering distribution pipelines to control corrosion and prevent the formation of solid hydrocarbon/methane hydrates (Kidnay, et al. 2011). To this end, technologies such as absorption, adsorption, condensation, and supersonic separation have been developed (Kidnay, et al. 2011, Netusil and Ditl 2011, Mokhatab and Poe 2012) As can be seen in Figure 2.1 dehydration unit is an essential part of the natural gas processing plants.

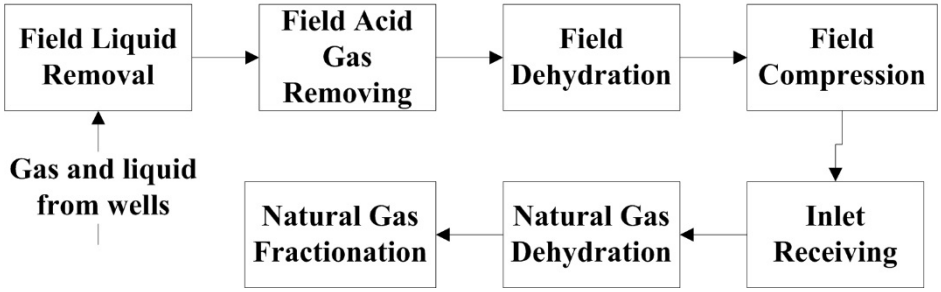

Figure 2.1: Overview of the a natural gas processing plant (Kidnay, et al. 2011)

Despite the results from these technologies, problems with pollution and high processing costs still exist (Ruthven 1984, Kidnay, et al. 2011, Netusil and Ditl 2011, Mokhatab and Poe 2012). For examples, glycol absorption process was the most widely used process in the natural gas industry (Gandhidasan 2003, Kidnay, et al. 2011, Mokhatab and Poe 2012). It is strictly prohibited in recent decades due to pollution issues (BTEX)(Mokhatab and Poe 2012). In addition, this process is energy intensive due to a distillation column and other equipment used to regenerate the glycol. Furthermore, temperature swing adsorption (TSA) process using commercial adsorbents such as molecular sieves and alumina has also been used in the natural gas processing industry (Ruthven 1984, Ruthven, Farooq et al. 1994, Mokhatab and Poe 2012, Liu, Feist et al. 2014, Karimi, Ghobadian et al. 2016). Novel materials such as metal organic frameworks, SiO_2 composites, silver nanoparticles and hierarchical porous zeolites were used as an adsorbent to

improve this adsorption process (Mrowiec-Białoń, Jarzebski et al. 1999, Fukuda, Ishida et al. 2011, Herm, Swisher et al. 2011, Besser, Tajiri et al. 2016). These adsorbents, however, require high regeneration temperatures (250^{o}C and higher). The high operating temperatures (250°C or higher) of this process limits the application of biosorbents in this process because they decompose (pyrolysis) at high temperatures. Therefore, pressure swing adsorption (PSA) which is operated for adsorption at high pressure and desorption at low pressure seems to be a better option due to lower operating temperatures. This process can be advantageous for natural gas dehydration since natural gas emerges from the reservoir at high pressure.

Pressure swing adsorption (PSA) has been extensively used for air drying and gas separation since 1948 because the pressure can be change easier and faster. Furthermore, the operating temperatures are lower than those of the TSA process, and the control of PSA process is easier (Carter and Wyszynski 1983). The main challenges in PSA process are selectivity of the adsorbents and gas compression costs (Santos, Portugal et al. 2004, Babicki, Keefer et al. 2006, Ho, Allinson et al. 2008, Santos, Grande et al. 2010, Grande and Blom 2012, Kacem, Pellerano et al. 2015, Yang, Xu et al. 2016). Commercial adsorbents used for air drying have drawback similar to that exist in TSA process.

There is thus an incentive to explore novel strategies, materials, and approaches for the dehydration of natural gas. In recent years, biosorbents demonstrated promising performance in the dehydration of alcohols (Niu and Volesky 2007, Sun, Okoye et al. 2007, Thevannan, Mungroo et al. 2010, Thevannan, Hill et al. 2011, Ranjbar, Tajallipour et al. 2013, Tajallipour, Niu et al. 2013, Niu, Baylak et al. 2014, Yan and Niu 2017, Yan and Niu 2017). Tajallipour et al. used canola meal to dehydrate ethanol and investigated the effect of operating parameters in ethanol dehydration a PSA process (Tajallipour, et al. 2013). Ranjbar et al. demonstrated that canola meal after protein extraction was also able to dehydrate ethanol and had higher selectivity towards water vapor.(Ranjbar, et al., 2013). The authors concluded that lignocellulose materials similar to canola meal have suitable surface functional groups for water (polar molecules) adsorption. These promising results attracted the attention to the potential application of biosorbents in natural gas dehydration. Flax shives, a byproduct from agricultural industry, contain lignocellulose materials; hence, they have the potential to be used in a PSA process to effectively dehydrate non-polar gases

such as natural gas. However, to the best knowledge of the authors, the research was not reported yet prior to this work.

In this chapter, a reusable agricultural by-product, flax shives, was used to dehydrate methane (non-polar), main component of natural gas in a PSA process. Flax shives were characterized, and the effect of PSA operating parameters were studied. Surface chemistry and adsorption mechanisms were investigated. The water adsorption capacity was determined at various operating conditions, and analyzed by the Redhead and Fowler-Guggenhein Models. Moreover, mass transfer zone was determined. Finally, the biosorbent was regenerated and reused, and its stability after 70 adsorption-desorption cycles were assessed.

2.3 MATERIALS AND METHODS

2.3.1. Biosorbents

Biosorbents were developed form flax shives in this work. Raw flax shives were supplied from Schweitzer-Mauduit Canada, Inc., Winkler, Manitoba. The flax shives were ground, oven dried, and sieved. Biosorbents with two different particle size ranges of 0.425 – 1.18 mm, and 1.18 - 3 mm were used in this work.

2.3.2. Gases

Ultra-High Purity (5.0) CH_4, CO_2, N_2 and He gases were purchased from Praxair Canada Co.

2.3.3. Characterization of Biosorbent

2.3.3.1 Particle Size Distribution*:* The particle size distribution of flax shives was measured by a particle size analyzer (Mastersizer 2000, Malvern Instruments) via a laser diffraction method. The shives are cylindrical with a ratio of length to diameter being approximately 2. The shape factor was calculated by the device program based on the L/D ratio provided. Five grams of sample were loaded onto the feed chamber, and the feed injection rate was 1.6 g/s. Air was the gas used in the device to maintain a constant flow of particles through the analysis tube and sensor assembly. The particle size distribution was reported on a volume basis.

2.3.3.2 Brunauer-Emmett-Teller (BET) Surface Area: The surface area of the biosorbent was analyzed by a pore size analyzer (Micromeritics Inc. ASAP 2020) using nitrogen gas adsorption

at liquid nitrogen temperature (74.15 K). The biosorbent particles (0.425-1.18 mm) were first degassed at 385 K under a vacuum of 500 µHg for 12 h. The specific surface area was determined by the BET method via nitrogen adsorption.

***2.3.3.3 Composition**:* The ash, moisture, and volatile contents of flax shives were determined by proximate analysis according to the ASTM 3173-87 (2003), ASTM 3174-04 (2004), and ASTM D 3175-07 (2007) methods, and ultimate analysis using a PerkinElmer Elemental CHNS analyzer.

2.3.3.4 X-ray Photoelectron Spectroscopy: Surface functional groups are essential in the adsorption process. Surfaces with different functional groups have affinity towards different components, which determines the selectivity of an adsorbent towards a targeted component. Flax shives are a novel adsorbent for gas dehydration and limited information is available about their surface properties. X-ray photoelectron spectroscopy has been used to quantify the functional groups on the surface of materials. In this work, an AXIS Supra photoelectron spectrometer (Kartos Analytical CO.) was used to obtain the XPS spectra of the biosorbent. Wide scans were performed at different spots with a spot size of 250 µm x 250 µm. The device was operated at a very low vacuum (approximately 3.12 x 10^{-10} kPa). The sample was vacuum dried at 105 °C and 2 µmHg for 48 hours in a sealed sample tube using ASAP 2020 (micromeritics) system; and then were loaded onto a stainless steel stub. In order to minimize moisture adsorption from air, the sample was quickly mounted on the device sampling and degassed under vacuum again for another 30 minutes.

2.3.4. Pressure Swing Adsorption (PSA) Process

In this work, an adsorption column was used to study a pressure swing adsorption process for natural gas dehydration, and the key process parameters were analyzed. Figure 2.2 shows the schematic of the apparatus used in the experiments. The flow rate and composition of feed gas were adjusted using mass flow controllers and pressure regulators connected to the gas cylinders. The feed gas was humidified in the humidifier column (E-1) containing deionized water and its relative humidity was adjusted by mixing this humid gas with a portion of the dry gas using two metering valves (Figure 2.2, V-2, and V-4). The humidity of gas was measured using high accuracy relative humidity (RH) sensors (Honeywell, US, HIH9000). The temperature of the feed gas in the pipelines was adjusted using heating tapes. Then the wet feed gas was sent into a column with a height of 51 cm and inside diameter of 4.9 cm where adsorption and desorption take place at

high pressure and vacuum, respectively. Isothermal condition was maintained in the column using a jacket with oil circulation throughout the experiment. Two pressure transducers (Honeywell, US), and two temperature sensors (Honeywell, US) were installed to monitor pressure, and temperature at the top and bottom of the adsorption column (I-6 and I-8, and I-5 and I-7). The gas composition of the outlet gas from the column was measured with time during the adsorption using gas chromatograph equipped with a thermal conductivity detector (TCD) (SRI-58424HQ000, SRI International), and water vapor was measured by another relative humidity sensor (Honeywell, US, HIH9000).

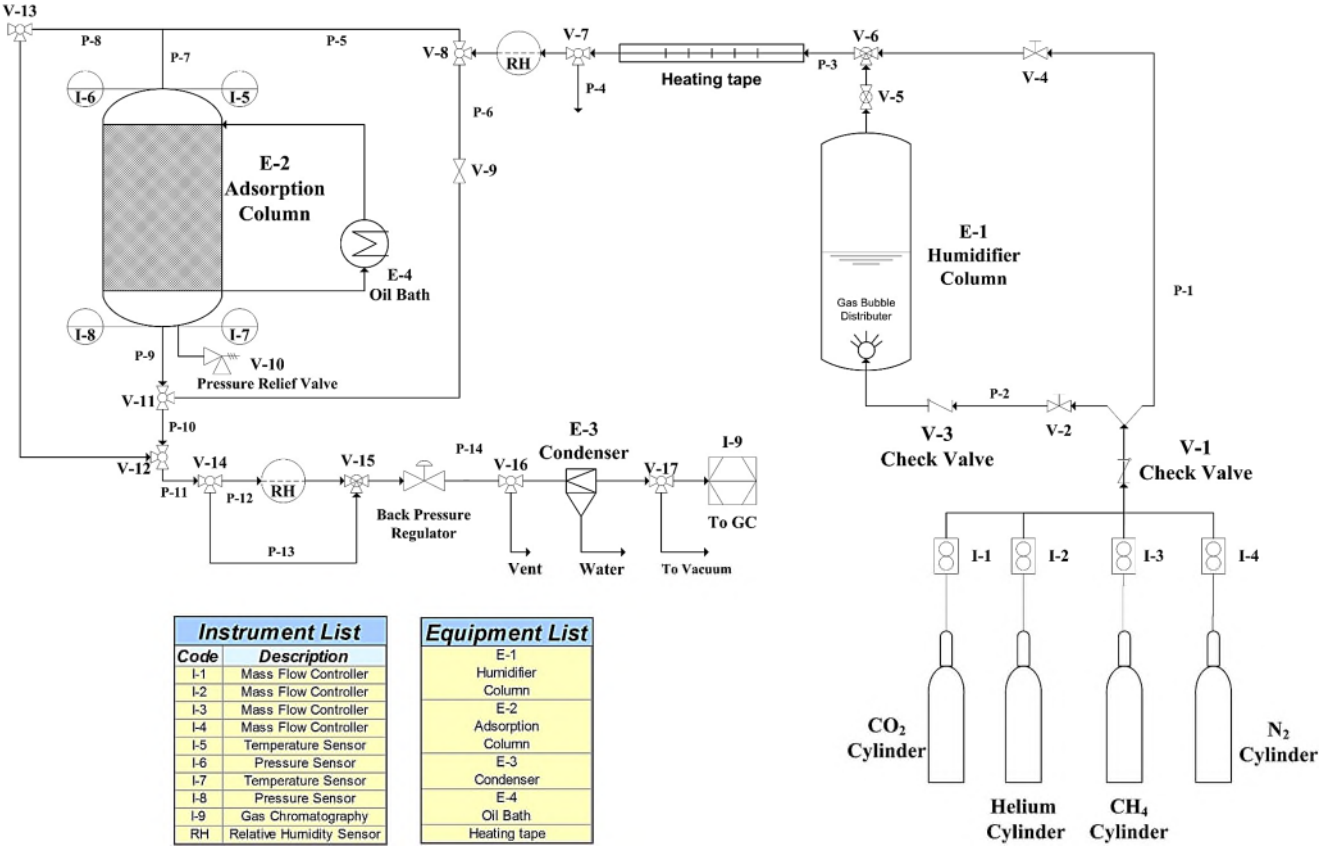

Figure 2.2: Schematic of the experimental set up

As can be seen in Figure 2.2, all sensors were connected to a data acquisition and monitoring system in a computer. As the gas stream passes through the bed, water and/or other gas molecules are adsorbed on the biosorbents with time, while unadsorbed components of gas leave the column from the bottom. A back-pressure regulator was used to maintain a constant- pressure in the column. The adsorption process was terminated when the mole fraction of species in the outlet gas was equal to 95 % of that in the inlet gas, which indicates a saturated

bed. Once the bed was saturated, the column was regenerated under vacuum with nitrogen purged to the column. In this work, methane, the major component of natural gas, was chosen to investigate the capability of the flax shives based biosorbent for dehydration of natural gas.

In contrast to previous works in the literature where it was assumed that the total flow rate of output gas from the column is the same as that in the inlet gas (carrier gas assumption) in order to do the mass balance, RH sensors allow accurate measurements without such assumptions. The molar flow rate of water vapor is determined by solving the following equation:

$$RH = \frac{P_t}{P_s} \times \frac{\dot{n}_w}{\dot{n}_w + \dot{n}_m + \dot{n}_c} \times 100 \qquad (2.1)$$

where RH is the relative humidity measured by the RH sensors, P_s is the vapor pressure of water at the gas temperature, P_t is the total pressure of the column (absolute), $\dot{n}_w$ is the molar flow rate of water vapor, $\dot{n}_m$ is the molar flow rate of methane, and $\dot{n}_c$ is the molar flow rate of carrier gas (helium or nitrogen). Helium was first used as a carrier gas for methane or nitrogen adsorption experiments. Once it was confirmed that adsorption of nitrogen gas by flax shives was negligible, nitrogen gas was used as the carrier gas for the experiments of methane dehydration, and water adsorption in the later stages. The molar flow rates of the carrier gas and methane in the inlet gas are known because they are adjusted using mass flow controllers. The molar flow rate of the carrier gas in the outlet is equal to that in the inlet. Gas chromatography (GC) was used to measure the content of methane in the outlet with time; however, since methane is not adsorbed by biosorbents, the molar flow rate of methane in the outlet is the same as that in the inlet. Therefore, the only unknown in Eq. 2.1 is the molar flow rate of water vapor, which is calculated at every time step using the values recorded by RH, temperature, and pressure sensors at the top and bottom of the column.

Since the PSA process using biosorbents is new to the natural gas dehydration, the effect of operating parameters must be studied. The main operating parameters that affect the process are the pressure of the column, temperature of the column, input gas flow rate, and the humidity of inlet gas (mole fraction of water vapor). To this end, a full factorial experimental design was considered using these four factors. Table 2.1 is a summary of this factorial design, which was later analyzed using statistical methods in order to find the main effects of and the interactions

among the factors. The values for these parameters were determined based on the system limitations, and/or industrial operation. Specifically, the temperature of sweat natural gas, which is the feed gas for the dehydration unit in the natural gas processing plants (see Figure 2.1), is between 35 to 38 °C. Hence, this temperature and room temperature were considered as the levels in the factorial experiment design. Due to safety issues (explosive methane gas), a pressure of 300 kPa was considered for the high level of pressure. The maximum water vapor mole fraction in a 100 % humid gas at 300 kPa and 24 °C is 0.0098. Water adsorption capacity was calculated by water mass balance when the adsorption reached equilibrium. Each experiment was done in duplicates, and the results were presented in average and standard deviation.

Desorption was done by connecting the column to a vacuum (46 kPa), while dry carrier gas (nitrogen) was passing through the column at the same temperature as that of the adsorption. The mole fraction of water in the outlet was measured with time using the RH sensor. The flow rate of the carrier gas was adjusted based on the flow rate of gas during the adsorption process (3 to 4.5 L/min at 46 kPa). Once the bed was approximately free of moisture, the bed was regenerated and ready for another adsorption experiment. To investigate the reusability and stability of the biosorbent, the biosorbent was repeatedly used in 70 completed adsorption-desorption cycles.

Table 2.1: Factors considered in the full factorial experiment design

Factors	**Levels**		
Pressure	P1 = 300.0 kPa	P2 = 101.3 kPa	
Temperature	T1 = 24 °C	T2 = 35 °C	
Gas flow rate	F1 = 2 L/min	F2 = 4 L/min	
Water vapor	C1 = 0.0098	C2 = 0.0083	C3 = 0.0068

2.4 RESULTS AND DISCUSSION

2.4.1. Characterization of Biosorbent

2.4.1.1. Main Properties of Flax Shives: Flax shives are categorized as a lignocellulose material, which is composed of cellulose, hemicellulose, lignin and protein. Its main properties are summarized in Table 2.2. Based on previous studies, cellulose and hemicellulos impart suitable surface functional groups for adsorption of polar compounds (Kataoka and Kondo 1998, Buranov

and Mazza 2010, Ranjbar, Tajallipour et al. 2013, Tajallipour, Niu et al. 2013). Since water is a polar compound, and methane is nonpolar, it is hypostatized that flax shives can selectively adsorb water vapor from natural gas.

Table 2.2: Main properties of flax shives

Composition (reported by manufacturer, SWM Inc.)	Cellulose (%)	53.2
	Hemicellulose (%)	13.6
	Lignin (%)	20.5
	Protein (%)	3.0
Ultimate analysis (CHNS)	H (%)	6.21±0.16
	N (%)	0.70±0.01
	S (%)	0.07±0.00
	C (%)	48.34±0.09
Proximate analysis	Volatile content (%)	84.62±0.19
	Ash content (%)	6.31±0.36
	Moisture content (%)	4.33±0.09
Bulk density (kg/m^3)	155.2	
BET surface area (N_2) (m^2/g)	1.34 ± 0.07	

2.4.1.2. Particle Size Distribution: The approximate size range of the flax shive particles which were mainly used in this work was 0.425-1.18 mm. The particle size distribution of the particles was further measured by a particle size analyzer, and is presented in Figure 2.3. The average diameter was 1097 μm. According to the results, 10% of the population have a diameter smaller than 750 μm, and 90% have a diameter smaller than 2561 μm.

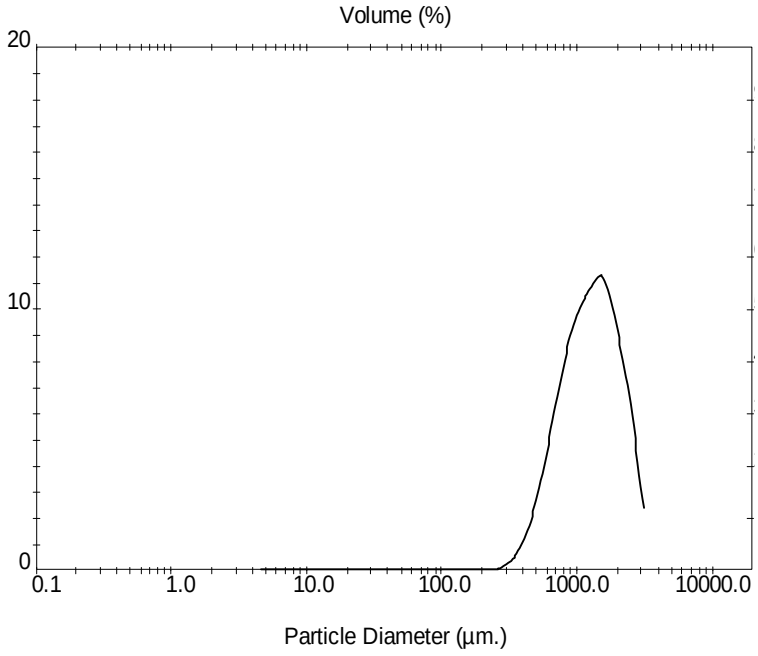

Figure 2.3: Particle size distribution of the biosorbent

***2.4.1.3. FE-SEM Analysis*:** The FE-SEM images of the flax shives based biosorbent are shown in Figure 2.4. As can be seen, the surface of the biosorbent is heterogeneous, on which the porous structure visible at the magnifications tested in this work is mostly comprised of large pores. Mesoporous structure inside these pores and also on the outer surface of the biosorbent can be also seen in Figure 2.4. Similar porous structure was observed in previous studies for biosorbents such as canola meal (Jayaprakash, Dhabhai et al. 2017). The flax shive based biosorbent is different from most conventional adsorbents such as molecular sieves and alumina, which have high surface area and mesoporous-microporous structure.

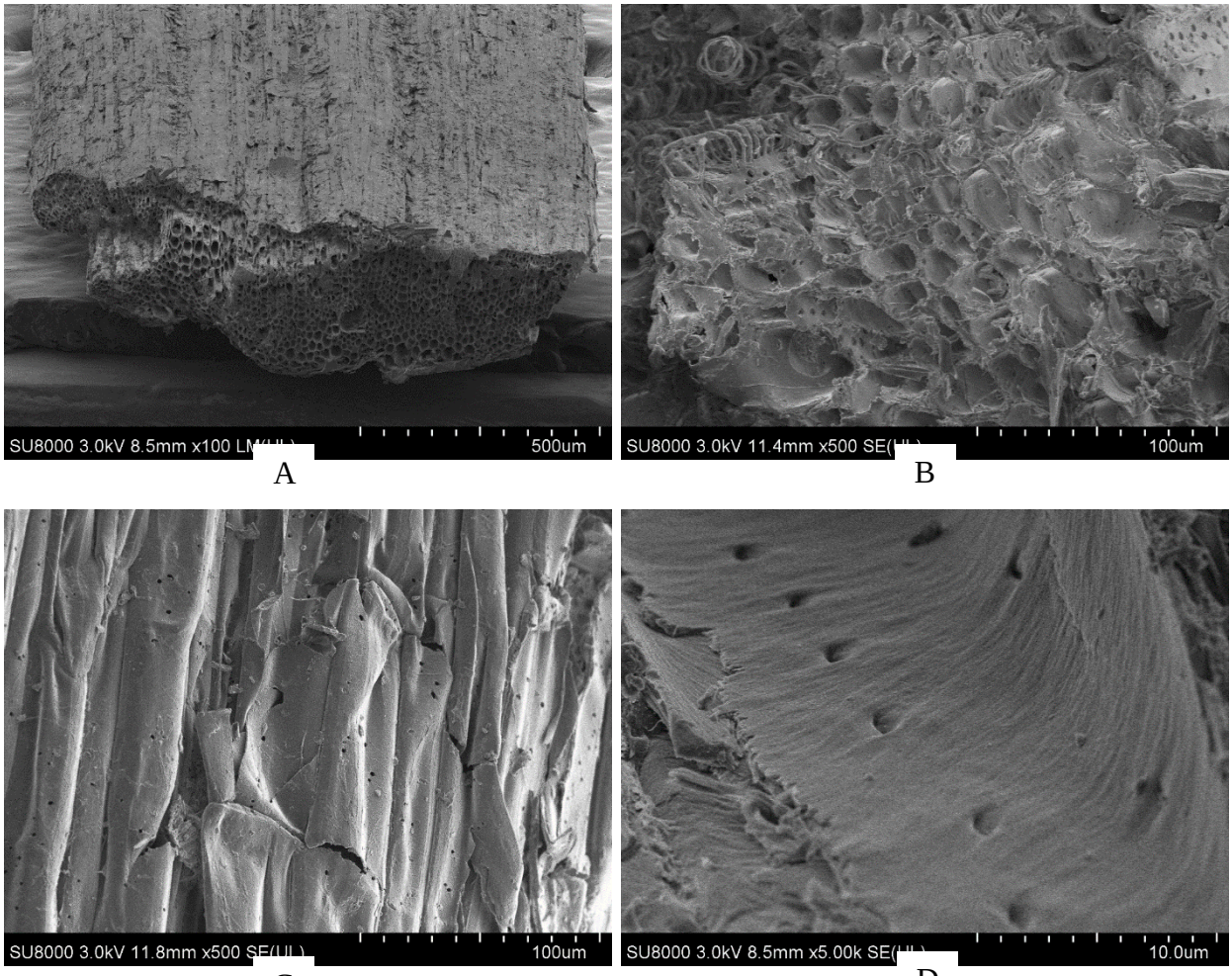

Figure 2.4: SEM ımages of used flax shives; A: The morphology of a piece of shive; B: The porous structure of flax shives; C: Small pores on the surface of flax shives; D: Small pores and the mesoporous parts of flax shives.

2.4.1.4. XPS:

Figure 2.5 shows the XPS wide scan spectrum of the flax shives based biosorbent. The results demonstrated that carbon, oxygen, nitrogen, calcium, and magnesium atoms presented on the surface of the biosorbent. According to this figure, 85.6 % of the atoms on the surface were carbon which was one of the main composition of cellulose, hemi-cellulose and lignin in flax shives. The next one was oxygen (8.6%) which existed in hydroxyl groups of the aforementioned components, and carboxyl groups in a small amount of protein in flax shives. Nitrogen (2.8%) is an element of

amine groups in protein molecules. Calcium and magnesium atoms on the surface presented in the form of MgO and $CaCO_3$, which were observed in ashes of most biomass.

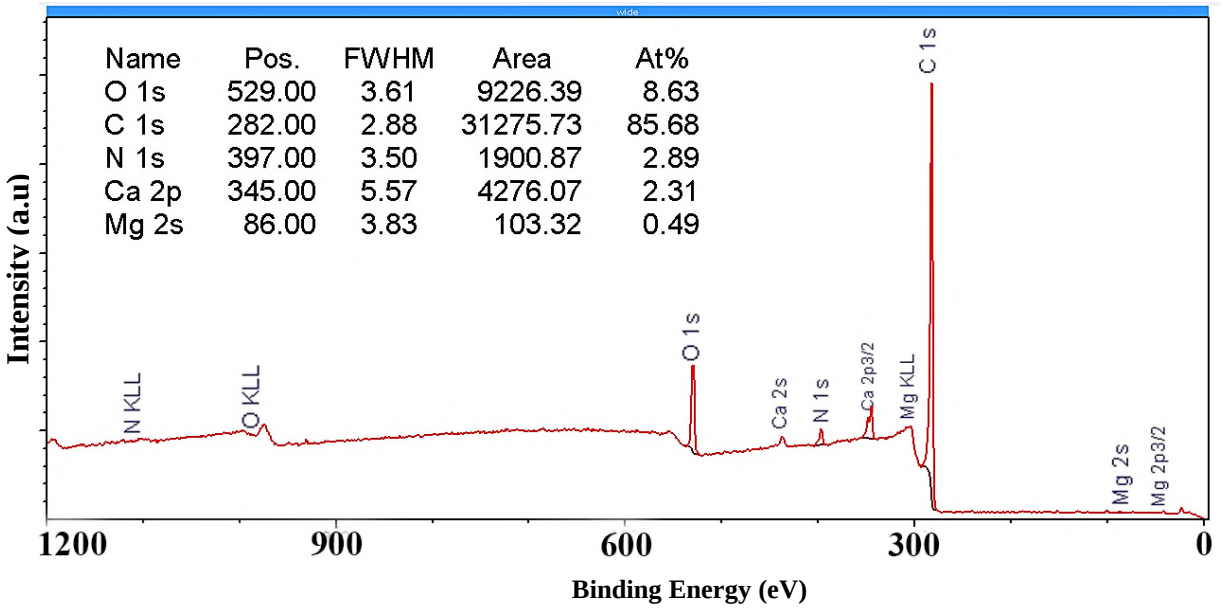

Figure 2.5: XPS spectrum of the biosorbent - wide scan (1200 – 0 eV); FWHM: Full width at half max; At%: Percentage of atoms on the sufrace

High resolution carbon C 1s and oxygen O 1s spectra are shown in Figure 2.6. These peaks were deconvoluted using CasaXPS software. As identified on the C 1s spectrum, most carbon atoms on the surface (62%) presented in the forms of C-C and C-H which were the main bonds of cellulose, hemicellulose, lignin and protein existing in the flax shives. Importantly, the rest total of ~ 38% carbon atoms were in the forms C-OH and C-O-C (29.7%), O-C=O (4.8%), and C=O (3.6%). The structures are polar, and exist in hydroxyl, carboxyl and other polar groups of the above mentioned components in flax shives. Such polar groups have potential for adsorbing polar water molecules. In addition, 1% carbon atoms were identified in the form of $(CO_3)^{2-}$ at the binding energy (BE) of 289.5 eV (Figure 2.6-B) on the spectrum of C 1s (Tan, Klabunde et al. 1991, Crist 1999, Zafeiropoulos, Vickers et al. 2003, Wallart, Henry de Villeneuve et al. 2005).

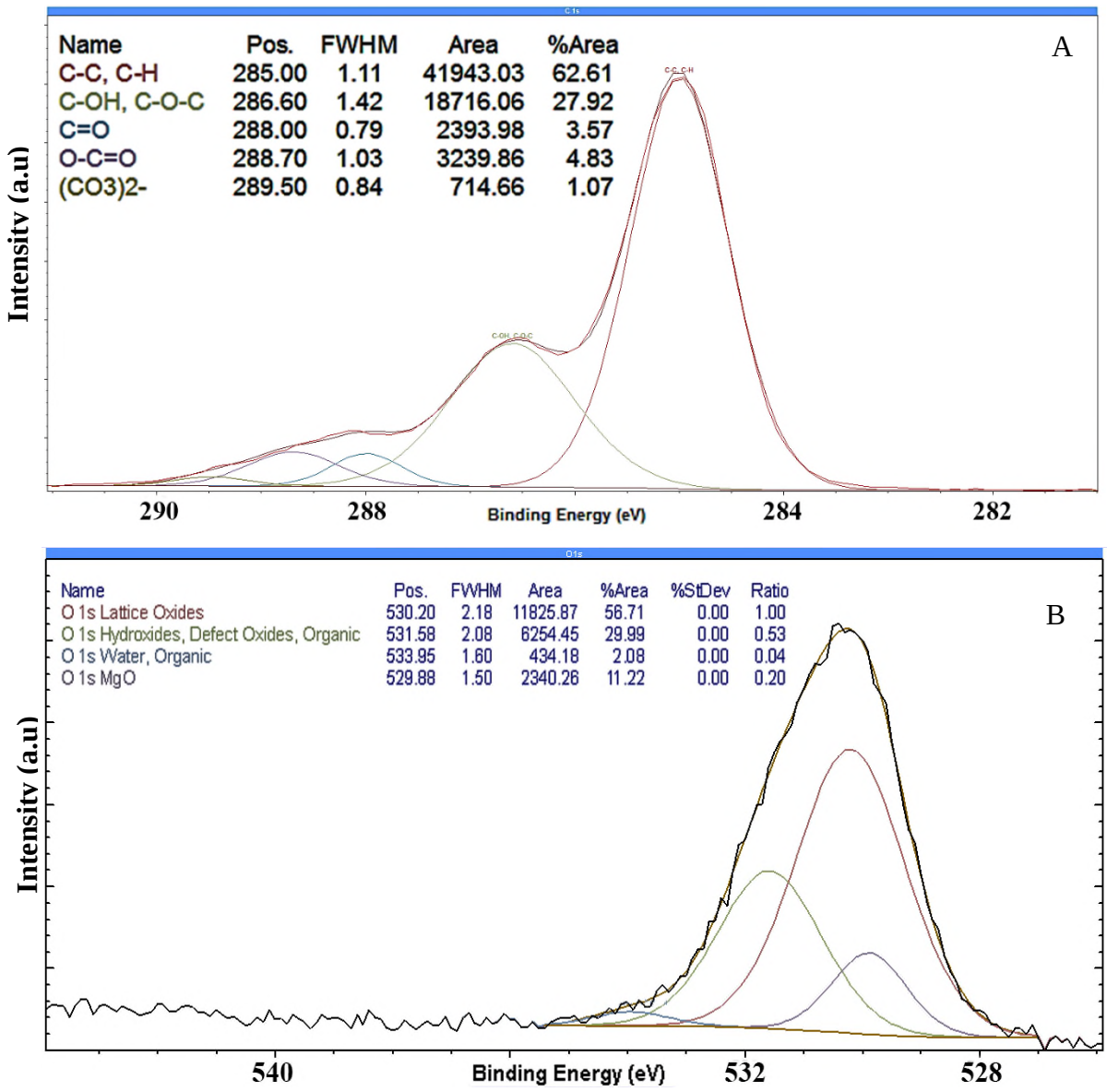

Figure 2.6: High resolution C 1s and O 1s scans. A: Deconvoluted C 1s peak, approximately 28% of the carbon atoms were in the form of alcohols (C-OH); B: Deconvoluted O 1s peak, 53% of oxygen atoms were presented in the form of hydroxides.

The spectrum of O 1s show that most oxygen atoms on the surface presented in the form of lattice oxides (56.7%), followed by hydroxides and organics (30%). The results are consistent to that of the C 1s spectrum that oxygen existed in polar groups. Inbound water peak (BE=533 eV) (1%) was also detected (Crist 1999, Liu, Ren et al. 2006, Sgriccia, Hawley et al. 2008).

In addition, MgO was identified at the binding energy (BE) of 529 eV on the spectrum, which may contribute to the ash contents reported in Table 2.2 of this work (Crist 1999).

Furthermore, the oxygen peak in the form of $(CO_3)^{2-}$ in $CaCO_3$ is at the same binding energy as that of lattice oxides (530 eV), thus the two cannot be distinguished; as such, $CaCO_3$ may also exist and contribute to the ash contents. In conclusion, the XPS results suggest that the surface of the biosorbent has abundant hydroxyl, carboxylic and additional polar groups, which can adsorb water vapor (polar molecules) from natural gas (non-polar).

2.4.2. Dehydration of Natural Gas (Methane)

To investigate the capability of the biosorbent for dehydration of natural gas, methane, the major component of natural gas, was used. Firstly, methane adsorption by biosorbent was investigated. A feed gas stream comprised of carrier gas helium, and methane was sent to the adsorption column under the conditions of 101-500 kPa, 24-50ºC, 2-4 L/min, and feed methane 10-50 v/v%. Gas chromatography was used to measure the concentration of methane in the feed and the effluent gas. The experimental results showed that the concentration of methane in the effluent gas was the same as that in the feed gas, demonstrating methane adsorption by the biosorbent was negligible.

Afterwards, the dehydration of wet methane (binary system) was investigated. Figure 2.7 shows a representative concentration profile of water vapor in the effluent during the adsorption process. The wet methane has a water molar fraction of 0.0082 ± 0.0001 which was fed to the adsorption column at 35 ºC, 300.0 kPa, and carrier gas flowrate of 2 L/min. As can be seen in this figure, dry gas was obtained from the column for around one hour; afterward, the water breakthrough point was reached (defined as the point where the water content in the effluent equals to 1% of that in the inlet stream in this work.) and the water vapor concentration in the outlet gradually increased to the saturation point. The results demonstrated that the flax shive based biosorbent had high selectivity for water adsorption and successfully dehydrated methane.

Methane is a non-polar compound (

Table 2.3). Previous results demonstrated that biomaterials have affinity to polar compounds due to their hydrophilic surface (Kataoka and Kondo 1998, Ranjbar, Tajallipour et al. 2013, Tajallipour, Niu et al. 2013). In this work, hydroxyl, carboxyl and additional polar groups on the surface of the biosorbent identified by the XPS

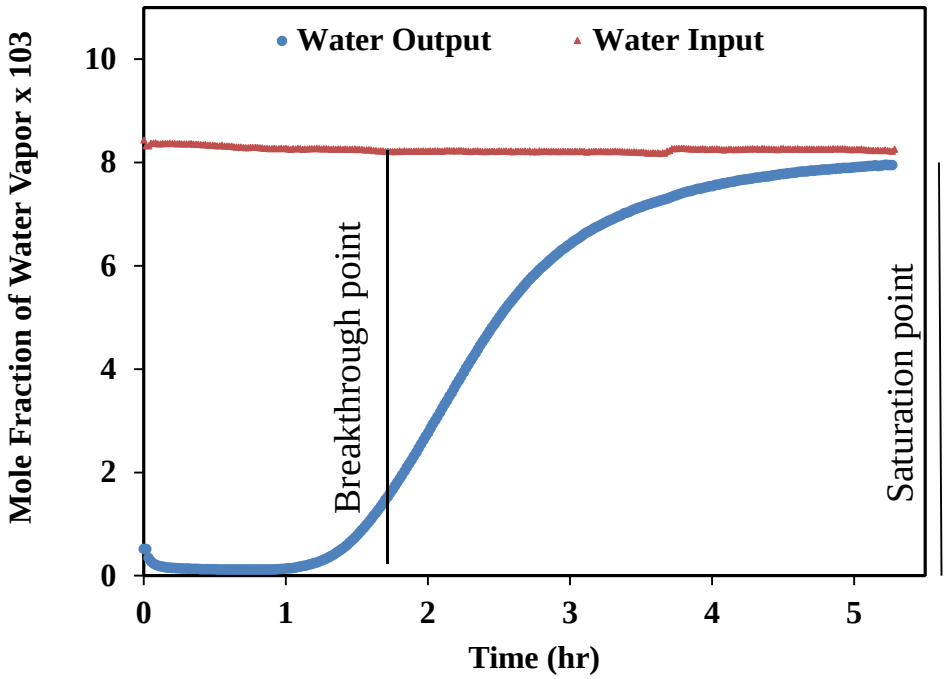

Figure 2.7: Water concentration profiles in the effluent during the adsorption experiment; Average standard deviation of all water input and output mole fraction data points is $0.05X10^{-3}$; 300 kPa, 35 °C, 2 L/min.

analysis in this work could be responsible for water vapor adsorption.

Table 2.3: Molecular structures of water and methane (Green and Perry 1973)

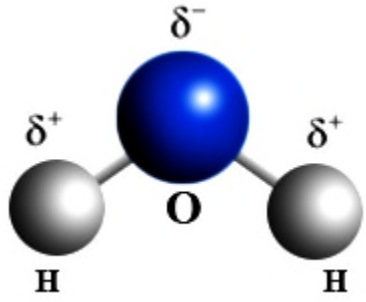	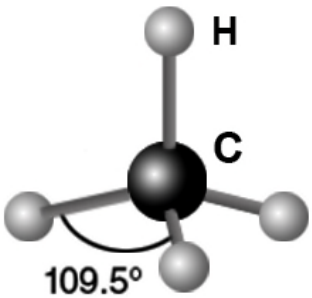
Effective diameter = 2.75 °A	Effective diameter = 3.988 °A

In addition, experiments were also carried out to test the adsorption of nitrogen, and carbon dioxide. Again, adsorption of nitrogen, and carbon dioxide was negligible, either. The results confirmed that water adsorption by the biosorbent was effective while adsorption of non-polar gases such as methane, nitrogen, and carbon dioxide was negligible. Therefore, the biosorbent seems to be a promising adsorbent for dehydration of natural gas and other non-polar gases. Based on the achieved results, the characteristics of water vapor adsorption were further investigated and the results are presented below.

2.4.3. Water Adsorption Equilibrium

***2.4.3.1 Effects of Parameters*:** The effects of key operation parameters including temperature, pressure, feed concentration and gas flow rate on water adsorption were investigated. Table 2.1 shows the levels considered for these parameters. According to this full factorial design table, 48 experiments were done in random order, and each experiment was repeated twice to determine the averages and standard deviations. The achieved maximum water adsorption capacity in this work was 0.90 g/g. It was much higher than that of commercial adsorbents for dehydration purposes that have been used in natural gas industry, e.g. silica gel (0.35-0.5 g/g), molecular sieves (0.21-0.26 g/g), and alumina (0.25-0.33 g/g).(Green and Perry 1973) The water adsorption capacities achieved under different experimental conditions are reported in Table 2.4 on the next page.

Table 2.4: Summary of data obtained from the full factorial experiments

ID	T (°C)	P (kPa)	Flowrate (L/min)	Mole Frac.	q (g/g) run 1	q (g/g) run 2	Average	Standard Deviation
1	24	300.0	2	0.0098	0.91	0.89	**0.90**	**0.01**
2	24	300.0	2	0.0083	0.57	0.50	0.53	0.04
3	24	300.0	2	0.0068	0.38	0.41	0.39	0.02
4	24	300.0	4	0.0098	0.85	0.86	0.85	0.00
5	24	300.0	4	0.0083	0.50	0.54	0.52	0.02
6	24	300.0	4	0.0068	0.36	0.35	0.36	0.00
7	24	101.3	2	0.0098	0.05	0.04	0.04	0.00
8	24	101.3	2	0.0083	0.04	0.04	0.04	0.00
9	24	101.3	2	0.0068	0.04	0.03	0.04	0.00
10	24	101.3	4	0.0098	0.05	0.05	0.05	0.00
11	24	101.3	4	0.0083	0.04	0.04	0.04	0.00
12	24	101.3	4	0.0068	0.03	0.03	0.03	0.00
13	35	300.0	2	0.0098	0.22	0.23	0.22	0.00
14	35	300.0	2	0.0083	0.20	0.20	0.20	0.00
15	35	300.0	2	0.0068	0.16	0.20	0.18	0.02
16	35	300.0	4	0.0098	0.23	0.23	0.23	0.00
17	35	300.0	4	0.0083	0.20	0.19	0.20	0.00
18	35	300.0	4	0.0068	0.17	0.16	0.17	0.00
19	35	101.3	2	0.0098	0.03	0.03	0.03	0.00
20	35	101.3	2	0.0083	0.04	0.03	0.03	0.00
21	35	101.3	2	0.0068	0.02	0.02	0.02	0.00
22	35	101.3	4	0.0098	0.03	0.03	0.03	0.00
23	35	101.3	4	0.0083	0.03	0.03	0.03	0.00
24	35	101.3	4	0.0068	0.03	0.03	0.03	0.00

The experimental results were analyzed using SPSS (Statistical Package for Social Science) software in order to determine the main effects of the factors (operating parameters) on the water adsorption capacity of the biosorbent, and the interactions among these factors. A significance level of $\alpha = 0.05$ was considered. The detailed results are reported in Table 2.5. The values of partial estimated squared measured the proportion of total variance in the ANOVA method. They were used to determine which factor has the most significant effect on the water

adsorption capacity, and interactions among the factors. The closer the value of partial estimated squared to one, the higher the contribution of the factor to the dependable variable.

It was shown that pressure had the most significant effect on the adsorption capacity. Temperature and mole fraction were the second and third important factors, respectively. The water adsorption capacity increased with an increase in pressure, and/or feed water content while it decreased as the temperature was increased. The interaction among temperature, pressure and feed water content are all significant. This was determined by the thermodynamics of water vapor adsorption in this system. Total gas flow rate did not have any effects on equilibrium water adsorption, but it may affect the diffusion rate in the particles and void volume of the bed which will be analyzed in a separate work.

Table 2.5: Statistical analysis of the full factorial experiment design

Tests of Between-Subjects Effects

Dependent Variable: adsorption capacity, q (g/g)

Source	F-Test	Significance Level	Partial Estimated Squared
Temperature	3957.07	0.000	0.999
Pressure	12772.85	0.000	1.000
Flowrate	5.29	0.083	0.570
Mole Fraction	701.10	0.000	0.997
Temperature * Pressure	3558.95	0.000	0.999
Temperature * Flowrate	3.39	0.139	0.459
Temperature * Mole Fraction	448.52	0.000	0.996
Pressure * Flowrate	6.82	0.059	0.631
Pressure * Mole Fraction	621.36	0.000	0.997
Flowrate * Mole Fraction	0.42	0.681	0.175
Temperature * Pressure * Flowrate	5.12	0.086	0.562
Temperature * Pressure * Mole Fraction	418.43	0.000	0.995
Pressure * Flowrate * Mole Fraction	0.48	0.647	0.196

Since pressure and temperature have the most significant effects on the adsorption capacity of flax shives, a contour plot of adsorption capacity can be very useful for the design of PSA columns (Figure 2.8). The highest adsorption capacity (optimum conditions) was achieved at high pressure and low temperature (300 kPa and 24 ° C).

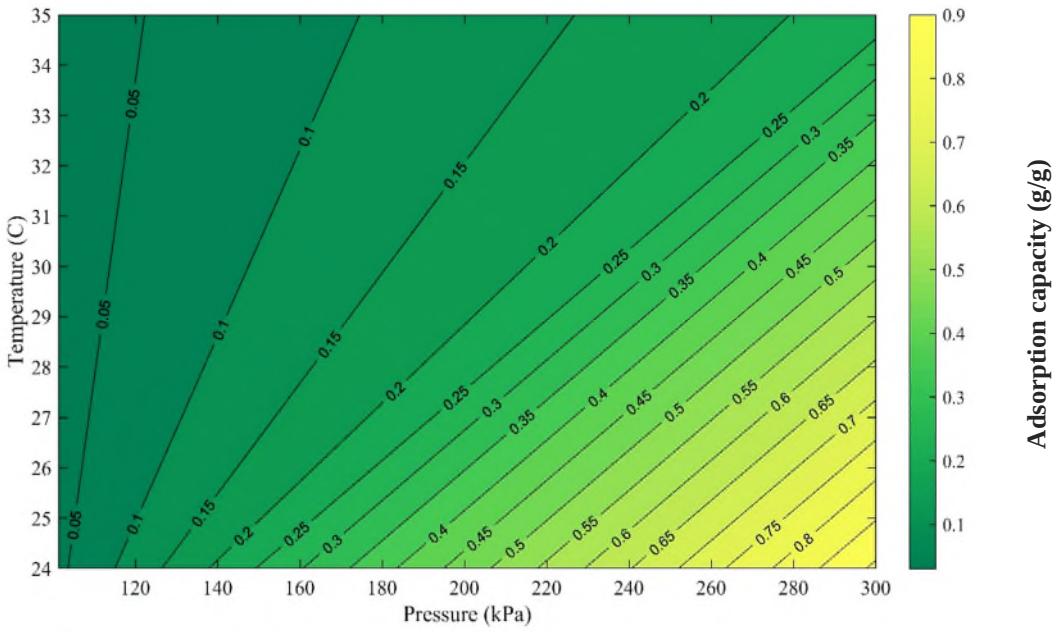

Figure 2.8: Contour plot of adsorption capacity as a function of temperature and pressure

2.4.3.2 Isotherms: Isotherm studies provide useful information about adsorption such as equilibrium, surface affinity towards adsorbates, etc. In this work, the isotherms of the water vapor adsorption by the biosorbent were obtained at temperatures of 24, 35, and 50 ^{o}C at a pressure of 300 kPa and a flowrate of 2 L/min. The results are presented in Figure 2.9. As temperature was increased, adsorption capacity decreased, demonstrating that water adsorption is exothermic. In addition, the shape of isotherm changed from type III isotherm (obtained at 24^{o}C) to type I isotherm (35-50 ^{o}C) with increase in the temperature.

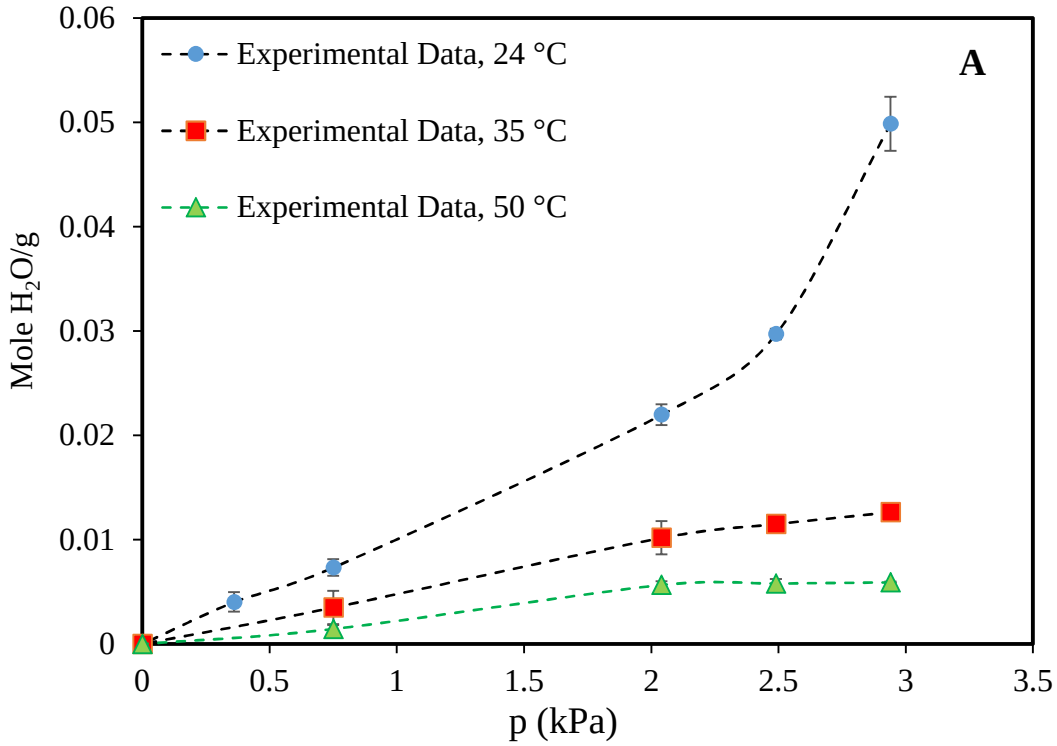
A
Experimental Data, 24 °C
Experimental Data, 35 °C
Experimental Data, 50 °C
Mole H2O/g
p (kPa)
0.06
0.05
0.04
0.03
0.02
0.01
0
0
0.5
1
1.5
2
2.5
3
3.5

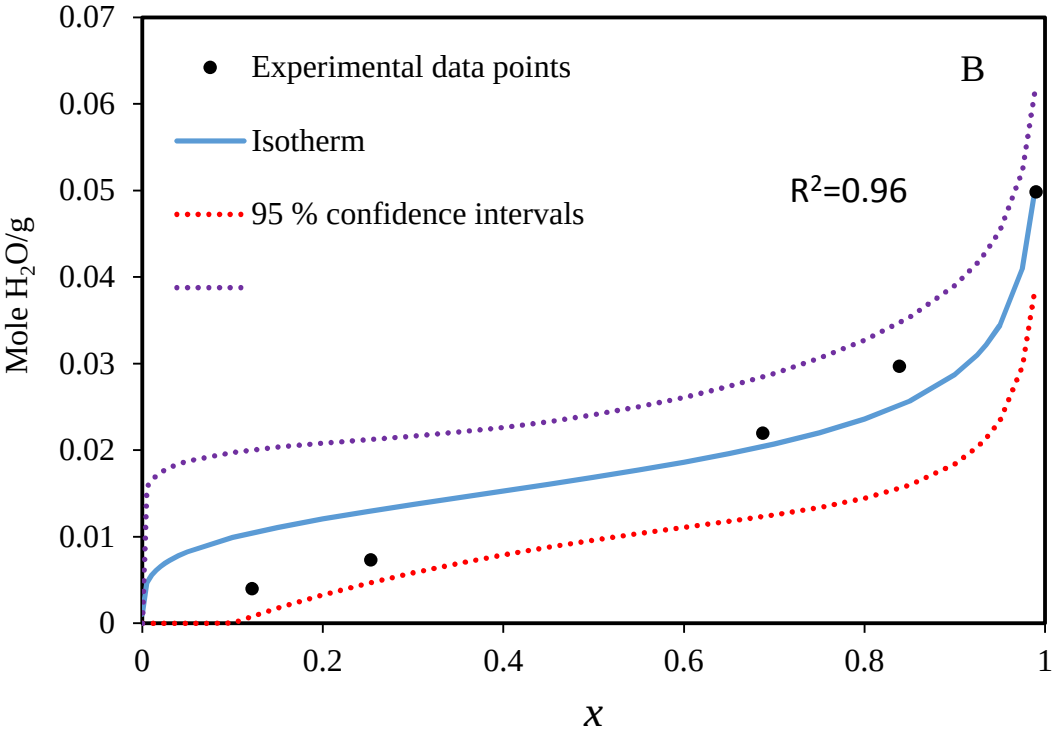
B
Experimental data points
Isotherm
95 % confidence intervals
R2=0.96
Mole H2O/g
x
0.07
0.06
0.05
0.04
0.03
0.02
0.01
0
0
0.2
0.4
0.6
0.8
1

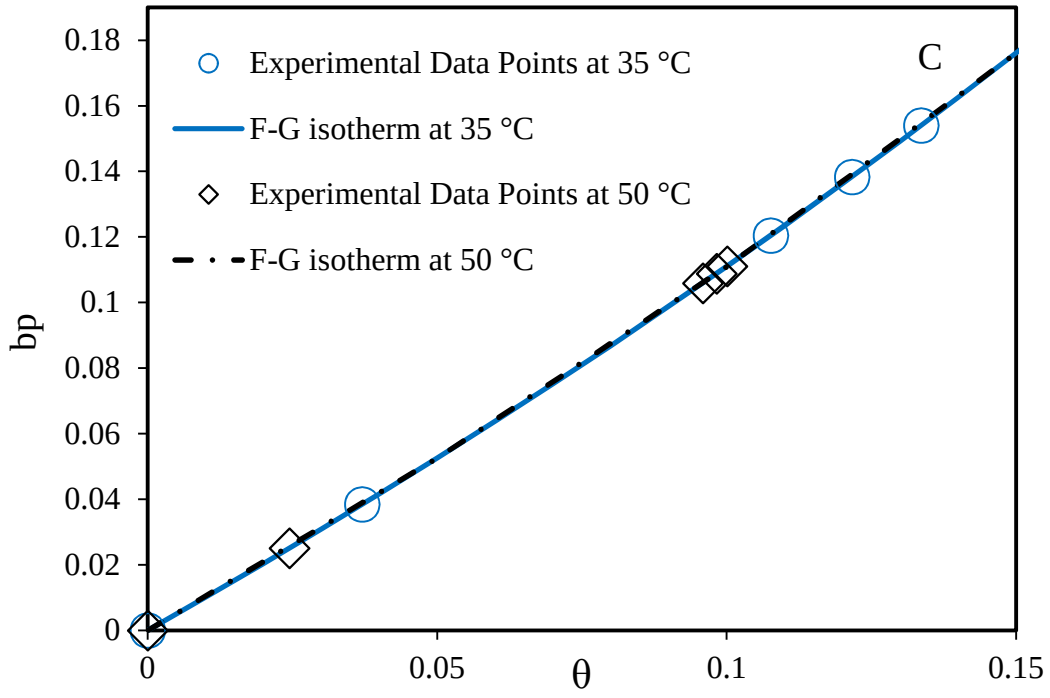

Figure 2.9: Water adsorption isotherms at 300 kPa and various temperature; A: Isotherm experimental data points; B:Redhead isotherm fitted on the experimental data points at 24 °C; B:F-G isotherm fitted on the experimental data points at 35 and 50 °C; flow rate 2 L/min for all isotherms.

2.4.3.3. Redhead Model*:* The Redhead model has been successfully used for simulation of type III isotherms such as adsorption of argon on alumina, neopentane on silica, and nitrogen on anatase (Ruthven 1984, Do 1998). This type of isotherm is usually involved in multiplayer adsorption. Similar to the BET model, the Redhead model provides the information of monolayer adsorption capacity however it extends the narrow range of validity of the BET equation (P/P_s between 0.05 to 0.35; where P is partial pressure and P_S is vapor pressure.) (Do 1998). Thus it finds wide applications. From the Redhead model, monolayer adsorption capacity can be determined, based on which surface area of an adsorbent can be determined (Ruthven 1984, Do 1998). The model is as follows:

$$\frac{q}{q_m} = \left[\frac{(2n-1)x}{(1-x)}\right]^{\frac{1}{n}} \qquad (2.2)$$

where q and q_m are total and monolayer adsorption capacities, respectively; x is relative pressure, P/P_s and n is a model fitting parameter. This model was used to simulate the isotherm obtained at 24°C and 300 kPa in this work. The modeling results are presented in Figure 2.9, and Table 2.6. It was shown that the Redhead model simulated the isotherm reasonably well. All experimental data points were within the 95% confidence intervals, and a high value of R squared was achieved. The monolayer adsorption capacity was 0.0104±0.0006 mole/g.

Table 2.6: Adsorption isotherm modeling results

		Redhead Model			
P (kPa)	**T(°C)**	**n**	**$q_{m\ (mole/g)}$**		**R^2**
300	24	4.1260 ± 0.1465	0.0104 ± 0.0006		0.96
		Fowler-Guggenhein Model			
P (kPa)	**T(°C)**	**b (pa^{-1})**	**c**	**W (J/mole)**	**R^2**
300	35	0.0524 ± 0.0034	0.0100 ± 0.0000	6.40	1.00
300	50	0.0433 ± 0.0057	0.0124 ± 0.0005	8.33	0.99

In general, the BET model is popular for determination of specific surface area; however, due to the limited validity range ($0.01 < P/P_S < 0.3$) of the BET model, the Redhead model has been successfully applied to many systems. In this work, the specific surface area for water adsorption was determined using the monolayer adsorption capacity q_m obtained from the Redhead modelling results for the data at 24°C and 300 kPa. The following equation was used to calculate the specific surface area A:

$$A = q_m \, \mathbb{N}_a \, a_m \quad (\frac{m^2}{g}) \tag{2.3}$$

where $\mathbb{N}_a$ is the Avogadro number, and a_m is the molecular projected area, which was reported to be 16 $A^2/molecule$ in the case of water.(Ruthven 1984, Do 1998) As such, a specific surface area of 1005 ± 81 m^2/g was obtained by Eq. 2.3 based on the results obtained at 24°C and 300 kPa. This value is much higher than that measured by the BET model via nitrogen adsorption, being 1.34 ± 0.07 m^2/g. The results indicated that the water adsorption sites were beyond the surface area identified by the BET method using nitrogen adsorption which provided information about the mesoporous/microporous volumes of the biosorbent. In this work, the results of SEM and XPS analyses show the flax shive based biosorbent has abundant hydrophilic groups such as hydroxyl, carboxyl and additional groups. Water molecules may be able to penetrate into the material inner structure to access those functional groups while nitrogen could not. In addition, water absorption may also contribute to total water uptake by the flax shive material. All these reasons can lead to the remarkably high apparent water adsorption capacity of the biosorbent. Thus the surface area determined from the Redhead model based on the water adsorption capacity is much higher than that of the BET surface area determined by nitrogen adsorption.

It was reported that in the cases of adsorption of argon on alumina, neopentane on silica, and nitrogen on anatase (Ruthven 1984, Do 1998), the specific surface areas obtained based on the Redhead modeling results were very close to the values obtained from the BET model using nitrogen (Ruthven 1984, Do 1998). In such cases, argon and nitrogen have similar properties. The results obtained in this work using two different adsorbate demonstrated the significant difference between the values of specific surface area determined by different methods. Therefore, type of adsorbate, and method used in surface area analysis is important. In this work, it is considered that using water vapor as the adsorbate and the Redhead model provided reasonable results in surface area determination for water adsorption.

2.4.3.4. Fowler-Guggenhein Model: The Fowler-Guggenhein (F-G) model has been effectively used to describe Type I isotherms. It was derived from the general Gibbs isotherm equation considering the van der Walls equation of state to describe the surface phase. This model was also derived from the statistical thermodynamics approach by Rudzinski and Everett (Ruthven 1984, Do 1998). Importantly, this model considers lateral interactions among the adsorbed atoms and can predict the two dimensional condensation. The model is as follows:

$$bp = \frac{\theta}{1-\theta}\exp(-c\theta) \qquad (2.4)$$

where p is partial pressure of water vapor, kPa, b is surface affinity towards water vapor, kPa^{-1}, c is model parameter, and θ is the surface coverage. The model parameter c can take a value from 0 to 7.(Do 1998) This parameter is related to the interactions among adsorbed molecules through Eq. 2.5:

$$c = \frac{zw}{R_g T} \qquad (2.5)$$

where z is the coordination number, w is the interaction parameter, J/mol; R_g is the universal gas constant, J/mol.K; and T is absolute temperature, K. A positive value for w indicates attraction among the adsorbed molecules on the surface, while a negative value indicates repulsion. The isotherm model was chosen in this work to simulate the isotherms obtained at 35, and 50 ^{o}C and determine the interaction forces among water molecules adsorbed on the surface.

The fitted isotherms are shown in Figure 2.9-C. The results demonstrated that the G-F model provided satisfactory prediction for the isotherms obtained at elevated temperatures 35, and 50 ^{o}C. The regressed model parameters are summarized in Table 2.6.

It can be noticed from the modeling results that the surface affinity towards water vapor, represented by the value of b, slightly decreased with increase in the temperature. In the current system, water adsorption is exothermic. Thus at elevated temperature, surface affinity decreased, and adsorption capacity reduced. The lateral interactions was also increased with increase in the temperature, which seems to be due to higher internal energy and more collisions among atoms on the surface. These pieces of information were determined by the nature of water adsorption thermodynamics.

In addition, the value of c was 0.0100 ± 0.0000, which is smaller than 4, indicating that no two-dimensional condensation took place in the system operated at 35, and 50 ^{o}C.(Do 1998) Furthermore, the interaction parameters (w) were calculated using Eq. 2.5 and are listed in Table 2.6 as well. A value of 4 was used for the water's coordination number, which was calculated from molecular dynamic simulations (Do 1998). In this work, the values of w are all positive, indicating attraction between adsorbed water molecules on the surface. Furthermore, the value of w representing interaction force did not change significantly with the change of temperature under the experimental conditions. The attraction forces among water molecules adsorbed onto the

surface of flax shives are much lower than the van der Walls weak forces (400 – 4000 J/mol) and hydrogen bonds such as HO-H$^{\cdots}$OH$_3^+$ (18,000 J/mol) (Markovitch and Agmon 2007). This demonstrated that water vapor adsorption on the surface of flax shives is physisorption.

2.4.4. Mass Transfer Zone

Information about mass transfer zone is important for design and scale-up of PSA operations. The length of mass transfer zone plays a critical role in the design and operation of PSA systems, which can be determined using the following equation (Ruthven 1984):

$$MTZ = 2 \times H \times \left(1 - \frac{\int_0^{t_b} \left(1 - \frac{C}{C_o}\right) dt}{\int_0^{t_s} \left(1 - \frac{C}{C_o}\right) dt} \right) \tag{2.6}$$

where *MTZ* is the length of mass transfer zone (cm), *H* is the height of the column packed with adsorbents (cm), t_b is the breakthrough time, and t_s is the stoichiometric time. Stoichiometric time is the time that divides the mass transfer zone into equal areas.

Eq. 2.6 was used to calculate the length of mass transfer zone. The representative breakthrough curves for determining the length of mass transfer zone are shown in Figure 2.10. The values are summarized in Table 2.7. In this work, the breakthrough point for water was defined to be the point where C/C_0 of water vapor equals to 0.01 and equilibrium or saturation point was considered to be the point where C/C_0 of water vapor equals to 0.95; where C is the concentration in the outlet and C_0 is the concentration in the inlet (Ruthven 1984).

Table 2.7: Length of mass transfer zone (MTZ) calculated at various operating conditions.

Pressure (kPa)	**Temperature (°C)**	**Flow rate (L/min)**	**Particle Size (mm)**	**MTZ (cm)**
300	24	2	0.425 -1.18	10.81
300	24	4	0.425 -1.18	11.59
300	35	2	0.425 -1.18	7.09
300	35	4	0.425 -1.18	8.02
101.3	24	2	0.425 -1.18	8.49
101.3	24	4	0.425 -1.18	11.49
101.3	35	2	0.425 -1.18	8.18
101.3	35	4	0.425 -1.18	9.23
300	24	4	0.425 -1.18	10.3
300	24	4	1.18 – 3.0	9.6

It is critical to predict the length of mass transfer zone while the PSA operating conditions are changed. In this work, it was observed that the length of mass transfer zone increased with increase in the total gas flow rate. On the other hand, the length of mass transfer zone was decreased as the temperature was increased, which is believed to be due to faster molecular diffusion and decrease in the water adsorption capacity with increase in temperature (equilibrium effect). The effect of pressure was different at low and high temperatures, which is likely to be due to the different adsorption mechanisms as discussed in the section of adsorption equilibrium (monolayer and multilayer adsorption mechanisms). Serbezov studied the mass transfer in a

packed bed of biosorbents based on tea wastes for the adsorption of chromium (VI), and also reported an increase in the length of mass transfer zone with increase in the flow rate, and pressure; however, the author did not report the results obtained at various temperatures (Serbezov 2001). Dynamic modeling of PSA process can provide detailed information on this subject, which is outside the focus of this paper.

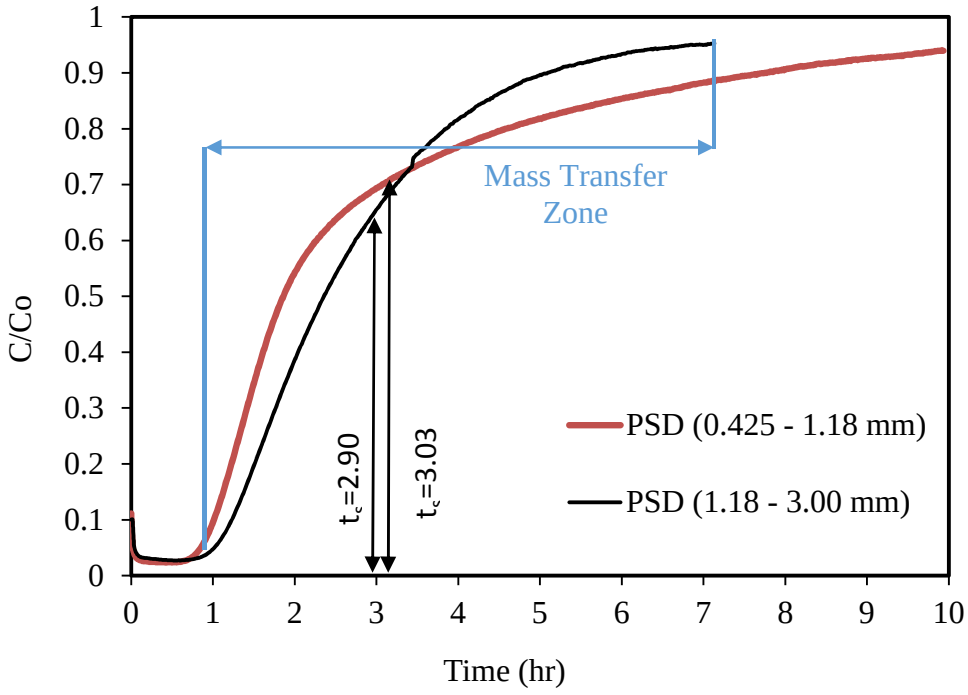

Figure 2.10: Representative breakthrough curves, and length of mass transfer zone.

t_b is breakthrough time; t_s is the stoichiometric time; conditions: 300 kPa, 24 °C, feed water mole fraction: 0.0098, and flow rate: 4 L/min.

Effect of biosorbent particle size on the length of mass transfer zone was also evaluated using two different particle size ranges (0.425-1.18 mm, and 1.18-3.00 mm). The results show that the length of mass transfer zone is insignificantly affected by the particles size under the experimental conditions (300 kPa and 24 ^{o}C). However, the slope of the water breakthrough curve obtained by the biosorbent of smaller particle sizes was steeper than that by the bigger size biosorbent, as shown in Figure 2.10. The steeper the slope, the higher the mass transfer rate. This is because smaller particles have higher specific surface area which enhance mass transfer rate. However, the particle size does not affect adsorption capacity which is determined by thermodynamic equilibrium.

A low pressure drop in the range of 2.9 – 5.8 kPa was observed in the experiments. Using the Ergun equation, values of 0.32 and 0.24 were calculated for the bed voidage at 101.3 kPa, and 300 kPa, respectively. Pressure drop was reduced to 1.8 kPa when biosorbents with particle size distribution of 1.18 – 3.00 mm were packed in the column.

2.4.5. Cycle of Adsorption and Desorption

To complete the pressure swing adsorption process, a cycle of adsorption and desorption was operated. The carrier gas was nitrogen for both the processes. Before the cycle, gas flow direction was first chosen for the adsorption and desorption process. The gas flow through the column could be upward or downward. To study the effect of flow direction, two experiments were run at same operating conditions, yet different flow direction (upward and downward). Same adsorption capacity and similar breakthrough curves were obtained indicating that the flow direction did not affect the process under the experimental conditions. Thus, downward flow was chosen for adsorption, and upward flow for desorption. For this experiment, adsorption was operated at 24 °C, 300 kPa, and 2 L/min and desorption was at 24ºC, 46 kPa, and 3 L/min. Figure 2.11 on the next page shows the profiles during a complete adsorption-desorption cycle in one column.

In a general dual-column PSA process, also called Skarstrom cycle, there are four steps in each cycle. Each bed experiences pressurization, adsorption at high pressure, blowdown, and desorption at low pressure (vacuum). Cycle time can be from a few seconds to a few minutes depending on the type of process in which adsorption usually does not reach equilibrium/saturation. However, in this work, adsorption was operated till equilibrium and desorption till the column was full dried in order to obtain complete operation data. Thus, Figure 2.11 shows the profiles of one column up to complete saturation and complete regeneration point. It can be seen that desorption rate on average was much faster than the adsorption rate at room

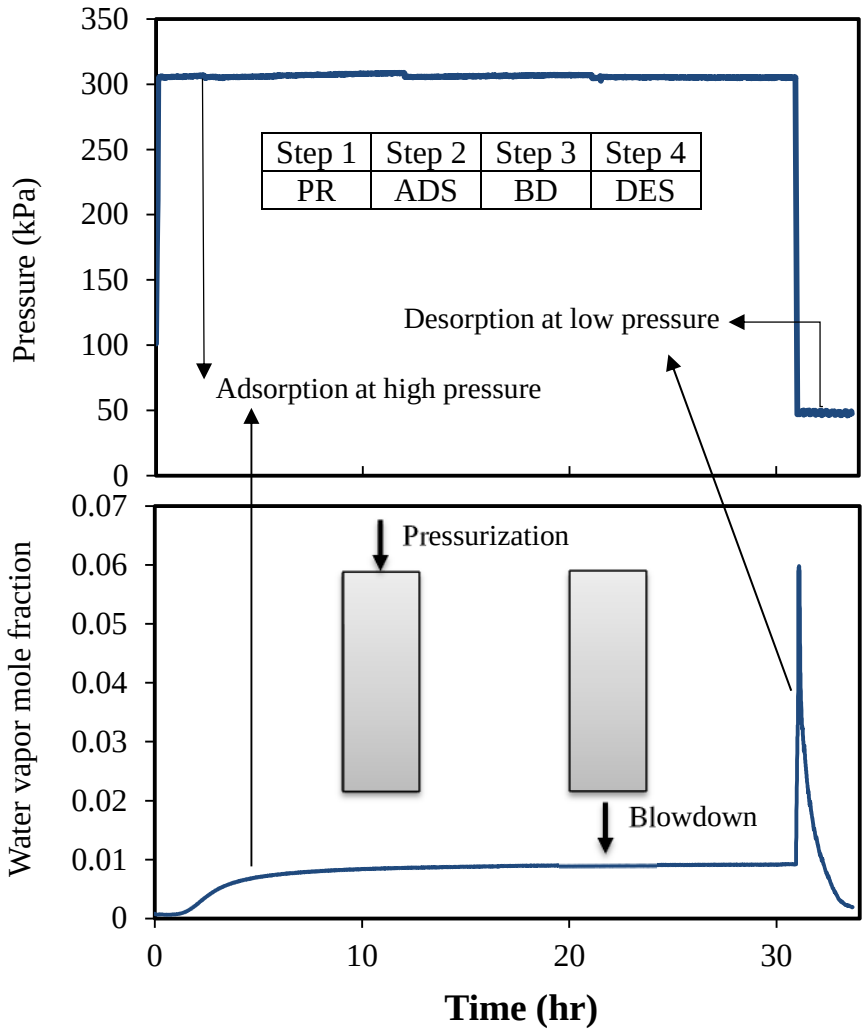

Figure 2.11: Column profiles during one complete adsorption-desorption cycle at 24 °C; PR: Pressurization; ADS: Adsorption at high pressure (300 kPa); BD: Blowdown; DES: Desorption under vacuum (46 kPa).

temperature (31 hours of adsorption and 2.5 hours of desorption). It is critical that the column is sufficiently regenerated during a specific cycle time; otherwise, accumulation of water vapor in the column over time would lead to premature breakthrough in the PSA process, and natural gas could not be sufficiently dehydrated. In an industrial PSA process, the bed temperature is sometimes increased in order to increase the desorption rate; however, in this work biosorbents were regenerated at a fast rate at room temperature, which demonstrated the advantages of using the biosorbents for the PSA process. Future work needs to be done on detailed adsorption-

desorption rate measurement, dual-column process, and additional analysis in regards to the product purity and recovery.

2.4.6 Reusability of Biosorbent

Biosorbents are expected to dehydrate natural gas during their lifetime with negligible deterioration and loss of adsorption properties. For that, the performance of the biosorbent has been evaluated for 70 adsorption-desorption cycles. Furthermore, thermal stability of the biosorbents was also investigated using the TGA analysis.

Figure 2.12 shows the breakthrough curves of water adsorption by the fresh, 2nd time used, and 70th time used biosorbents. As can be seen, the breakthrough curves overlapped with one another. The achieved water adsorption capacities are similar, the average of which had a small standard deviation. The slight difference among the breakthrough curves could be due to uncontrollable environmental disturbances to temperature and pressure control. Therefore, the performance of the biosorbent is stable and the results are repeatable. Investigation on effect of aging over a longer period of time would be necessary in the future.

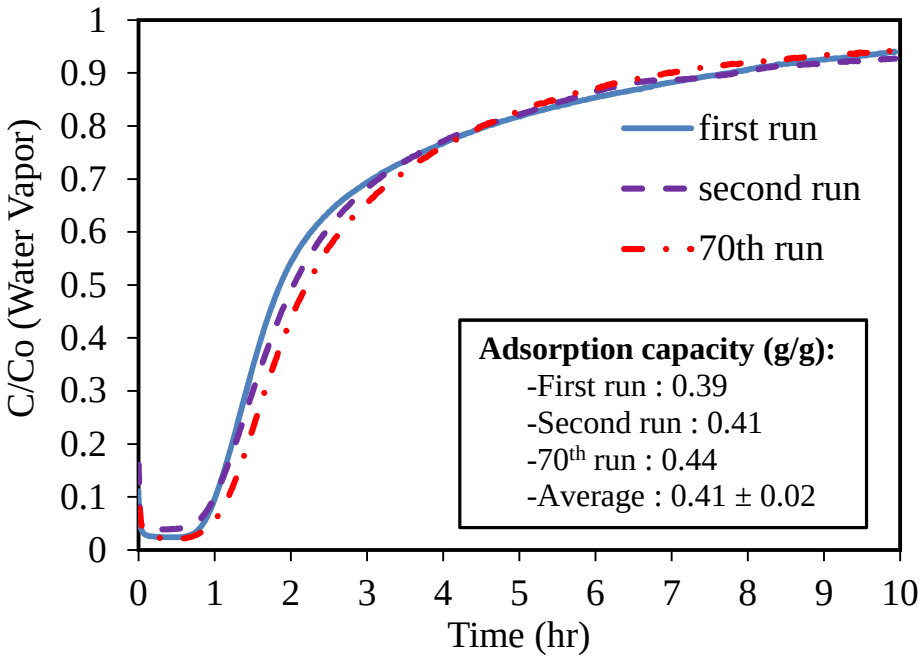

Figure 2.12: Reusability of flax shives for natural gas (methane) dehydration; Dimensionless concentration of water vs. time; 300 kPa, 24 °C, and flow rate 4 L/min.

The thermogravimetric analysis (TGA) was also done to determine the thermal stability of the biosorbent. The TGA results are presented in Figure 2.13. According to this figure, flax shives started to decompose at around 200° C. The sharp blue peak indicates the decomposition of cellulose at around 380 °C. These temperatures are much higher than the operating temperatures of the PSA process using the biosorbents (24 to 50 °C) in this work, which confirmed that flax shive biosorbent is stable and suitable for dehydrating natural gas.

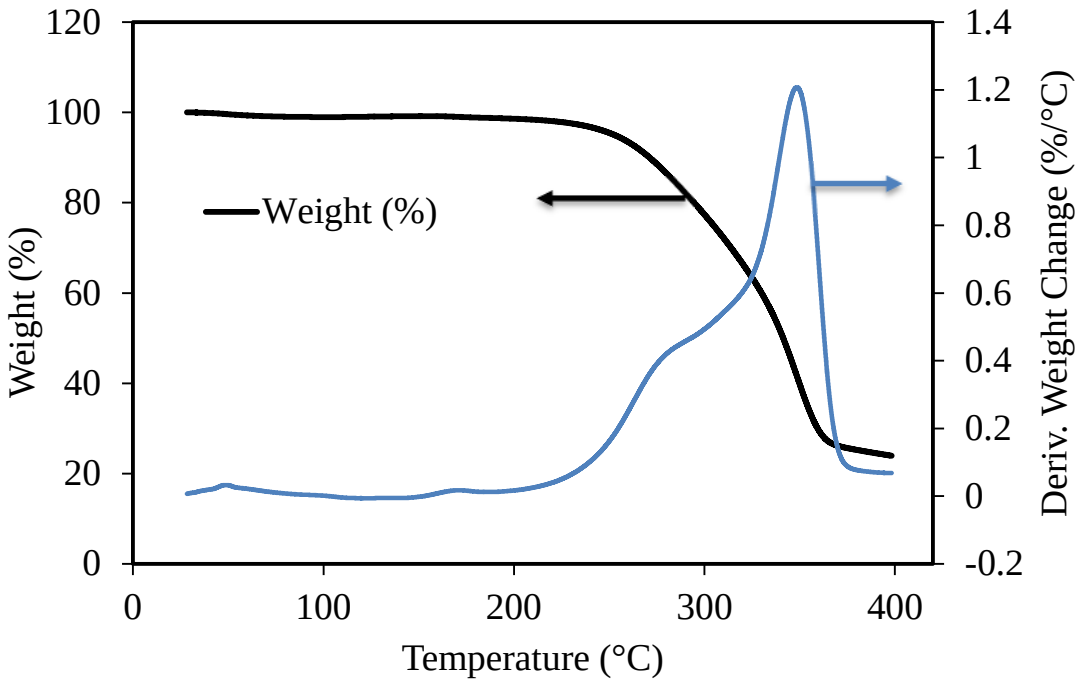

Figure 2.13: TGA results of flax shives; Sample weight loss due to thermal degradation and pyrolysis was measured over time as the temperature was gradually increased.

2.5 SUMMARY

The biosorbent developed from flax shives was able to effectively dehydrate methane (major component of natural gas) with high selectivity for water adsorption. It demonstrated much higher water adsorption capacity (0.9 g/g) than most of the commercial adsorbents. Adsorption of methane, nitrogen and carbon dioxide was negligible. The water saturated biosorbent was regenerated at a fast rate at room temperature under vacuum, and had stable performance after 70 adsorption-desorption cycles. The biosorbent was also stable at temperatures up to 200 °C. The

results show that the flax shive biosorbent is promising in the dehydration of methane (natural gas), and other non-polar gases in a PSA process.

The biosorbent has porous structure, and contains hydroxyl, carboxyl, and additional polar groups as evidenced by the SEM and XPS analyses, which are considered to play important roles for the high water adsorption capacity achieved in this work. The total pressure has the most significant effect on water adsorption capacity, followed by temperature and feed water content. The interaction among temperature, pressure and feed water content are all significant. The water adsorption is exothermic, but mechanisms are different at lower (24^{o}C), and higher temperature (35-50^{o}C). The isotherm changed from type III isotherm at 24^{o}C to type I at 35-50^{o}C. The Redhead model provided satisfactory simulation for the isotherm obtained at 24^{o}C, and the F-G model for the isotherms at 35-50^{o}C. The surface area available for water adsorption was calculated to 1005 m^2/g based on the Redhead modeling results, which is significantly higher than that determined by the BET model via nitrogen adsorption. Selecting proper adsorbate for determination of surface area for adsorption is important. The F-G modeling results indicated that the adsorbed water molecules on the surface of the flax shive biosorbent were attractive to one another, however, the interaction force was very weak.

The length of mass transfer zone determined at various conditions showed that it increased with increase in the total gas flow rate, and decrease in temperature. Pressure did not have consistent effect at the tested conditions. More research in the regards is necessary.

2.6 ABBREVIATIONS

BE	Binding energy (eV)
BTEX	Benzene, Toluene, Ethylbenzene and Xylene
FE-SEM	Field emission scanning electron microscopy
FT-IR	Fourier transform Infrared spectroscopy
FWHM	Full width at half max
GC	Gas chromatography
ID	Identification number

MTZ	Mass transfer zone
PSA	Pressure swing adsorption
PSD	Particle size distribution
RH	Relative humidity (%)
SPSS	Statistical Package for Social Science
SD	Standard deviation
TSA	Temperature swing adsorption
TCD	Thermal conductivity detector
TGA	Thermo gravimetric analysis
XPS	X-ray photoelectron spectroscopy

2.7 NOMENCLATURE

a_m	Molecular projected surface (m^2)
At%	Percentage of atoms on the surface
b	Surface affinity (pa^{-1})
c	Model parameter in Anderson isotherm
C	Concentration in the column outlet
C_0	Concentration in the column inlet
C 1s	Carbon peak in the XPS spectrum
Ca 2p	Calcium peak in the XPS spectrum
H	Height of the column (cm)
j	Model parameter in Anderson isotherm
k	Surface affinity (pa^{-1})

$\dot{m}_i$	Mass flow rate of component i (g/hour)
Mg 2s	Magnesium peak in the XPS spectrum
$\mathbb{N}_a$	Avogadro number
N 1s	Nitrogen peak in the XPS spectrum
n	Model parameter in Redhead isotherm
$\dot{n}_c$	Molar flow rate of carrier gas (mole/s)
$\dot{n}_m$	Molar flow rate of methane (mole/s)
$\dot{n}_w$	Molar flow rate of water vapor (mole/s)
O 1s	Oxygen peak in the XPS spectrum
p	Partial pressure of water (kPa)
P	Partial pressure (kPa)
P_s	Vapor pressure at a reference temperature (kPa)
P_t	Total pressure of the column (absolute, kPa)
t_b	Breakthrough time
t_s	Stoichiometric time
q	Adsorption capacity (gram water/gram adsorbent)
q_m	Monolayer adsorption capacity (gram water/gram adsorbent)
x_w	Mole fraction of water vapor
w	Lateral interactions among adsorbed molecules on the surface (J/mole)
Greek letter	
α	Statistical significance level

2.8 REFERENCES

Babicki, M. L., B. G. Keefer, A. C. Gibbs, A. I. IaCava and F. Fitch (2006). PSA with adsorbents sensitive to contaminants, Google Patents.

Besser, B., H. A. Tajiri, G. Mikolajczyk, J. Möllmer, T. C. Schumacher, S. Odenbach, R. Gläser, S. Kroll and K. Rezwan (2016). "Hierarchical porous zeolite structures for pressure swing adsorption applications." ACS applied materials & interfaces **8**(5): 3277-3286.

Buranov, A. U. and G. Mazza (2010). "Extraction and characterization of hemicelluloses from flax shives by different methods." Carbohydrate polymers **79**(1): 17-25.

Carter, J. and M. Wyszynski (1983). "The pressure swing adsorption drying of compressed air." Chemical Engineering Science **38**(7): 1093-1099.

Crist, B. (1999). XPS Handbook of the Elements and Native oxides, XPS International, Inc.

Do, D. D. (1998). Adsorption Analysis: Equilibria And Kinetics: (With CD Containing Computer Matlab Programs), World Scientific.

Fukuda, N., N. Ishida, K. Nomura, T. Wang, K. Tamada and H. Ushijima (2011). "Analysis of adsorption and binding behaviors of silver nanoparticles onto a pyridyl-terminated surface using XPS and AFM." Langmuir **27**(21): 12916-12922.

Gandhidasan, P. (2003). "Parametric analysis of natural gas dehydration by a triethylene glycol solution." Energy Sources **25**(3): 189-201.

Grande, C. A. and R. Blom (2012). "Dual pressure swing adsorption units for gas separation and purification." Industrial & Engineering Chemistry Research **51**(25): 8695-8699.

Green, D. W. and R. H. Perry (1973). Perry's Chemical Engineers' Handbook/edición Don W. Green y Robert H. Perry.

Herm, Z. R., J. A. Swisher, B. Smit, R. Krishna and J. R. Long (2011). "Metal− organic frameworks as adsorbents for hydrogen purification and precombustion carbon dioxide capture." Journal of the American Chemical Society **133**(15): 5664-5667.

Ho, M. T., G. W. Allinson and D. E. Wiley (2008). "Reducing the cost of CO2 capture from flue gases using pressure swing adsorption." Industrial & Engineering Chemistry Research **47**(14): 4883-4890.

Jayaprakash, D., R. Dhabhai, C. H. Niu and A. K. Dalai (2017). "Selective Water Removal by Sorption from Butanol–Water Vapor Mixtures: Analyses of Key Operating Parameters and Site Energy Distribution." Energy & Fuels **31**(5): 5193-5202.

Kacem, M., M. Pellerano and A. Delebarre (2015). "Pressure swing adsorption for CO 2/N 2 and CO 2/CH 4 separation: comparison between activated carbons and zeolites performances." Fuel Processing Technology **138**: 271-283.

Karimi, S., B. Ghobadian, M.-R. Omidkhah, J. Towfighi and M. T. Yaraki (2016). "Experimental investigation of bioethanol liquid phase dehydration using natural clinoptilolite." Journal of advanced research **7**(3): 435-444.

Kataoka, Y. and T. Kondo (1998). "FT-IR microscopic analysis of changing cellulose crystalline structure during wood cell wall formation." Macromolecules **31**(3): 760-764.

Kidnay, A. J., W. R. Parrish and D. G. McCartney (2011). Fundamentals of natural gas processing, CRC Press.

Liu, C.-F., J.-L. Ren, F. Xu, J.-J. Liu, J.-X. Sun and R.-C. Sun (2006). "Isolation and characterization of cellulose obtained from ultrasonic irradiated sugarcane bagasse." Journal of agricultural and food chemistry **54**(16): 5742-5748.

Liu, Y., S. D. Feist, C. M. Jones and D. R. Armstrong (2014). "Isopropyl alcohol dehydration by hot gas pressure swing adsorption: experiments, simulations, and implementation." Industrial & Engineering Chemistry Research **53**(20): 8599-8607.

Markovitch, O. and N. Agmon (2007). "Structure and energetics of the hydronium hydration shells." The Journal of Physical Chemistry A **111**(12): 2253-2256.

Mokhatab, S. and W. A. Poe (2012). Handbook of natural gas transmission and processing, Gulf professional publishing.

Mrowiec-Białoń, J., A. B. Jarzebski and L. Pajak (1999). "Water Vapor Adsorption on the SiO2− CaCl2 Sol− Gel Composites." Langmuir **15**(19): 6505-6509.

Netusil, M. and P. Ditl (2011). "Comparison of three methods for natural gas dehydration." Journal of Natural Gas Chemistry **20**(5): 471-476.

Niu, C., T. Baylak, D. Wilson and M. Zhang (2014). "Pelletisation of canola meal by extrusion–spheronisation for ethanol dehydration." Biomass and bioenergy **66**: 116-125.

Niu, C. H. and B. Volesky (2007). "Modeling chromium (VI) biosorption by acid washed crab shells." AIChE journal **53**(4): 1056-1059.

Ranjbar, Z., M. Tajallipour, C. H. Niu and A. K. Dalai (2013). "Water removal from ethanol vapor by adsorption on canola meal after protein extraction." Industrial & Engineering Chemistry Research **52**(40): 14429-14440.

Ruthven, D. M. (1984). Principles of adsorption and adsorption processes, John Wiley & Sons.

Ruthven, D. M., S. Farooq and K. S. Knaebel (1994). Pressure swing adsorption, VCH publishers New York.

Santos, J., A. Portugal, F. Magalhaes and A. Mendes (2004). "Simulation and optimization of small oxygen pressure swing adsorption units." Industrial & engineering chemistry research **43**(26): 8328-8338.

Santos, M. n. P., C. A. Grande and A. r. E. Rodrigues (2010). "Pressure swing adsorption for biogas upgrading. Effect of recycling streams in pressure swing adsorption design." Industrial & Engineering Chemistry Research **50**(2): 974-985.

Serbezov, A. (2001). "Effect of the process parameters on the length of the mass transfer zone during product withdrawal in pressure swing adsorption cycles." Chemical engineering science **56**(15): 4673-4684.

Sgriccia, N., M. Hawley and M. Misra (2008). "Characterization of natural fiber surfaces and natural fiber composites." Composites Part A: Applied Science and Manufacturing **39**(10): 1632-1637.

Sun, N., C. Okoye, C. H. Niu and H. Wang (2007). "Adsorption of water and ethanol by biomaterials." International Journal of Green Energy **4**(6): 623-634.

Tajallipour, M., C. Niu and A. Dalai (2013). "Ethanol Dehydration in a Pressure Swing Adsorption Process Using Canola Meal." Energy & Fuels **27**(11): 6655-6664.

Tan, B. J., K. J. Klabunde and P. M. Sherwood (1991). "XPS studies of solvated metal atom dispersed (SMAD) catalysts. Evidence for layered cobalt-manganese particles on alumina and silica." Journal of the American Chemical Society **113**(3): 855-861.

Thevannan, A., G. Hill and C. H. Niu (2011). "Kinetics of nickel biosorption by acid‐washed barley straw." The Canadian Journal of Chemical Engineering **89**(1): 176-182.

Thevannan, A., R. Mungroo and C. H. Niu (2010). "Biosorption of nickel with barley straw." Bioresource technology **101**(6): 1776-1780.

Wallart, X., C. Henry de Villeneuve and P. Allongue (2005). "Truly quantitative XPS characterization of organic monolayers on silicon: study of alkyl and alkoxy monolayers on H− Si (111)." Journal of the American Chemical Society **127**(21): 7871-7878.

Yan, B. and C. H. Niu (2017). "Modeling and site energy distribution analysis of levofloxacin sorption by biosorbents." Chemical Engineering Journal **307**: 631-642.

Yan, B. and C. H. Niu (2017). "Pre-treating biosorbents for purification of bioethanol from aqueous solution." International Journal of Green Energy **14**(3): 245-252.

Yang, B., E. L. Xu and M. Li (2016). "Purification of coal mine methane on carbon molecular sieve by vacuum pressure swing adsorption." Separation Science and Technology **51**(6): 909-916.

Zafeiropoulos, N., P. Vickers, C. Baillie and J. Watts (2003). "An experimental investigation of modified and unmodified flax fibres with XPS, ToF-SIMS and ATR-FTIR." Journal of Materials Science **38**(19): 3903-3914.

CHAPTER 3. DRYING BUTANOL USING CANOLA MEAL AFTER PROTEIN EXTRACTION

3.1. ABSTRACT

In this chapter, selective water removal from butanol-water vapor mixture was carried out in a pressure swing adsorption (PSA) system using canola meal (CM) biosorbent. Five operating parameters (temperature, pressure, feed butanol concentration, feed flow rate, and CM particle size) were studied by the orthogonal array design method and range analysis to obtain the favorable process conditions for butanol drying. The performance of butanol dehydration was evaluated using five indices - water uptake; butanol uptake; water selectivity; butanol recovery; and maximum butanol concentration in the effluent. The obtained favorable dehydration conditions resulted in the maximum effluent butanol concentration of >99 v/v%, water uptake of 0.48 g/g-ads, water separation factor of 5.4, and butanol recovery of 90%. The Dubinin-Polanyi model for large pores fit the water adsorption isotherms reasonably well. Furthermore, site energy distribution of water adsorption was also estimated. Average site energy (3.33 kJ/mol) and standard deviation of the site energy distribution (2.36 kJ/mol) were determined and applied to analyze the interaction between the biosorbent and adsorbate, and adsorbent surface energy heterogeneity. Saturated CM was regenerated at 110°C under vacuum and reused for more than 16 cycles without deterioration and will be continuously used.

3.2 INTRODUCTION

Diminishing supplies of crude oil, coupled with increasing greenhouse gas emissions and carbon footprints, have led to a massive interest in renewable biofuels such as ethanol and butanol (Shah and Dhrubo, 2011). In recent years, biobutanol is preferred to bioethanol and other alcohols, mainly because of its superior fuel properties that are very similar to gasoline. It is less corrosive and can be easily transported through existing pipelines. Butanol also has higher combustion value, and octane rating with less ignition problems (Visioli et al., 2014). Most importantly, biobutanol can be used in place of gasoline without vehicle modifications – that means it can be integrated

seamlessly into the existing petroleum infrastructure. Butanol-gasoline blends of up to 85% butanol can be used in unmodified petrol engines (Nigam, 2011).

Biobutanol is often produced through acetone-butanol-ethanol (ABE) fermentation. However, as butanol is toxic to microorganisms above 2 v/v% in the fermentation broth (Moreira et al., 1981), it is difficult to obtain its high concentration. Thus, it is imperative to purify butanol from diluted aqueous media. Unless concentrated to over 99 v/v%, biofuels can neither be mixed with gasoline nor be used as a stand-alone fuel. Conventionally, for purification of butanol from ABE process, distillation is carried out which produces azeotropic vapor of about 55 v/v% butanol and 45 v/v% water followed by decantation. However, it is a costly and energy intensive process due to the need of multiple distillation and decantation steps (Gupta Kumar et al., 2013).

Commonly employed alternative techniques for biobutanol recovery and purification are adsorption, gas stripping, and membrane pervaporation (Quereshi and Blaschek, 2001). Various researchers have selectively adsorbed butanol from the fermentation broth using butanol adsorbing selective sorbents such as activated carbon (Xue et al., 2016), macroporous resins such as poly (styrene-codivinyl benzene) and cross-linked polystyrene framework named KA-I (Wiehn et al., 2014; Liu et al., 2014;), and microporous mordenite framework inverted (MFI) type zeolite (Faisal et al., 2014). Some have used integrated butanol production and recovery by gas stripping (Qureshi et al., 2014) or two stage energy efficient gas stripping (Xue et al., 2013).

Membrane based process pervaporation is also being widely employed for the integrated butanol purification. Polydimethylsiloxane composite membranes, either in combination with ceramic or polyvinylidene fluoride coating, have been used to efficiently separate butanol from fermentation broth ((Xue et al., 2014; Dong et al., 2014). Integrated or two stage processes such as combination of gas or vapor stripping–pervaporation or two stage pervaporation processes have also been employed for butanol recovery (Cai et al., 2017; Vane et al., 2013).

Distillation, followed by adsorption could be a cost-effective method in terms of energy requirement. A specific adsorption technique known as pressure swing adsorption (PSA) has been put to practice by most of the bioethanol industries to dry ethanol due to its low energy requirement to achieve anhydrous ethanol (Simo, 2008; Tajallipour et al., 2013). Most commonly, zeolites are used as adsorbents in the PSA process owing to their high adsorption capacity. However, the regeneration of water saturated zeolite bed is energy intensive and their disposal can be a threat to

environment. These shortcomings could be overcome with a more effective approach of using biomaterials as adsorbents as they are biodegradable, reusable Tajallipour et al., 2013; Sun et al., 2013), and safe (Boonfung et al., 2010), require relatively low temperature for regeneration, and do not pose a threat to be disposed of into the environment. However, there has been scarce literature for drying of butanol in a PSA process.

Agriculture byproduct like canola meal can be a potential biosorbent, as canola is abundantly cultivated in Canada (Canadian Canola 2017; Newkirk, 2009). This byproduct has not been thoroughly investigated as an adsorbent for drying of butanol, although canola meal has been reported to have a relatively high water adsorption capacity of about 303-390% of its initial dry weight (Aider and Barbana, 2011). Research has demonstrated that canola meal, before (Baylak et al., 2012) and after protein extraction (Ranjbar et al., 2013), is capable of drying ethanol, thus, showing its potential for drying other alcohols. There is a great incentive in examining the potential of CM biomaterial for drying of butanol.

In this work, a pressure swing adsorption process using canola meal based biosorbent was investigated to selectively remove water from lower grade butanol-water vapors including the simulated azeotropic butanol concentration (55 v/v %) from preliminary distillation in biobutanol production industry, to optimize the crucial parameters affecting the performance of drying butanol, and to explore the water selective adsorption mechanism. An important aspect of this study was the approach of butanol drying by selective water adsorption from the butanol-water vapor mixture on a biosorbent packed PSA column which produced fuel grade (>99 v/v%) butanol. The process was aimed to be an alternative to the use of multiple decantation and distillation units in the biobutanol production industry. In addition, the site energy distribution of water adsorption was analyzed based on the Dubinin-Polanyi isotherm model which helped to understand the adsorbate-adsorbent interactions and the water adsorption process.

3.3. MATERIALS AND METHODS

3.3.1 Biosorbent preparation. Canola meal (CM) after protein extraction was obtained from Bunge Global Innovation, White Plains, NY, USA. The material was oven dried at 105°C for 24 h followed by sieved using Canadian Standard Sieves Series (Combustion Engineering Canada Inc.) to collect particles in the size range of 0.43-1.18 mm. This size range of CM were used in

the present work based on the available surface area and ease of operation. In addition, CM pellets were made with the particles in the size range of 0.43-1.18 mm using a California Pellet Mill (CPM-Laboratory Model CL-5, California Pellet Mill Co., Crawfordsville, IN, USA). The pellet diameter was about 4.7 mm and length of 7-10 mm.

3.3.2 Feed solution preparation. Butanol solutions of different concentrations were prepared by mixing butanol (Fisher Scientific, ACS reagent grade; >99.4 v/v %) with deionized water.

3.3.3 Physico-chemical characterization of biosorbents. The composition of CM was determined by Intertek Labs, Saskatoon, Canada as per AOAC International. The organic elemental content was analyzed using an Elementar Vario III CHNS analyzer. 4-6 mg of sample was weighed and packed along with a tin boat and placed in the designated chambers for analysis. Sulfalinic acid ($C_6H_7NO_3S$) was used as a standard for analysis. Fourier transform infrared (FTIR) spectroscopy (Bruker Vertex 70 FTIR spectrometer, MA, USA) analysis was carried out to identify the significant functional groups in biomass with respect to adsorption. Each spectrum was the average of 16 co-addition of scans with a total scan time of 15 s in the IR range of 400–4000 cm^{-1} at 4 cm^{-1} resolution. The devolatilization characteristics of the biomass with temperature were investigated by thermogravimetric analysis (TGA) (Perkin Elmer Pyris Diamond TG/DTA) in the range of 22°C to 400°C at the heating rate of 5°C/min. Particle size of CM was measured using the Mastersizer MS-64 sample dispersion analyzer by means of dry method. A 1000F lens was utilized and the particle size analysis was performed using 10,000 sweeps, and the obtained particle obscuration was comprehended between 10% and 30%.

3.3.4 Design of experiments by orthogonal array design (OAD). In order to evaluate the effects of operating parameters on butanol drying, the orthogonal array design (OAD) was used (Medina et al., 2009). Five operating parameters including temperature (A), pressure (B), butanol feed concentration (C), feed flow rate (D), and size of adsorbent particles (E) were chosen for the present study as shown in Table 3.1.

Table 3.1. Factors and levels in orthogonal array design experiments

	Factors				
	A	**B**	**C**	**D**	**E**
Levels	Temperature (°C)	Pressure (kPa)	Bu-OH Feed Concentration (v/v %)	Feed flow rate (mL /min)	Particle sizes (mm)
L 1	95	135	55	1.5	0.425-1.18
L 2	111	201	95	3.0	4.7

The butanol feed concentrations of 55 and 95 v/v% were chosen to mimic the azeotropic distillate butanol concentration and the high end of concentration, and the corresponding boiling points (95 and 111°C) were chosen to study the effect of operation temperature. A pressure range of 135-201 kPa was chosen to avoid high pressure operation demanding high energy consumption.

The effect of these parameters on performance indices, including water uptake, butanol uptake, water selectivity, butanol recovery, and maximum effluent butanol concentration were determined using a statistical treatment called the "range analysis" (Sharma et al., 2005). This analysis provided relevant information to optimize the butanol dehydration performance by choosing appropriate operation conditions. The details of range analysis are given in the supplementary information. All the experiments were replicated and the average results with standard deviation were reported.

3.3.5 Adsorption/regeneration experiments.

It is noted that the aim of this work was to develop an alternative technology of adsorption to remove water directly from the azeotrope of 55 v/v% butanol vapor generated from the preliminary distillation in biobutanol industry in a hope to reduce or replace the downstream multiple decantation and distillation. For the interest of both industrial application and scientific research, adsorption was investigated at a wider concentration range of 55-95 wt% butanol at 95-

110^{o}C in this work to simulate the butanol vapor product in biobutanol industry. Even though in the lab scale experiments in this work, heat was provided to generate such butanol-water vapor, no heat was needed in real industrial adsorption process because the butanol vapor is generated from the preliminary distillation and can be directly fed to the adsorption column.

The PSA system used in this study has been used previously for ethanol drying and the schematic drawing is presented in Fig. 3.1.

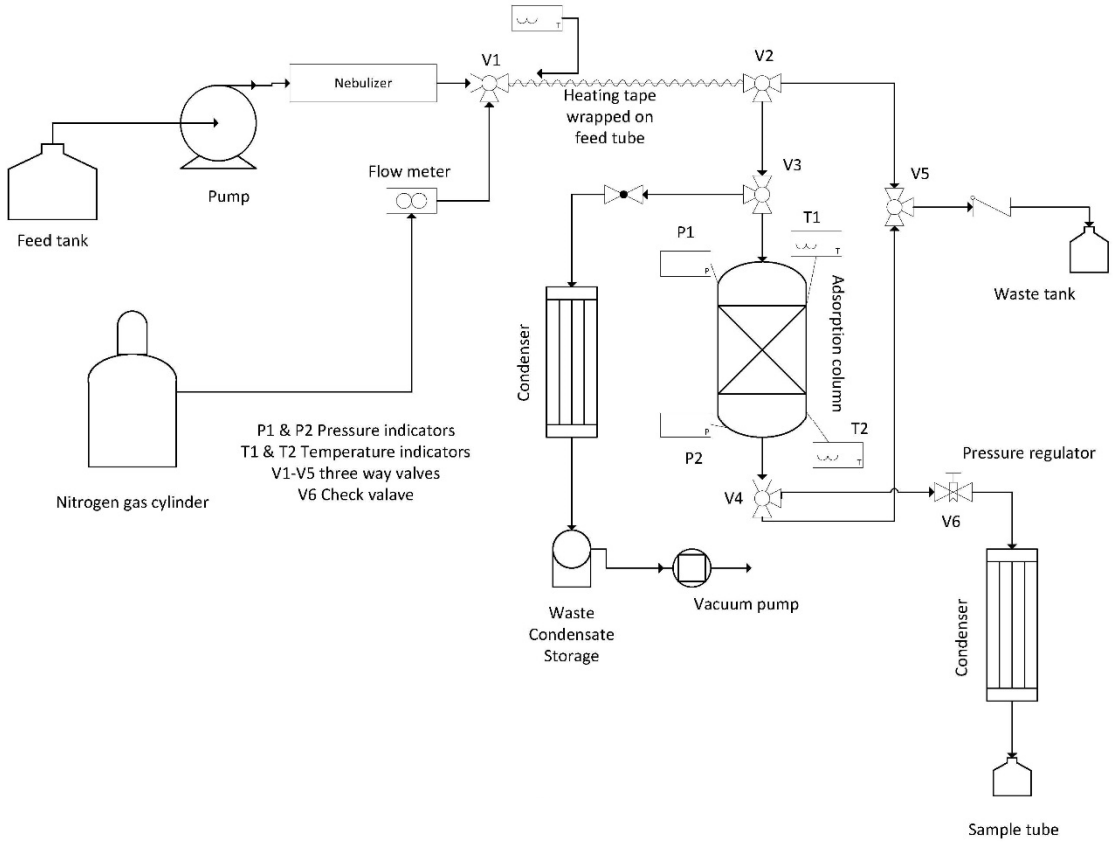

Figure 3.1. Schematic diagram of the experimental PSA setup

The PSA system has been described in detail in previous reports (Tajallipour et al., 2013; Ranjbar et al., 2013). In order to simulate the butanol-water vapor generated by preliminary distillation in biobutanol production industry, the butanol-water solution stored in a jacketed sealed feed tank with stirring was pre-heated to 90°C. Then it was pumped through a digital piston pump (Cole-Parmer, RK-74930-05) through a nebulizer to stainless steel tubing equipped with heating tapes (Cole-Parmer; 50-60Hz, 120 V, 624W, 5.20A). It was then mixed with preheated nitrogen (carrier gas) at a flow rate of 850 mL/min to completely vaporize the feed butanol solution before it is

reached to the adsorption column. The 316-stainless steel adsorption column with dimensions (length 500 mm, internal diameter 47.5 mm, wall thickness 1.65 mm) contained randomly packed canola meal adsorbents. The vapor feed entered the column from the top through a three-way valve. The temperature and pressure of the bed were measured both at the top and the bottom of the column. The pressure drop along the column during the adsorption process was 2.1-3.2 kPa, which is negligible compared with the operation pressure range of 135-201 kPa. Water got selectively adsorbed onto the adsorbent bed and the dried butanol vapor effluent exited from the bottom of the column. The effluent sample was then condensed and collected for water content analysis by a Karl-Fischer (KF) titrator. The sample was collected at an interval of 5 min and the adsorption process lasted for a total duration of about 2.5 h till equilibrium (bed saturation) was achieved. After adsorption, desorption process was carried out by purging heated nitrogen gas at 110°C (850 mL/min) from the bottom of the column with a vacuum 33 kPa for 5.5 h. Desorbed water was condensed and collected. Desorption process conditions were confirmed adequate not only to dry the wet column, but also to preserve the chemical properties and stability of the adsorbent.

Water or butanol uptake was determined by the mass balance, i.e. the water/butanol input subtracted from the water/butanol output per g of dry adsorbent in the column. Recovery of butanol was defined as the ratio of the amount of butanol in effluent to the amount of butanol in influent. Water separation factor over butanol (α) was calculated according to Eq. 3.1:

$$\alpha = (X_w/X_b) \,/\, (Y_w/Y_b\ ) \qquad (3.1)$$

where X_w is mole fraction of water in the adsorbed phase, X_b is the mole fraction of butanol in the adsorbed phase, Y_w is the mole fraction of water in the vapor phase and Y_b is the mole fraction of butanol in the vapor phase.

In the adsorption process, the feed butanol concentration varied from 55 to 95 v/v%, and the rest is water. The lower end of the feed butanol concentration was chosen in order to simulate the butanol concentration in the butanol-water azeotrope obtained from the initial distillation process in industry. The feed of butanol-water liquid solution was 1.5-3 mL/min in order to provide sufficient amount of water and butanol to the adsorption column. The pressure of 135-201 kPa and temperature of 95-111ºC were chosen to investigate their effects, while ensuring adsorption of butanol and water to be operated in vapor-solid phases without burning the adsorbents. The amount

of CM packed in the adsorption column depended on the particle size of CM. In the case of CM particles (0.425-1.18 mm), the full packing required about 215 g CM, while in the case of CM cylindrical pellets (4.7 mm in diameter and 5 mm in length) about 515 g were packed. Each experiment was run at least in duplicate. The results were presented in average and standard deviation.

3.3.6 Analytical methods. The water content in the feed and effluent was determined by an automated KF coulometric titrator (Mettler Toledo DL 32) using methanol as diluent. Butanol mass in the effluent samples was calculated by subtracting the mass of water from the total mass of sample, these results were cross-validated with that measured by a gas chromatograph (GC) (Agilent Technologies 7890A GC System; 7683B Series Injector) with a flame ionization detector. The coefficient of variation (CV) for water content determination by the KF titrator was 0.05%, while for GC analysis, CV was 1.5%, based on the analysis of a standard of 1% water or butanol in 4 trials. Butanol analysis by GC was carried out at the following conditions - flow rate 2.6 mL/min, average velocity 40 cm/s, hold up time 1.25 min, inlet temperature 150°C, oven temperature 40°C and detector temperature 250°C. 25 µL sample was injected into the column with a split ratio of 100:1.

3.3.7 Dubinin-Polanyi isotherm and site energy distribution

The Dubinin-Polanyi model used in this work is based on the adsorption potential theory, which has been recognized as a useful model both gas and aqueous phase adsorption on energetically heterogeneous surfaces such as biomaterials. As per this model, for any molecule, the magnitude of adsorption potential varies within the adsorption space depending on its proximity to atoms on the adsorbent surface (Polanyi, 1920). Polanyi theory assumes that the adsorption potential, ε is independent of temperature and the adsorbed gas phase molecules have similar properties as the corresponding bulk gas phase (Chang et al., 2006). Meanwhile, the adsorption potential ε is given by

$$\varepsilon = RT \ln\left(\frac{P^s}{P_i}\right) \quad (2)$$

The Dubinin–Polanyi equation for microporous and large pore materials is described in Eqs. 3.3 and 3.4, respectively, as shown below.

$$\ln q = \ln q_0 - \frac{K_1}{\beta}\left[RT \ln\left(\frac{P^s}{P_i}\right)\right]^2 \quad (3.3)$$

$$\ln q = \ln q_0 - \frac{K_2}{\beta}\left[RT \ln\left(\frac{P^s}{P_i}\right)\right] \quad (3.4)$$

where q is the mass adsorbed per unit mass of adsorbent (mol/g adsorbent), q_0 denotes the limiting mass for adsorption (mol/g adsorbent), K_1 and K_2 are pore constants for micropore and large pore materials, β is an affinity coefficient, P_i represents partial pressure of the adsorbate (kPa), and P^s is saturated vapor pressure of the adsorbate (kPa). These relationships can be helpful to estimate the adsorption capacity and affinity, and to evaluate the potential application of CM as a sorbent.

Site energy distribution can be determined from the isotherm representing the experimental equilibrium data (Kumar et al., 2011). The interaction forces between solutes and sorbents could be indicated by the mean of the site energy distribution, while the surface energy heterogeneity of sorbent could be interpreted by the width of the site energy distribution (Shen et al., 2015). Most biosorbents are composed of multiple components and thus are heterogeneous in their structure. The basic integral equation defining adsorption distribution is:

$$qe(P) = \int_0^\infty q(h)\ (E,p) f(E) dE \quad (3.5)$$

As per Eq. (3.5), the total adsorption, qe, by a heterogeneous surface is the integral of energetically homogeneous isotherm ($q(h)$) multiplied by a site energy frequency distribution, $f(E)$. E is the difference between the solute and solvent adsorption energies for a given site. The maximum (E_{max}) and minimum (E_{min}) limits of energy space are generally ∞ and 0 which are directly related to the partial pressure of adsorbate in the isotherm for a gas phase adsorption. Eq. (3.5) is difficult to solve and has no analytical solution, however, approximate solutions have been developed. The most employed method in literature is the condensation approximation method, originally proposed by Cerofolini (1974). It estimates site energy distribution function from the isotherm equation. The partial pressure of adsorbate can be correlated with the energy of adsorption as:

$$P_i = P^s . \exp\left(-\frac{E-E^s}{RT}\right) \quad (3.6)$$

Defining E*=E-E^s gives

$$P_i = P^s . \exp\left(-\frac{E^*}{RT}\right) \quad (3.7)$$

where P_i and P^s are the partial and saturation pressure of adsorbate at a fixed temperature. The E^s reference state for E represents the lowest physically realizable sorption energy (kJ/mol). Incorporation of Eq. (3.7) into Eq. (3.5) will lead to an approximate site energy distribution, $f(E^*)$(g.mol/g.J), which is the differentiation of the isotherm, $q_e(E^*)$, with respect to E^*:

$$f(E^*) = \frac{dq_e(E^*)}{d(E^*)} \quad (3.8)$$

As such, the area under the distribution curve is equal to the maximum adsorption capacity, q_m, and is given by:

$$\int_0^\infty f(E^*)d(E^*) = q_m \quad (3.9)$$

Eq. (3.8) can be used to estimate $f(E^*)$ by differentiating the corresponding isotherm expression with respect to E^*. The value of $f(E^*)$ was determined by plugging Eq. (3.7) into Eq. (3.4) and then incorporating into Eq. (3.8):

$$f(E^*) = \left(qo.\frac{K_2}{\beta}.E^*\right).\exp\left(-\frac{K_2}{\beta}.E^*\right) \quad (3.10)$$

The average site energy μ(E*) (kJ/mol) and the surface energy heterogeneity in the tested range of temperature and partial pressure were also estimated. μ(E*) can be calculated by integrating the value of $f(E^*)$ in the minimum and maximum range (0 and ∞, respectively) (Yan and Bei, 2017):

$$\mu(E^*) = \int_0^\infty E^* f(E^*)dE^* / \int_0^\infty f(E^*)dE^* \quad (3.11)$$

Incorporating Eq. (3.10) into the above equation, and integrating, the average site energy for the present case can be determined,

$$\mu(E^*) = 2/(\frac{k2}{\beta}) \quad (3.12)$$

With site energy distribution model, sorption site heterogeneity can also be determined by calculating the standard deviation (σ^*_e) (kJ/mol) which can be determined by first calculating $\mu(E^{*2})$ which is given by:

$$\mu(E^{*2}) = \int_0^\infty E^* f(E^{*2}) dE^* / \int_0^\infty f(E^*) dE^* \quad (3.13)$$

$$\mu(E^{*2}) = 6/(k2/\beta)^2 \quad (3.14)$$

Once $\mu(E^*)$ and $\mu(E^{*2})$ are determined, the standard deviation can be simply calculated as (Yan and Bei, 2017):

$$\sigma_e^* = \sqrt{\mu(E^{*2}) - \mu(E^*)^2} \quad (3.15)$$

The units of the site energy distribution function depend on the units of the isotherm parameters.

3.4. RESULTS AND DISCUSSION

3.4.1 Physico-chemical characterization of CM biosorbents. The major composition of CM is presented in Table 3.2. CM contains over 26% cellulose and lignin, and 6.3% hemicellulose. The high content of cellulosic components is desirable in biomass as these groups are responsible for water adsorption (Ranjbar et al., 2013). Even after protein extraction, the residual protein of CM was 27.1%. The efficiency of protein extraction from CM in the industry is outside the scope of this work. Other components, such as crude fibre, aromatics, fats, and inorganics, which make up the rest of the composition of CM, were not analyzed.

Table 3.2. Composition of canola meal

Content in CM	**Composition (wt. %)**
Protein	27.1±0.53*
Starch	< 1.5
Acid detergent fibre (Cellulose +Lignin)	26.4±0.42
Hemicellulose (%)	6.3±0.56
Ash	3.6±0.17
Moisture	4.2±0.9

*All results were presented in average ± standard deviation.

The affinity of water for biomaterials is predominantly due to the presence of polar functional groups such as hydroxyl and carboxyl. For instance, it was reported that hydroxyl groups in cellulose/hemicellulose (Okewale et al., 2013) and starch (Beery and Ladisch, 2001) are responsible for water adsorption by forming hydrogen bond between the hydroxyl groups and water molecules (Boonfung and Rattanaphanee, 2010).

The major elements composition of fresh and used CM is presented in Table 3.3. CM primarily consists of carbon which is due to the presence of protein, cellulose, hemicellulose, and lignin. It also had higher nitrogen content due to the residual protein. Oxygen is one of the major elements in cellulosic components in CM. However, because the CHNS analyzer does not provide with the oxygen data, the respective values were not available.

Table 3.3. Organic elemental composition of fresh and used canola meal (in wt. %)

Element	**Fresh (unused) CM**	**CM after adsorption and regeneration (after 16th reuse)***
C	46.34±0.04	46.85±0.13
H	6.15±0.03	6.60±0.04
N	3.78±0.08	3.85±0.07
S	0.35±0.06	0.33±0.01

*All results were presented in average ± standard deviation.

In order to determine the presence of various functional groups present in CM, the FTIR spectrum was obtained as shown in Fig. 3.2. The spectrum showed an intense peak at 1050 cm^{-1} indicating the presence of C-O and CHO groups in polysaccharides (Himmelsbach et al., 2002) such as cellulose, and hemicellulose. The C–N stretching vibration of aliphatic amines is observed

as medium or weak bands in the region of 1250-1020 cm^{-1} which is indicative of presence of amino acid groups in residual protein (Theivandran et al., 2015). It is known that appreciable amounts of O-acetylated glucomannans and xylans are part of hemicellulose. Thus, the presence of acetyl functional groups observed by C=O band at 1730 cm^{-1} along with CH_3 and CH_2 asymmetric and symmetric stretching vibrations at 2950 cm^{-1} provide information about presence of hemicellulose (Himmelsbach et al., 2002). A prominent peak at 1700 cm^{-1} is due to C=O stretching attributed to lignin in biomass. The asymmetric stretching vibration observed at 1650 cm^{-1} is most likely due to the strongest band for the carboxyl groups COO^- (Himmelsbach et al., 2002; Xu et al., 2013). The spectrum also confirms the presence of hydroxyl functional groups (3350 cm^{-1}) in cellulose and hemi-cellulose. The FTIR results demonstrated that CM has carboxyl, amino and hydroxyl groups, which are polar and have the potential for water adsorption.

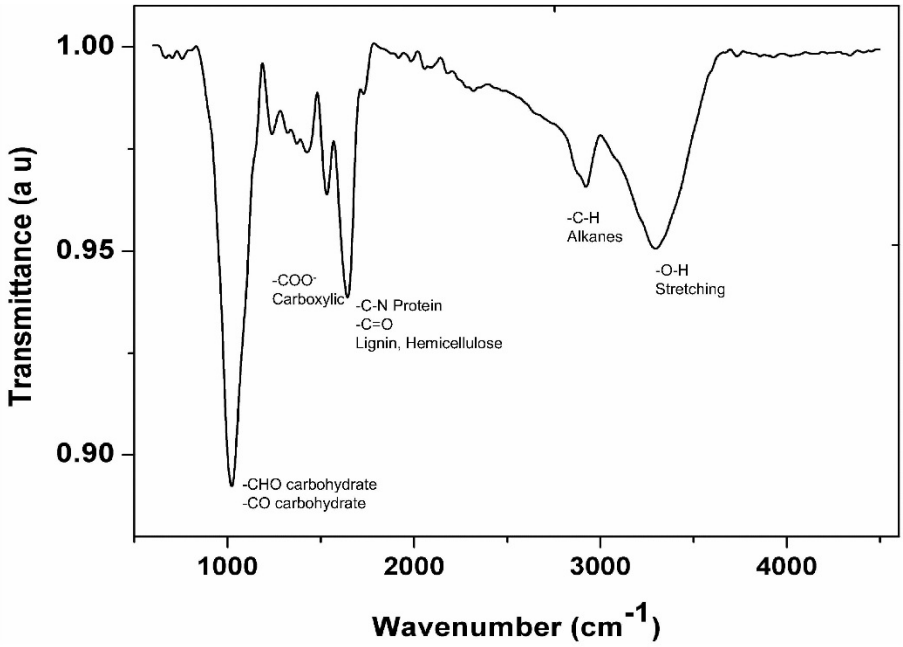

Figure 3.2. FTIR spectrum of canola meal

The devolatilization characteristics of CM obtained from TG/DTA analysis is depicted in Fig. 3.3. As it can be seen, the weight loss began gradually up until 200°C, then significant weight loss occurred in the range of 200°C-320°C. The devolatilization behavior of biomass is associated

with the presence of cellulose, hemicelluloses and lignin (Raveendran et al., 1996). Biagini et al. (2006) investigated the devolatilization of hemicelluloses, cellulose and lignin and reported the onset temperature of these chemical constituents for decomposition to be 253°C, 319°C and 253°C, respectively. The weight loss at temperatures <100°C can be attributed to the loss of easily volatiles, while the weight loss occurring between 100 and 130°C is due to loss of water. The results showed that CM is stable and suitable for butanol dehydration at a bed temperature no higher than 130°C which was used in the dehydration and regeneration process in this work.

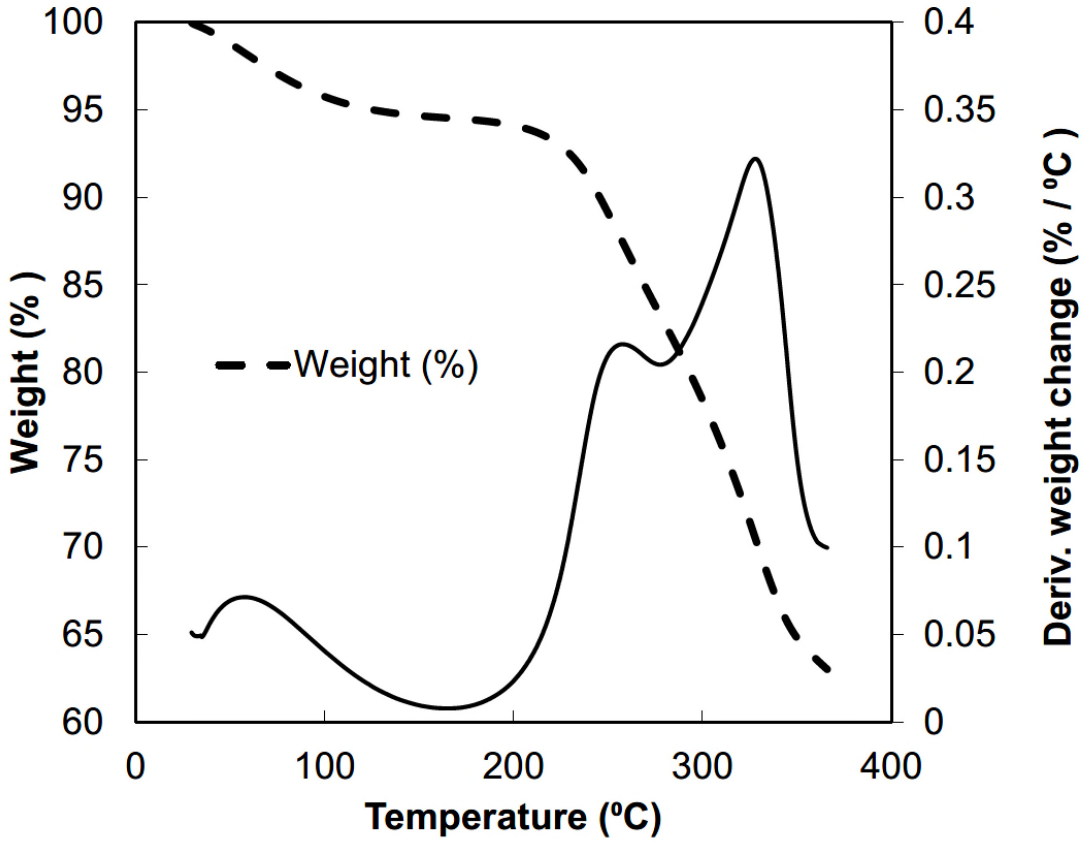

Figure 3.3. TG/DTA analysis of canola meal

The particle size distribution of CM initially sieved in the range of 0.43-1.18 mm was analyzed by the particle size analyzer. About 62 vol.% of particle sizes were within the range of

0.47-1.19 mm, 28% were smaller than 0.47 mm and only 9% bigger than 1.19 mm. The median of the size was 0.6 mm. These particles were used in the present work.

3.4.2 Dehydration of butanol using canola meal. Initial experiments were carried out to examine the capability of CM for butanol dehydration at the following conditions: temperature of 100°C; total pressure of 135 kPa; feed butanol concentration of 79 v/v%, feed butanol-water liquid flow rate of 3 mL/min; and adsorbent particles size of 0.43-1.18 mm. The butanol and water breakthrough curves are presented in Fig. 3.4 (a) and (b).

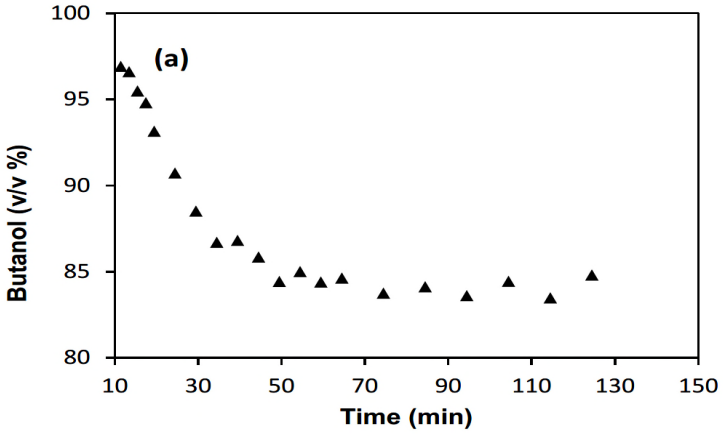

Figure 4(a)

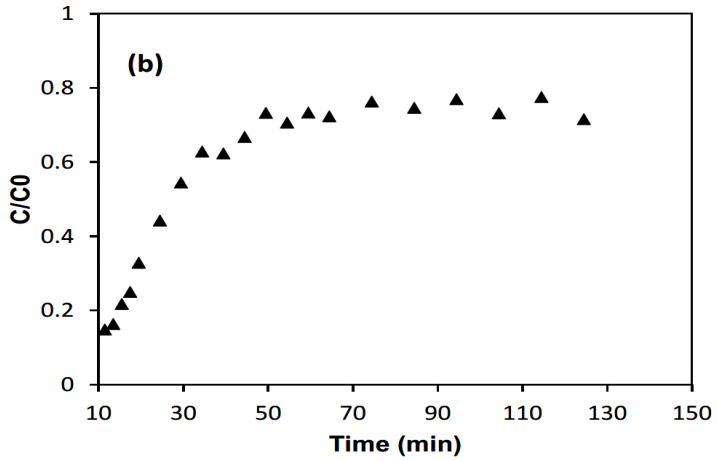

Figure 3.4. Butanol (a) and water (b) breakthrough curves for canola meal(a) Butanol and (b) water breakthrough curves for canola meal. All runs were at a temperature of 100°C, pressure of 135 kPa, butanol feed concentration of 79 v/v %, feed flow rate of 3 mL/min and particle size of canola meal in the sieved range of 0.43−1.18 mm.

The results demonstrated that CM successfully dried a lower grade butanol 79 v/v% and achieved over 97 v/v% butanol with a water uptake of 0.21 g/g-ads. This proves the hypothesis that CM was able to concentrate butanol by selective removal of water, demonstrating a potential for application in butanol drying.

3.4.3 Effect of operating parameters on butanol drying. In order to further investigate the effects of operating parameters on butanol dehydration, the orthogonal array design (OAD) method was used to design the experiments. Table 3.4 summarized the experimental conditions and their corresponding results. The experimental data were further treated by the range analysis (Sharma et al., 2005) to determine the most significant parameters for the butanol dehydration performance.

It was noted that the standard deviation of butanol recovery in experiment 8 in Table 3.4 (67.48±10.26) was larger than that of the rest experiments. This may be because the experiment was run under a higher pressure (201 kPa) and lower butanol feed concentration (55.50 v/v%, i.e. higher water concentration). Under such conditions, it was relatively more difficult to control the pressure as more water vapor was adsorbed. This may bring in operation errors leading to the larger standard deviation value of butanol recovery.

Based on the range analysis, butanol feed concentration had the most significant effect on water uptake, followed by temperature. Pressure was found to be the most influencing parameter in terms of butanol uptake, equilibrium water selectivity, butanol recovery, and maximum effluent butanol concentration. Furthermore, in addition to pressure, feed flow rate, had an equal influence on maximum effluent butanol concentration. Particle size of the adsorbents in the tested range showed effect on water uptake but did not significantly affect butanol uptake, water selectivity, recovery, and butanol concentration in the effluent. Based on the range analysis of OAD in this work, a set of optimum conditions for butanol dehydration were proposed in order to achieve higher water uptake, lower butanol uptake, higher water selectivity, higher butanol recovery and higher butanol concentration in the effluent. The specific conditions are as follows: temperature of 111°C, pressure of 135 kPa, butanol concentration of 55 v/v%, feed flow rate of 3 mL/min, and particle size of 0.425-1.18 mm.

Since the above proposed favorable conditions were not included in the original OAD design (Table 3.1), in order to confirm their validity, the experiments were carried out in duplicate at the proposed optimum operation conditions. The average results are presented in Table 3.5.

Apparently, a higher water separation factor of 5.4, butanol recovery of 90%, and a maximum effluent butanol concentration of 99.2 v/v% (fuel grade) were achieved, which are better than that obtained at any other conditions (Table 3.4) investigated in this work. The result confirmed that the optimum conditions proposed based on the range analysis was reasonable.

Table 3.4. Experimental combinations using OAD and the corresponding results

Exp. No.	Factors					Experimental results				
	A	B	C	D	E					
	Temp (°C)	Pressure (kPa)	Inlet Bu-OH Conc. (v/v %)	Inlet flow rate (mL/min)	Particle size (mm)	Water Uptake*	Butanol uptake*	Equilibrium water separation factor**	Recovery (%)	Max. Effluent Bu-OH conc. (v/v %)
1	95	135	55.99 ± 1.03	1.5	0.425-1.18	0.36±0.02	0.21±0.02	1.77±0.03	58.03±3.17	99.17 ± 0.09
2	95	135	55.39±0.14	3.0	4.7	0.16±0.00	0.06±0.02	3.22±0.92	83.56±5.57	96.65 ± 0.01
3	95	201	95.33±0.02	1.5	0.425-1.18	0.02±0.00	0.80±0.00	0.40±0.11	6.88±0.03	88.82 ± 1.89
4	95	201	94.02±0.76	3.0	4.7	0.05±0.01	0.59±0.00	1.05±0.02	15.40±0.17	99.19 ± 0.11
5	111	135	95.72±0.10	1.5	4.7	0.01±0.00	0.11±0.00	1.95±0.10	71.16±0.82	99.13 ± 0.03
6	111	135	94.96±0.06	3.0	0.425-1.18	0.03±0.00	0.25±0.01	2.05±0.03	85.63±0.91	99.17 ± 0.55
7	111	201	56.50±0.33	1.5	4.7	0.14±0.00	0.10±0.00	1.42±0.04	49.79±1.18	93.67 ± 2.44
8	111	201	55.50±0.91	3.0	0.425-1.18	0.64±0.01	0.32±0.11	2.13±0.67	67.48±10.26	98.86 ± 0.41

* g adsorbed/ g dry net weight of adsorbent at equilibrium conditions.

**All results were presented in average ± standard deviation.

Table 3.5. Validation test results for the most favorable process conditions for drying of butanol

[Experimental conditions: Temperature 111°C, pressure 135 kPa, butanol concentration 55 v/v%, feed flow rate 3 mL/min, and particle size 0.425-1.18 mm]

Water uptake (g/g-ads)*	**Butanol uptake (g/g-ads)**	**Water separation factor**	**Recovery (%)**	**Max. Butanol concentration achieved (v/v %)**
0.48±0.02	0.09±0.00	5.43±0.08	90.11±0.26	99.20 ±0.79

*All results were presented in average ± standard deviation.

3.4.4 Water Adsorption Equilibrium. In this work, water adsorption equilibrium was achieved when the adsorption column reached saturation. The water adsorption isotherms were obtained at temperatures of 95, 100 and 111℃ and the water feed concentrations in the range of 5-45 v/v% corresponding to 95 – 55 v/v% butanol. The pressure of the system was maintained at 135 kPa, and the feed liquid flow rate was held at 3 mL/min. The adsorbent particle size chosen for this study was 0.425-1.18 mm.

Modelling approach based on the Dubinin-Polanyi model has been employed for water adsorption equilibrium on carbon nanomaterials (Wu et al., 2012), modified rice husk (Ou et al., 2015), corn meal (Chang et al., 2006) and canola meal (Ranjbar et al., 2013). This model has been found to give the most reasonable representation of the equilibrium isotherm data in this study.

Temperature-invariant characteristic curve was observed for the polycyclic aromatic hydrocarbons (PAH) adsorption by carbon nano-particles (CNPs), which indicates that the Polanyi theory also captures the gas adsorption process mechanistically (Wu et al., 2012). The above Eqs. 3.3 and 3.4 were used to fit the equilibrium water adsorption data. The resultant graphs are presented as Fig. 3.5 (a) and (b), respectively.

Table 3.6 summarizes the Dubinin-Polanyi model parameters for the micropore and large pore materials. As it can be seen, Eq. 3.4 representative of large pore materials, gave a better fit

compared to Eq. 3.3. Similar modeling results were obtained for ethanol dehydration by canola meal (Polanyi, 1920). However, elucidation of actual adsorption mechanisms requires further investigation.

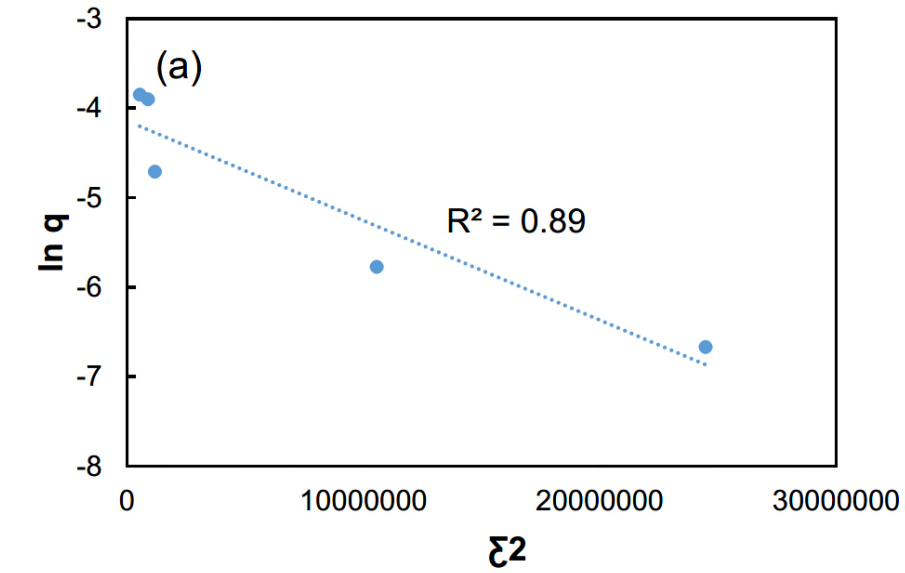

ig. 5a

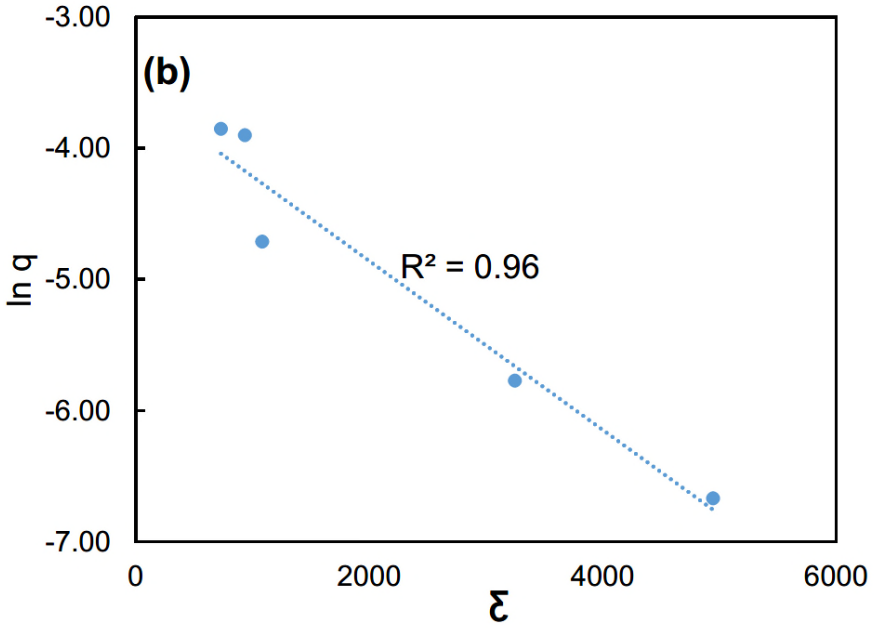

Figure 3.5 Dubinin−Polanyi model for (a) micropores and (b) large pores: (●) experimental data; (−) model

Table 3.6. Modeling results of Dubinin-Polanyi equations

Model Type	**K/β**	**Mean free energy of adsorption (kJ/mol)**	**q_0 (mol/g-ads)**	**r^2**	**ARE % ***
Micropore in this work	1E-07	2.24	0.016	0.89	11
Large pore in this work	6E-04	0.04	0.028	0.96	7
Canola meal for drying ethanol (Ranjbar et al., 2013)	4E-04	0.04	0.038	0.97	5
Corn meal for drying ethanol (Chang et al., 2006)	3E-04	0.04	0.009	0.96	-

*ARE - Average Relative Error

According to Eq. 3.5, the values of the limiting mass for adsorption (q_0) and the coefficient $\frac{K_2}{\beta}$ were estimated from the intercept and slope to be 0.028 mol/g-ads and 6×10^{-4}, respectively. Chang et al. (2006) reported these values to be 16.33% and 3.28×10^{-4} and Ranjbar et al. (2013) reported these to be 69.59% and 4×10^{-4}, in an ethanol-water binary vapor system using corn meal and canola meal as adsorbents, respectively. The mean free energy of adsorption was thus evaluated based on the large pores D-P modeling results using the following equation:

$$\bar{E} = \frac{1}{\sqrt{2\frac{K_2}{\beta}}} \tag{3.16}$$

The value of the mean free energy is an indication of the nature of the adsorption process. For those values of $\bar{E}$ above 8 kJ/mol, the adsorption process is considered to be predominantly chemisorption while the process is predominantly physisorption for the values of $\bar{E}$ lower than 8 kJ/mol (Ruthven, 1984). The mean free energy obtained in this work for the large pore model was 0.04 kJ/mol, indicating the water adsorption is physisorption. It is consistent with water adsorption

studies on corn meal (Chang et al., 2006) and canola meal (Ranjbar et al., 2013) as shown in Table 3.6.

3.4.5 Site energy distribution. In the section, the isotherm modeling results demonstrated that the D-P model for the larger pores fit the experimental data better, indicated by R^2 of 0.96. For this reason, site energy distribution analysis was carried out by using the D-P model for larger pores only. The site energy, E^* as a function of the equilibrium water uptake at different temperature, is shown in Fig. 3.6. E^* decreased as the water uptake increased, revealing that water molecules first occupied the high-energy sorption sites on CM at low water uptake, then spread to low-energy sorption sites.

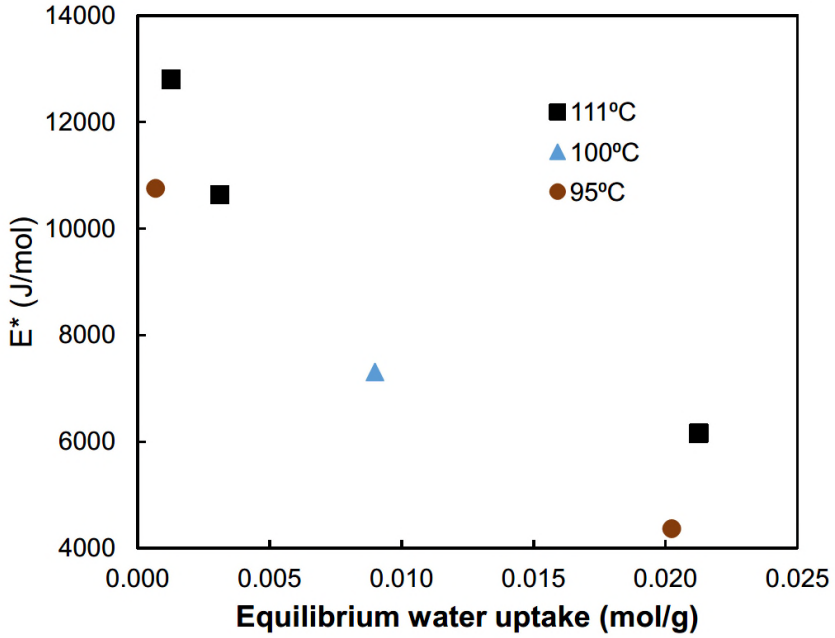

Figure 3.6. Dependence of site energy on equilibrium water uptake at different temperature

The site energy distribution for water adsorption is presented in Fig. 3.7. It is to be pointed out that the shape and intensity of site energy distribution curve calculated using the condensation approximation method will vary depending on the isotherm model applied (Kumar et al., 2010). In the present case, site energy distribution curve was constructed using the D-P isotherm model for larger pores. It is important to note that no similar site energy distribution analysis for the

adsorption of water molecules on biomaterials was found in literature. Thus, the discussion of the results has been developed with reference to the available site energy distribution studies.

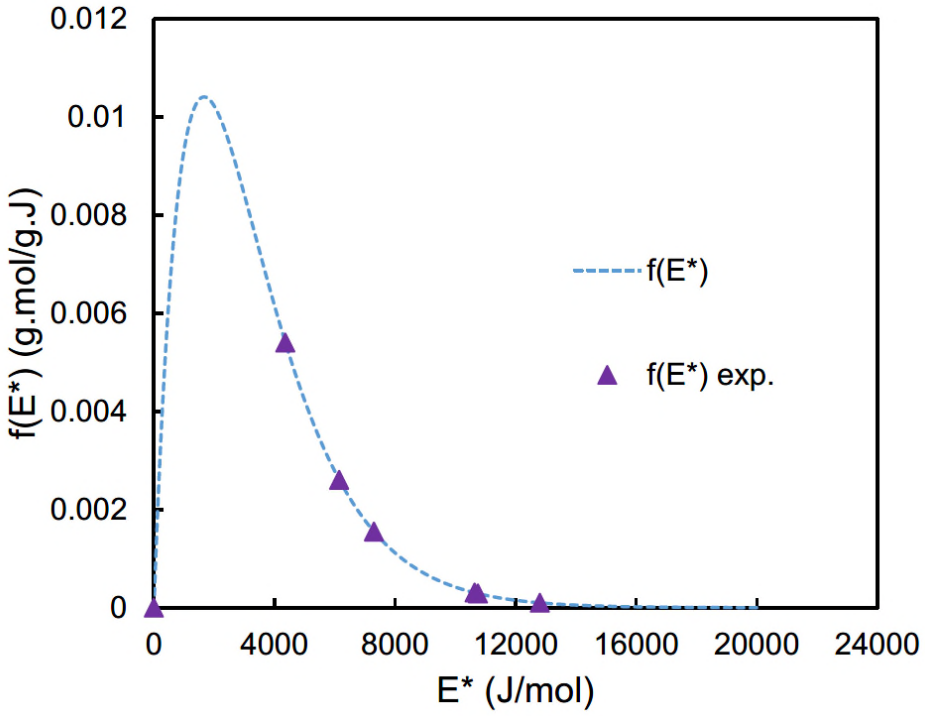

Figure 3.7 Site energy distribution of water adsorption on CM

Site energy distribution curve was found to be the typical bell shaped unimodal curve obtained in other similar studies (Kumar et al., 2011; Yan and Bei, 2017; Kumar et al., 2010). Site energy curve had two characteristic regions: (1) a sharp peak area corresponding to high energy binding sites and, (2) a decaying region relating to higher energy sites. As the site energy (E^*) increased, the frequency function $f(E^*)$ increased up to a point, and then asymptotically decreased to zero at about 14,000 J/mol. This implied that CM had negligible sites with high energy (e.g., >15,000 J/mol) in the tested range of parameters. Similar observations were obtained for site energy distribution of gases and other organic compounds (Kumar et al., 2011; Shen et al., 2015; Kumar et al., 2010). Theoretically, the area under the curves in Fig. 3.8 reveals the number of the available sorption sites in a specific energy range as depicted in Eq. 3.9 which is equal to the theoretical maximum adsorption capacity q_m.

In order to deduce the adsorbent-adsorbate interaction, average site energy $\mu(E^*)$ was calculated as described in Eq. 3.12. The average site energy $\mu(E^*)$ can be used as a measure of the affinity of the adsorbate for the adsorbent surface. The higher the value of the average site energy, the higher the sorption affinity. In the present case, $\mu(E^*)$ was 3.33 kJ/mol, which implies that the water adsorption can be predominant physical adsorption. Yan and Niu (2017) obtained $\mu(E^*)$ in the range of 26.3-28.1 kJ/mol for the adsorption of levofloxacin on pretreated barley straw in which chemisorption was considered to be predominant. In this work, the average site energy was much lower, demonstrating low affinity and binding force between water and the biosorbent surface. This is consistent to the result of mean free energy determined by the D-P isotherm model in this work which indicates physisorption in the system.

The standard deviation (σ_e^*), which is a measure of the adsorbent site energy heterogeneity, was calculated to be 2.36 kJ/mol. The higher the value of σ_e^*, the higher is the heterogeneity. As described earlier, CM is composed of cellulose, hemicellulose, lignin, protein, and starch which consists of carbonyl, hydroxyl and other oxygen containing groups. This may account for the adsorbent site energy heterogeneity. For adsorption of antibiotics on pretreated barley straw, Yan and Niu (2017) obtained value of σ_e^* in the range of 1.4-4.2 kJ/mol which again indicates the heterogeneous nature of biomaterials.

3.4.6 Regeneration and reusability. It is important to regenerate the water saturated column for reuse. For that end, it is essential to ensure that the bed has been sufficiently dried for the next cycle of adsorption. Regeneration of the column was done by purging heated nitrogen gas at 110°C (850 mL/min) from the bottom of the column with a vacuum 33 kPa. The temperature profile for both adsorption and desorption is shown in Fig. 3.8. During the regeneration process, initially, the temperature decreased, indicating that water desorption is an endothermic process. After a while, when the water content in the bed decreased, the temperature started increasing until the initial bed temperature was attained. A similar trend was reported by Simo (2008) for regeneration of type 3A molecular sieves for ethanol dehydration.

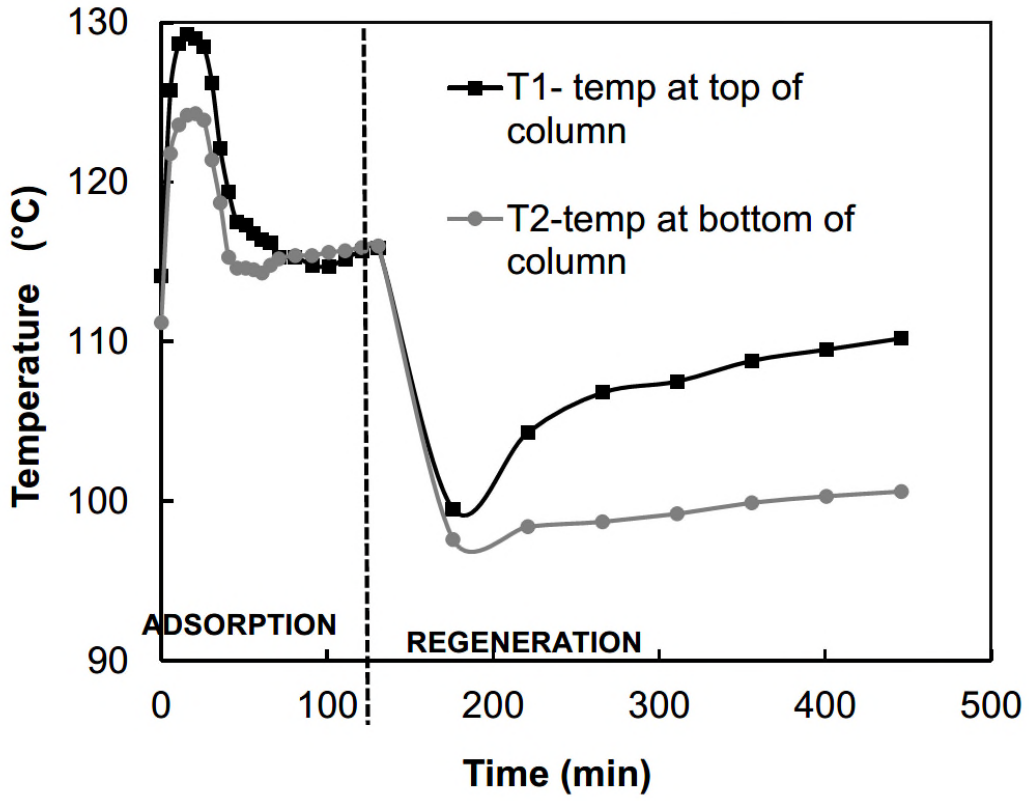

Figure 3.8. Bed temperature profile during adsorption-desorption cycle in PSA

The adsorbent was examined for 16 cycles and are still used without deteriorated quality. Fig. 3.9 shows examples of the butanol production profiles of fresh, and regenerated CM for the 1st, 2nd, 3rd reuse, 15th, and 16th reuse. The breakthrough curves for the first three reuse are overlapped showing that the fresh and the regenerated CM biosorbents have similar performance, and are capable of producing fuel grade butanol of over 99 v/v%. Though the breakthrough curves for the 15th, and 16th reuse were slightly below the other three runs, above 96 v/v% butanol was produced. The slightly decrease of the performance may be because more water was accumulated in the column, and longer regeneration time is required. This can form an area of future research. Table 3 shows that the elements composition of fresh and regenerated CM is very much similar, once again confirming CM is stable after regeneration.

The results demonstrated that CM was easily regenerated at 110°C, a temperature much lower than that required for regenerating molecular sieves commonly used in dehydration in ethanol production industry, around 220°C-240°C (Simo, 2008). In addition, the water selective

adsorption approach was unlike the butanol selective adsorption approach that normally has regeneration issues like sequential heating desorption method at high temperature leading to adsorbent damages, incomplete butanol recovery (Barshad,1960) and use of an external agent like methanol for regeneration (Kumar et al., 2010). The high water uptake capacity, coupled with lower regeneration temperature, and a relatively easy disposal makes CM to be a promising material for drying of butanol vapor.

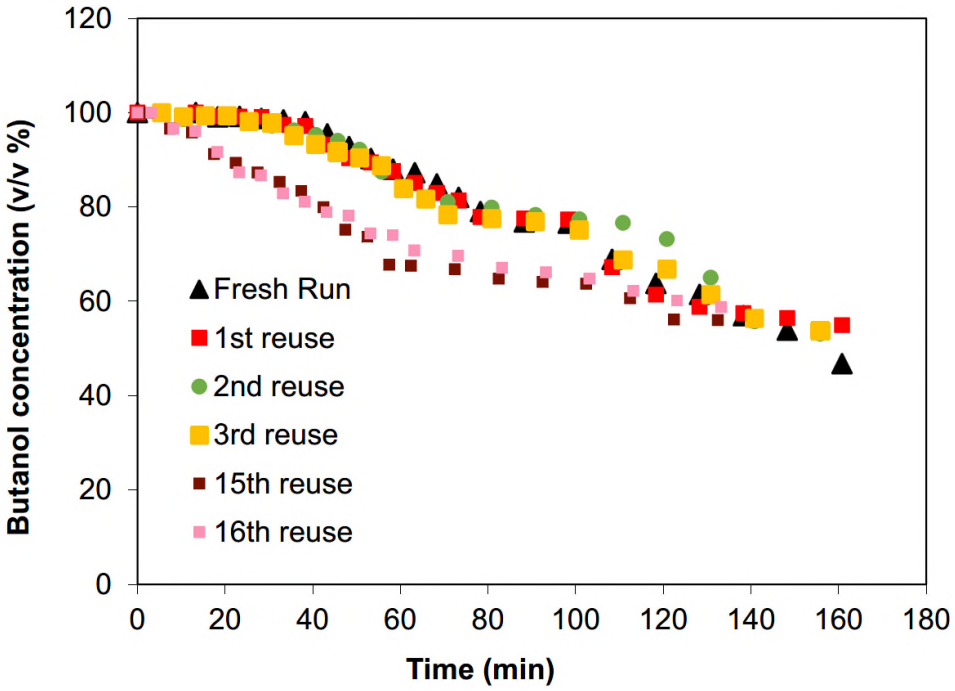

Figure 3.9 Butanol breakthrough curves to evaluate reusability of CM as adsorbent.

All runs were at a temperature of 111°C, pressure of 201 kPa, butanol feed concentration of 55 v/v %, feed flow rate of 3 mL/min and particle size of canola meal in the sieved range of 0.43−1.18 mm.

3.4.7 Contribution of the major components of canola meal to drying of butanol

Canola meal is a multi-component material as it's found to contain over 26% cellulose and lignin, and 6.3% hemicellulose, as shown in Table 3.2. Even after protein extraction, the residual protein of CM was found to be around 27%. The efficiency of protein extraction from CM in the industry is outside the scope of this work. In the previous ethanol dehydration process, it was demonstrated that cellulose (Al-Asheh et al., 2004), and protein (Hong et al., 1982; Ostroff et al., 1988) has important roles in water adsorbing capabilities. To better understand the mechanism of

selective water adsorption of CM, it also becomes important to investigate the contribution of the major components of CM like cellulose and protein towards butanol dehydration. Thereby, it can help comprehend and differentiate the cumulative effect from the individual effect.

For that purpose, cellulose (C-6288, major particle size range 0.015-0.088 mm) and protein (S-9633, major particle size range <0.12 mm) were obtained from Sigma Aldrich and were used as such without any pretreatment as they were dry enough. Corn meal samples (0.2-1.19 mm) were also purchased from Purity Inc, a trademark company of ADM Agri-Food Industry Ltd for comparison as it represents starchy material. Corn meal was dried for 6h at 105°C to remove any residual moisture and was then used. Owing to the fact that it is difficult to obtain the sizes of commercial cellulose, and protein same as those of the cellulose, and protein in CM, the cellulose, and protein materials used here are only considered to approximate the performance of butanol dehydration of actual cellulose, and protein in CM. For the experiments, the above mentioned samples of cellulose, protein, corn meal and canola meal cylindrical pellets (4.7 mm in diameter, which was chosen to simulate the industrially feasible size) were used as adsorbent for drying 55 v/v% butanol at 110^{o}C, 135 kPa, and carrier gas 850 mL/min. The results are shown in Table 3.7.

Table 3.7. Butanol dehydration performance indices for different biosorbents

Adsorbents	Water uptake (g/g-ads)	Butanol uptake (g/g-ads)	Water selectivity	Butanol recovery (%)	Max. Effluent butanol concentration achieved (v/v %)
Canola meal	0.47 ± 0.01	0.04 ± 0.06	5.25 ± 0.28	89.67 ± 0.68	98.86 ±0.67
Cellulose	0.29 ± 0.03	0.07 ± 0.02	4.27 ± 1.04	84.36 ± 1.26	93.43 ± 1.31
Protein	0.20 ± 0.00	0.08 ± 0.00	2.79 ± 0.17	82.47 ± 1.06	84.56 ± 0.64
Corn meal	0.18 ± 0.00	0.04 ± 0.00	4.79 ± 0.23	87.76 ± 0.81	98.44 ± 0.27

Canola meal showed a water separation factor of about 5.25, butanol recovery of 90%, and a maximum effluent butanol concentration of 99 v/v% which are higher than those of cellulose,

protein and corn meal. In addition, CM had the highest water uptake of 0.47 g/g-ads and lowest butanol uptake of 0.04 g/g-ads, which is desirable.

The cellulose was able to remove water from butanol and had a water adsorption capacity of 0.29 g/g-ads, butanol uptake of 0.07 g/g-ads and water selectivity of 4.8 which were lower than that of CM at the same operation conditions. However, the achieved equilibrium water uptake of cellulose 0.29 g/g-ads in this work is similar to that reported for oak chips, and kenaf core being 0.28 g/g-ads, and 0.20 g/g-ads, respectively (Benson and George, 2005). In addition, it is higher than that of the type 3A molecular sieves at 0.18-0.25 g /g-ads (Simo, 2008) which is most often used in industrial ethanol dehydration process. An interesting observation in this work is that the water uptake and water selectively of cellulose is inferior to that of the CM material though the cellulose has smaller particle sizes. The results are suggestive that the physical structure of CM and its natural multi-components may have a synergetic effect on selective water adsorption from butanol solution.

On the other hand, protein also showed capability to dehydrate butanol and had a water uptake of 0.20 g/g-ads. Protein-water interactions have been expressed by varying terminologies like water retention, water binding, water imbibing, water adsorption, and so on. Although water binding can depend on composition and conformation of protein molecules, it also exhibits the swelling behavior due to spontaneous water uptake by protein matrix like that of starch molecules (Zayas, 1997). In this work, protein displayed the least equilibrium water selectivity and butanol recovery amongst all materials studied which was about 2.79 and 82% respectively. It also resulted in a similar lower butanol uptake of 0.07g/g-ads as compared with the cellulose material. The lower butanol uptake might be because of the less accessible structure of the protein material and the interference of the protein hydrophobic regions with adsorption of polar water and butanol molecules. This result is consistent with the study carried out by Ostroff et al., (1998) wherein they showed that the whey proteins were able to adsorb water to some extent due to the presence of hydrophilic polar groups while its affinity for ethanol is less. In one of the studies by Hong et al. (1982), protein in the form of bovine serum albumin (BSA) was examined for the water adsorption capability from water-ethanol mixture as protein along with starch and xylan is one of the three major components of corn meal. They demonstrated similar results of protein with little to no capacity to adsorb ethanol whereas it weakly adsorbed water as compared to other major ingredients- starch and xylan. It proved that protein had a less significant role in water adsorption

properties of corn meal (Hong et al., 1982). The results obtained from this work also (Table 3.7) demonstrated that protein was the least effective component for selective water uptake compared to other tested biosorbents.

The results reveal that CM containing cellulose in this work has higher water uptake than starch-rich corn meal, which could be due to its presence of multi-components such as cellulose, hemicellulose, lignin, protein, etc. It is also demonstrated that the water uptake and selectivity from the cellulose are much higher than those from protein, affirming that cellulose plays a more important role in the butanol dehydration of CM. However, the performance of pure cellulose is not as effective as that of the CM material. A synergetic effect of all components and physical properties and molecular structural makeup of CM may have attributed to the high water uptake and selectivity and thus it could serve as a promising material for butanol dehydration. However, further investigations are required in regards to the synergetic effect of CM.

3.5. SUMMARY

It was demonstrated that CM has the capability to dry butanol from the azeotropic butanol concentration 55 v/v% to high purity butanol of 99 v/v%. Pressure was found to be the most significant factor at the tested conditions, affecting butanol uptake, water selectivity, butanol recovery, and maximum effluent butanol concentration. The optimum conditions obtained from the statistical design resulted in a water separation factor of 5.4, butanol recovery of 90%, water uptake of 0.48 g/g-ads and fuel grade butanol of >99 v/v%. The Dubinin- Polanyi (D-P) model based on the adsorption potential theory for large pore materials gave a better fit to the water adsorption isotherms. The mean free energy indicated that water adsorption is predominantly physisorption. The approximate site energy distribution based on the D-P isotherm elucidated the uptake of water on the heterogeneous CM biosorbent. The high-energy sorption sites were first occupied at low concentration, followed by the low-energy sorption sites. Site energy distribution curve revealed that CM had negligible sorption sites with very high energy (e.g., >15,000 J/mol) in the tested range of parameters. The average site energy $\mu(E^*)$ was 3.33 kJ/mol, which again indicated physical nature of water adsorption, while the standard deviation σ_e^* of 2.36 kJ/mol indicated the heterogeneous nature of biosorbents. Saturated CM was regenerated at 110°C under vacuum and reused for more than 16 cycles.

The results also reveal that CM containing cellulose in this work has higher water uptake than starch-rich corn meal. It is also demonstrated that the water uptake and selectivity from the cellulose are much higher than those from protein, affirming that cellulose plays a more important role in the butanol dehydration of CM. However, the performance of pure cellulose is not as effective as that of the CM material. A synergetic effect of all components and physical properties and molecular structural makeup of CM may have attributed to the high water uptake and selectivity and thus it could serve as a promising material for butanol dehydration. However, further investigations are required in regards to the synergetic effect of CM.

3.6 NOMENCLATURE

Å angstrom

C water content at time t (wt%)

C_o initial water content (wt%)

C_e equilibrium water concentration in vapor phase (g/L)

$\bar{E}$ mean free energy of adsorption (kJ/mol)

E^s reference state for E, representing the lowest physically realizable sorption energy (kJ/mol)

E* $E-E^s$ (kJ/mol)

f (E) site energy frequency distribution (dimensionless)

f (E*) approximate site energy distribution (g.mol/g-J)

k_1, k_2 average values of the performance index for each of the parameters at levels 1 and 2 in OAD table (units of respective performance index)

K_1, K_2 pore constants for microspore and large pore materials (dimensionless)

P pressure (atm)

P_i partial pressure of the adsorbate (atm)

P_s saturated vapor pressure of the adsorbate (atm)

q mass adsorbed per unit mass of adsorbent (g/g-ads)

q_e equilibrium water uptake (g/g-ads and also expressed as mol/g)

q_o limiting mass for adsorption (g/g-ads and also expressed as mol/g)

R universal gas constant (J/mol K)

r^2 correlation coefficient (dimensionless)

T absolute temperature (K)

X_w mole fraction of water in the adsorbed phase (dimensionless)

X_b mole fraction of butanol in the adsorbed phase (dimensionless)

Y_w mole fraction of water in the vapor phase (dimensionless)

Y_b mole fraction of butanol in the vapor phase (dimensionless)

Greek Letters

α separation factor (dimensionless)

β affinity coefficient (dimensionless)

ε adsorption potential (J/mol)

Δ range value in statistical range analysis (units of the performance index)

3.7. ABBREVIATION

ARE	Average Relative Error
Bu-OH	Butanol
CM	Canola meal
CNPs	Carbon nanoparticles
FT-IR	Fourier Transform Infrared Spectroscopy
GC	Gas chromatography
OAD	Orthogonal array design

ppm	Part per million
PAH	Polycyclic aromatic hydrocarbons
PSA	Pressure Swing Adsorption
TGA	Thermogravimetric analysis

3.8. REFERENCES

Al-Asheh, S., F. Banat and N. Al-Lagtah, Chem. Eng. Res. Des. 2004. 82, 855-864.

Aider, M.; Barbana, C. Trends in Food Sci. Technol. 2011, 22, 21-39.

Barshad, I. Thermodynamics of water adsorption and desorption on montmorillonite; A. Swineford (Ed.)., Clays and Clay Minerals: Proc. Eighth Nat. Conf., Pergamon, New York, 1960.

Baylak, T.; Kumar, P.; Niu, H. C.; Dalai, A.; Energ. Fuel. 2012, 26, 5226-5231.

Beery, K. E.; Ladisch, M. R. Enzyme Microb. Technol. 2001, 28, 573-581.

Benson, T.J. and C.E. George, Adsorpt. 2005, 11, 697-701.

Biagini, E.; Barontini, F.; Tognotti, L. Ind. Eng. Chem. Res. 2006, 45, 4486-4493.

Boonfung, C.; Rattanaphanee, P. World Acad. Sci. Eng.Technol. 2010, 4, 557-560.

Cai, D.; Hu, S.; Miao, Q.; Chen, C.; Chen, H.; Chen, H.; Zhang, C.; Li, P.; Qin, P.; Tan, T. Bioresour. Technol. 2017, 224, 380–388.

Canadian Canola: Agriculture and Agri-Food Canada; [updated 2015 Mar 18 ; accessed 2017 Jan 20]:http://www.agr.gc.ca/eng/industry-markets-and-trade/exporting-and-buying-from-canada/buying-canadian-food-products/canadian-canola/?id=1426170869200.

Cao, Z.; Lin, X.-Q.; Xie, J.-J.; He, X.-J.; Ying H.-J. Biotechnol. Biofuels 2014, 7(5), 1-13.

Cerofolini, G. F. Thin Solid Films, 1974, 23, 129–152.

Chang, H.; Yuan, X.; Tian, H.; Zeng, A. Ind. Eng. Chem. Res. 2006, 45, 3916-3921

Dong, Z.; Liu, G.; Liu, S.; Liu, Z.; Jin, W. J. Memb. Sci. 2014, 450, 38–47.

Faisal, A.; Zarebska A.; Saremi, P.; Korelskiy, D.; Ohlin, D.; Rova, U.; Hedlund, J.; Grahn, M. Adsorption 2014, 20, 465–470.

Gupta Kumar, V.; Schmoll, M.; Makki, M.; Tuohy, M.; Antonio, M. M. Applications of Microbial Engineering; first ed., CRC Press: Austria, 2013; pp 282-296.

Himmelsbach, S. D.; Khalili, S.; Akin, E. D. J. Sci. Food. Agr. 2002, 82, 685-696.

Hong, J., M. Voloch, M.R. Ladisch and G.T. Tsao, "Adsorption of ethanol-water mixtures by biomass materials," Biotechnol. Bioeng**. 1982, 24, 725-730**.

Kumar, K. V.; De Castro, M. M.; Escandell, Sabio, M. M.; Reinoso, M. M. F. R. Phys. Chem. Chem. Phys. 2011, 13, 5753–5759.

Lin, X.; Wu, J.; Fan, J.; Qian, W.; Zhou, X.; Qian, C.; Jin, X.; Wang, L.; Bai, J.; Ying, H. J. Chem. Technol. Biotechnol. 2012, 87, 924-931.

Liu, D.; Chen, Y.; Ding, F.-Y.; Zhao, T.; Wu, J.-L.; Guo, T.; Ren, H.-F.; Li, B.-B.; Niu, H.-Q.;

Medina, A. R.; Gamero, P. M.; Almanza, J. M. R.; Cortes, D. A. H.; Vargas, G. G. J. Chil. Chem. Soc. 2009, 54, 244-251.

Moreira, A. R.; Ulmer, D. C.; Linden, J. C. Biotechnol. Bioengin, Symp. 1981, 11, 567-579.

Newkirk, R. Canola Meal Feed Industry Guide; fourth ed., Canola Council of Canada: [updated 2009 Dec 31; accessed 2014 May 11]: http://www.canolacouncil.org/.

Nigam, P.; Singh, A. Progr. Energ. Combust. Sci. 2011, 37, 52-68.

Okewale, A. O.; Babayemi, K. A.; Olalekan, A. P. Int. J. Appl. Sci. Technol. 2013, 3, 35-42.

Ostroff, A., E. Hatzidimitriu and J.L. Kokini, Biotechnol. Bioeng. 1988, 31, 880-884.

Ou, H.; Tan, W.; Niu, C. H.; Feng, R. Ind. Eng. Chem. Res. 2015, 54, 6100-6107.

Polanyi, M. Z. Elektrochem. 1920, 26, 370-374.

Qureshi, N.; Blaschek, H.P. Renew. Energ. 2001, 22, 557–564.

Qureshi, N.; Cotta, M. A.; Saha, B. C. Food Bioprod. Process. 2014, 92, 298–308.

Ranjbar, Z.; Tajallipour, M.; Niu, H. C.; Dalai, A. Ind. Eng. Chem. Res. 2013, 52, 14429-14440.

Raveendran, K.; Ganesh, A.; Khilar, K. C. Fuel, 1996, 75, 987-998.

Ruthven, D. M. Principles of Adsorption and Adsorption Processes; John Wiley & Sons: first ed., USA, 1984, pp 323-329.

Shah, R. Y.; Dhrubo, J. S. Int. J. Cur. Sci. Res. 2011, 2, 57-62.

Sharma, P.; Verma, A.; Sidhu, R. K.; Pandey, O. P. J. Mater. Process. Technol. 2005, 168, 147-151.

Shen, X.; Guo, X.; Zhang, M.; Tao, S.; Wang, X.; Environ. Sci. Technol. 2015, 49, 4894-4902.

Simo, M. Pressure Swing Adsorption Process for Ethanol Dehydration; first ed., ProQuest: USA, 2008, pp 102-107.

Sun, J.; Wang, W.; Wan, P.; Hao, L.; Luo, X.; Gao, H. Adsorpt. Sci. Technol. 2013, 31, 829-844.

Tajallipour, M.; Niu, C.; Dalai, A. Energ. Fuel. 2013, 27, 6655-6664.

Theivandran, G.; Ibrahim, M. S.; Murugan, M. J. Med. Plants. Stud. 2015, 4, 30-32.

Vane, L. M.; Alvarez, F. R.; Rosenblumb, L.; S. Govindaswamy, J. Chem. Technol. Biotechnol. 2013, 88, 1448–1458.

Visioli, J. L.; Enzweiler, H.; Kuhn, C. R.; Schwaab, M.; Mazutti, A. M. Sustainable Chem. Processes. 2014, 2, 1-9.

Wiehn, M.; Staggs, K.; Wang, Y.; Nielsen, D. R. Biotechnol. Prog. 2014, 30(1), 68-78.

Wu, P.; Gao, H.; Sun, J. S.; Ma, T.; Liu, Y.; Wang, F. Bioresour. Technol. 2012, 107, 437-443.

Xu, F.; Yu, J.; Tesso, T.; Dowell, F.; Wang, D. Appl. Energ. 2013, 104, 801-809.

Xue, C.; Du, G.-Q., Chen, L.-J.; Ren, G.-J.; Bai, F. J. Biotechnol. 2014, 188, 158–165.

Xue, C.; Liu, F.; Xu, M.; Tang, I.-C.; Zhao, J.; Bai, F.; Yang, S.-T. Bioresour.Technol. 2016, 219, 158–168.

Xue, C.; Zhao, J.; Liu, F.; Liu, L.; Xu, M.; Yang, S.-T.; Bai, F. Bioresour. Technol. 2013 135, 396–402.

Yan, B.; Niu, C. H. Chem. Eng. J. 2017, 307, 631–642.

Zayas, F.J., "Water Holding Capacity of Proteins," in "Functionality of Proteins in Food," Anonymous Springer Berlin Heidelberg, Germany, 1997, pp. 76.

CHAPTER 4. DRYING BIO-BUTANOL BY OAT HULLS

4.1 ABSTRACT

Bio-butanol is an important source of renewable biofuels. It contains significant amount of water in the production process through fermentation. The current technologies to remove water from butanol is energy intensive and costly. In this work, oat hulls, representative of cellulosic materials abundantly generated as agricultural by-products, was used to dehydrate butanol in a packed column in order to produce biofuel product. The results demonstrated that the oat hull based biosorbent was able to effectively remove water from butanol. The biosorbent was characterized by Brunauer, Emmett and Teller (BET) surface area, thermogravimetric analysis (TGA), Fourier transform infrared (FTIR) spectroscopy and scanning electron microscope (SEM). The adsorption performance and breakthrough curve of the single component (butanol or water) adsorption on the biosorbent was investigated separately. Besides, the separation factors of water over butanol on the biosorbent were determined according to the equilibrium data in the butanol-water binary system. The effects of feed concentration and temperature on adsorption capacity were investigated. The water adsorption equilibrium data in the single water system and the butanol-water binary system were fitted to the Dubinin-Polanyi model. The approximate sorption site energy distribution was calculated to analyze the adsorption equilibrium data on the biosorbent. The results indicate the oat hulls based biosorbent has the capability for butanol dehydration.

4.1. INTRODUCTION

The biofuel, a renewable energy, is a competitive additive and an alternative to fossil fuel. Bio-butanol is a biofuel source, which can be produced from acetone 1-butanol and ethanol (ABE) fermentation. One of the key steps of this process is the recovery of low concentrated butanol from fermentation broth. The concentration of butanol in the broth is often no more than 20 g/L or 5 wt% (Liu et al. 2005; Maddox 1989), because of the butanol inhibition to culture. The product inhibition results in high cost and large volume water removal in the purification process (Qureshi and Blaschek 2001). In biobutanol production

industry, butanol was usually separated from the fermentation broth first by distillation to achieve the azeotrope 55.5wt% butanol, then followed by a multiple number of decantation and distillation to remove the remaining water, which is energy intensive and costly (Luyben 2008).

Efforts have been made to develop various approaches to recover butanol from the fermentation broth. These separation techniques include adsorption (Lin et al. 2012; Oudshoorn et al. 2009; Qureshi et al. 2005; Saravanan et al. 2010) , gas stripping (Groot et al. 1989; Qureshi and Blaschek 2001), membrane pervaporation (Liu et al. 2005; Qureshi and Blaschek 2000), extraction and supercritical extraction (Davison and Thompson 1993; Groot et al. 1990), and hybrid recovery technologies (Kraemer et al. 2011; Xue et al. 2014). Currently, adsorption is known as an effective method for separation and purification due to its low cost, high efficiency, and easy operation (Grande 2012). It has been used for butanol purification in some studies (Lin et al. 2012; Oudshoorn et al. 2009; Qureshi et al. 2005; Saravanan et al. 2010). Recently, many adsorbents such as zeolite, molecular sieves, and polymeric resins have been used to purify bio-alcohols (Carmo and Gubulin 1997; Lin et al. 2012; Oudshoorn et al. 2009; Qureshi et al. 2005; Saravanan et al. 2010). However, most of them are expensive. The adsorption process using molecular sieves such as zeolites as adsorbents accompanies with high regeneration temperature and potential environmental problems.

Moreover, there are increased studies on low-cost biosorbents, because these potential adsorbents are environmentally friendly, easy to be regenerated, and more cost-effective (Benson and George 2005; Ladisch and Dyck 1979). Starch-based and cellulose-based natural materials were employed in water adsorption (Benson and George 2005; Crawshaw and Hills 1990; Kim et al. 2011; Rebar et al. 1984). Dehydration of butanol using appropriate biomaterials provides a promising alternative way for bio-butanol production, which is more cost-efficient and more environmentally friendly compared with conventional distillation (Jayaprakash et al. 2017).

Adsorption could be a promising method for removing water from butanol efficiently. However, there are limited studies in butanol dehydration by adsorption using biosorbents. Oat is an important cereal crop globally. The annual global production of oats

is nearly 22.5 million tons. The waste oat hulls have been used as fuel, packing material and animal feed, but the output of them is higher than utilization (Banerjee et al. 2016). Thus, a significant amount of oat hulls, the agricultural by-product of oat, are discarded. The waste oat hulls need to be utilized in a feasible and environmentally friendly way. Oat hulls, composed of cellulose, hemicellulose, and lignin (Paschoal et al. 2015), have potential to remove water from butanol based on the conclusions from other studies that lignocellulosic materials can be a potential option for ethanol dehydration (Quintero and Cardona 2009; Rakshit et al. 1993). There are some studies on oat hulls for dye removal (Banerjee et al. 2016); however, it has not been studied for butanol dehydration. Its water adsorption capability is unknown.

Thus this work investigated adsorption of water, and butanol vapor using the oat hull biosorbent. The aim of this work was to develop an alternative technology of adsorption to remove water directly from the azeotrope of 55.5 wt% butanol vapor generated from the preliminary distillation in biobutanol industry in a hope to reduce or replace the downstream multiple decantation and distillation in bio-butanol industry. . For the interest of both industrial application and scientific research, adsorption was investigated at a wider concentration range of 55-92 wt% butanol. The water/butanol adsorption capability and characteristics of the oat hulls based biosorbent were investigated respectively in the single component systems. The butanol-water binary system was also used to determine the competitive adsorption of water and butanol on the biosorbent. Furthermore, the site energy distribution based on equilibria data were investigated.

4.2. MATERIALS AND METHODS

4.2.1 Agricultural byproduct biosorbent and other materials

Oat hulls particles were obtained from Richardson Millings Ltd, Warman, SK, Canada. The raw materials were air dried, and sieved by Canadian Standard Sieves Series (Combustion Engineering Canada Inc.) to sizes of 0.425-1.18 mm. After that, the materials were dried in an oven at 105 ^{o}C for 48 hr and kept in desiccators. Butanol used in the

experiments was 1-Butanol purchased from Fisher Scientific (ACS reagent grade). All the water used in this study was distilled water.

4.2.2 Characterization of the biosorbent

The surface area and pore volume of the biosorbent were determined through N_2 adsorption-desorption isotherm at 77 K using the BET theory by a surface area analyzer (Micromeritics ASAP 2020). The thermal stability of the biosorbent was estimated by TA Instruments Q500 thermogravimetric analyzer. The functional groups of the biosorbent were determined by Fourier transform infrared spectroscopy (JASCO FT-IR 4100). The surface morphology of the biosorbent was investigated by JEOL JSM- 6010LV scanning electron microscope.

4.2.3 Adsorption

The pressure swing adsorption (PSA) system was used to study the dehydration performance of the biosorbent based on oat hulls. The stainless-steel adsorption column packed with the biosorbent was used as a fixed-bed reactor. This experimental apparatus was composed of an adsorption column, a feed pump, a gas flow meter which was used to adjust the flow rate of the carrier gas (N_2), a heating jacket, temperature controllers, thermocouples, pressure transducers, a back pressure regulator which was used to regulate the pressure and a condenser. The details of experimental apparatus were described in the study of Ranjbar et al (Ranjbar et al. 2013).

It is noted that the feed of 55-92 wt% butanol-water vapor, and adsorption temperature (381-392K) were used in this work to simulate the butanol vapor product. Even though in the lab scale experiments in this work, heat was provided to generate such butanol-water vapor, no heat was needed in real industrial adsorption process because the butanol vapor is generated for the preliminary distillation and can be directly fed to the adsorption column

For that purpose, before the adsorption experiment, the system temperature was adjusted to the desired temperature by the heating jacket and temperature controller. Once the desired temperature was achieved, the feed pump was switched on. The feed was pumped to the pipelines and carried by nitrogen. The pipelines were equipped with heating

tapes to vaporize the liquid feed. The feed was led to bypass before it was vaporized. After the feed was vaporized completely, the feed stream was directed to the top of the column. The pressure of the column was adjusted to a desired value by the back-pressure regulator. During adsorption process, the temperature and pressure were measured by thermocouples and pressure transducers. The effluent flowing out from the column was condensed in a condenser and collected every 5 or 10 min. The bed was considered saturated when the content in the effluent reached the same level in the feed. In the PSA system, desorption (regeneration) was carried out in the same column after adsorption. Once the biosorbent packed in the column was saturated, the pump was switched off, and the valve of feed line was closed at the same time. The nitrogen gas entered column from the bottom under vacuum to flash out the adsorbates for 5 hours at 105 °C. This regeneration temperature is much lower than that of commercial adsorbents such as molecular sieves, silica gel, and alumina (at least 175 °C, and up to around 300^{o}C) (Beery and Ladisch 2001; Fahmi et al. 1999). It has been reported that the usage of biomass derived adsorbents is more beneficial compared to other types of adsorbents regarding the energy demand (Boonfung and Rattanaphanee 2010). For example, the energy requirement for the dehydration of ethanol with CaO was reported to be 3669 kJ/kg EtOH, while the energy consumed by the adsorption with cellulose was 2873 kJ/kg EtOH (Boonfung and Rattanaphanee 2010). Dehydration of ethanol by adsorption on molecular sieves has been applied in industry to replace the conventional separation techniques for breaking the ethanol-water azeotrope due to its low energy requirement (Simo et al. 2006; Vane 2008). The energy consumption and costs will be further evaluated in the next step of this research.

In single component system experiments, pure water or pure butanol was vaporized and carried by N_2 (680 mL/min). The liquid feed flow rate ranges from 0.3 to 5 mL/min. The oat hulls based biosorbent 300 ± 25 g (0.425-1.18 mm particle size) were packed in the column. The pressure of the system was maintained at 135 kPa by a back pressure regulator. 392 K was chosen as temperature to avoid the condensation of vapor feed in the column. The effluent was collected and weighed periodically after the first drop was collected. Water or butanol adsorption capability was determined by the mass balance, i.e. the water/butanol input minus the water/butanol output per g of biosorbent in the column.

For binary system study, the mixture of butanol and water vapor with different concentrations (55-92 wt% butanol) were used as feed. The butanol concentration of the feed has been used in this study was close to or higher than that of the binary azeotrope of butanol and water, which is generated from distillation in butanol production industry. The liquid feed rate was 3 mL/min. The liquid feed was vaporized and carried by N_2 (680 mL/min) to the column from the top. The adsorption column was packed with 300 ± 25 g oat hulls based biosorbent (0.425-1.18 mm). The pressure of the system was maintained at 135 kPa. The boiling point of the mixture of water and butanol is different from that of pure water or pure butanol. 381 K, 386 K, 392 K were chosen as the reaction temperature to make sure that the feed of selected concentration remained in gas phase after entering the column. The effluent was cooled, collected and weighed periodically. The water concentration in effluent was determined by Mettler Toledo Karl Fischer titrator to monitor the change in water concentration and the adsorption capacity was calculated.

4.3. RESULTS AND DISCUSSION

4.3.1 Results of characterization

The specific surface area, pore volume and porosity of the biosorbent were determined by N_2 adsorption-desorption measurements. The BET surface area analysis revealed that the biosorbent had the specific surface area of 3.0±1.1 m^2/g. The Barrett–Joyner–Halenda (BJH) pore size distribution showed 32% of the pores belonged to macropores (>50 nm), 65% of the pores belonged to mesopores (2–50 nm), and the remaining was in micropores (<2 nm) region. The average pore diameter and pore volume were 8.1 nm and 0.003 cm^3/g, respectively.

Figure 4.1 shows the result of the thermogravimetric analysis (TGA). The tested biosorbent had high thermal stability up to 220 °C which was higher than the chosen temperature of adsorption (up to 120°C) and desorption temperature (105 °C) in this work. There was a considerable weight loss at 220-315 °C, which corresponds to the decomposition of hemicellulose. The weight loss at 315-400 °C relates to the pyrolysis of cellulose (Yang et al. 2007). The pyrolysis of cellulose and hemicellulose mostly occurred

within a specific temperature range, while the decomposition temperature range of lignin was from 160 to 900 °C (Yang et al. 2007), so there was no characteristic weight loss for lignin in Fig. 4.1.

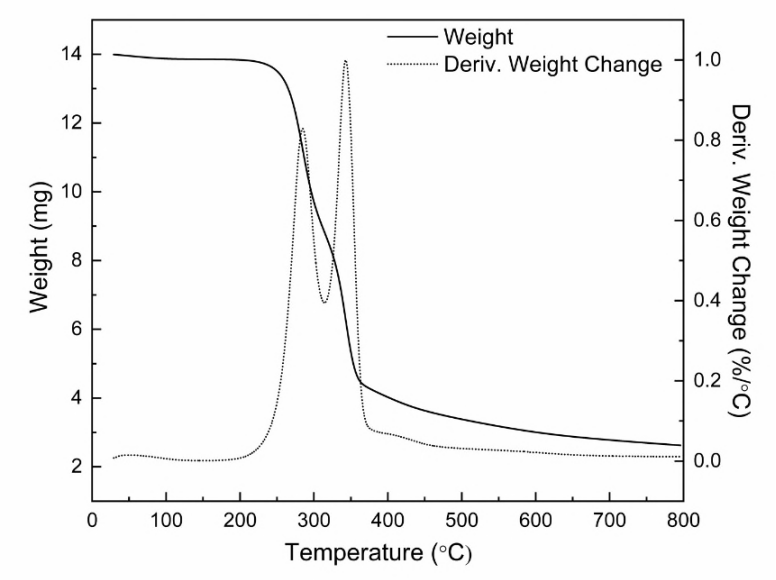

Figure 4.1. Thermogravimetric curves of the oat hulls based biosorbent

The functional groups in the biosorbent are observed in Fig. 4.2. The O-H stretching was found at a broad peak at 3323 cm^{-1}. The existence of OH group could prove the occurrence of H-bonding interactions which could play an important role in butanol dehydration. The adsorption band at 2921 cm^{-1} was attributed to C–H_n stretching; peaks at 1512 and 1726 were attributed to C=O stretching; the peak at 1633 cm^{-1} may indicate the existence of C=C of the aromatic ring in the lignin; the band at 1232 cm^{-1} may indicate the C-O stretching; adsorption band at 1022 and 1149 cm^{-1} was due to C–O–C stretching vibration. The FTIR spectra of the biosorbent (oat hulls) was largely consistent with FTIR spectra of cellulose, hemicellulose and lignin (Yang et al. 2007), the three main components of oat hulls.

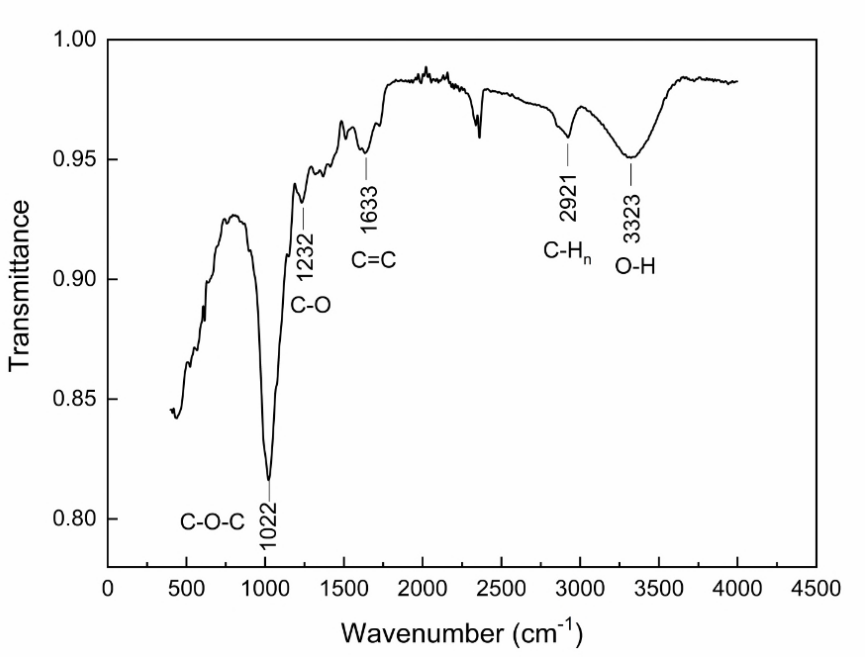

Figure 4.2. FTIR spectra of oat hulls based biosorbent

The SEM images of oat hulls based biosorbent before and after butanol dehydration are shown in Fig. 4.3. Figure 4.3a provides the texture and pore feature of the original biosorbent. There were deep holes and bundle-holes widely distributed on the original biosorbent. The deep pores and complicated reticular fiber structure probably play important roles in bonding water molecules. Fibered networks were clearly visible in the micrographs of the original biosorbent. The micrograph of the biosorbent after butanol dehydration and desorption shown in Figure 4.3b was captured to compare with that of the original biosorbent. The structure of fiber network and pores of the biosorbent before and after butanol dehydration are similar. The well-developed pores and bunchy fiber were also clear and distinct on the biosorbent after butanol dehydration, which indicates the structure of oat hulls based biosorbent was relatively stable during the butanol dehydration and desorption.

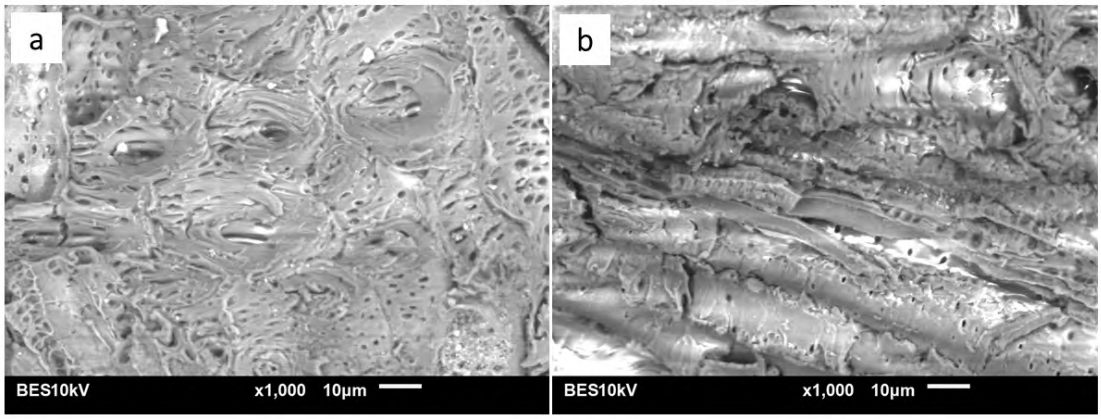

Figure 4.3. SEM images of oat hulls based biosorbent (a) before adsorption; (b) after adsorption and regeneration

4.3.2 Water/butanol adsorption on the biosorbent in the single system

Water and butanol vapor adsorption on the oat hulls based biosorbent were first determined for the single component system in the packed column.

The water breakthrough curves were plotted by the ratio of the mass of water (adsorbate) in the effluent to that in feed along with time. The breakthrough curves also provide the information of breakthrough time, equilibrium time, effluent concentration profile, and adsorption of adsorbate along with time. The shape of the breakthrough curve can determine the utilization of adsorption bed and the rate of mass transfer. The breakthrough curves of water and butanol adsorption on the oat hull biosorbent were depicted in Figs. 4 and 5 respectively. It can be seen from Figs. 4 and 5 that the first drop time changes with different feed concentration. The higher the feed concentration, the shorter the first drop time. When adsorbates with higher concentration passed into the column, it took less time to reach equilibrium. The breakthrough curves in Figs. 4 and 5 showed higher adsorption rate during the first half and a slower rate of adsorption while approaching equilibrium. At the beginning of adsorption, the slope of the breakthrough curve was steep, since there was high concentration gradient between the biosorbent and the feed. The shape of the breakthrough curves and the equilibrium time suggested that the

feed concentration of adsorbates would affect the adsorption rate in this system. The higher the feed concentration, the higher the mass transfer rate.

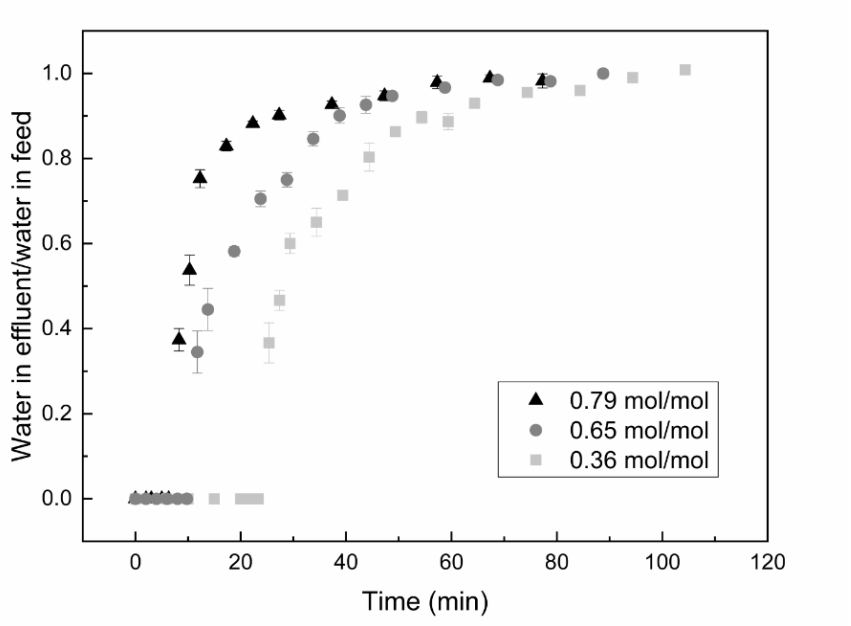

Figure 4.4. The breakthrough curve of water adsorption on the biosorbent at 392 K, 135 kPa at different feed concentrations

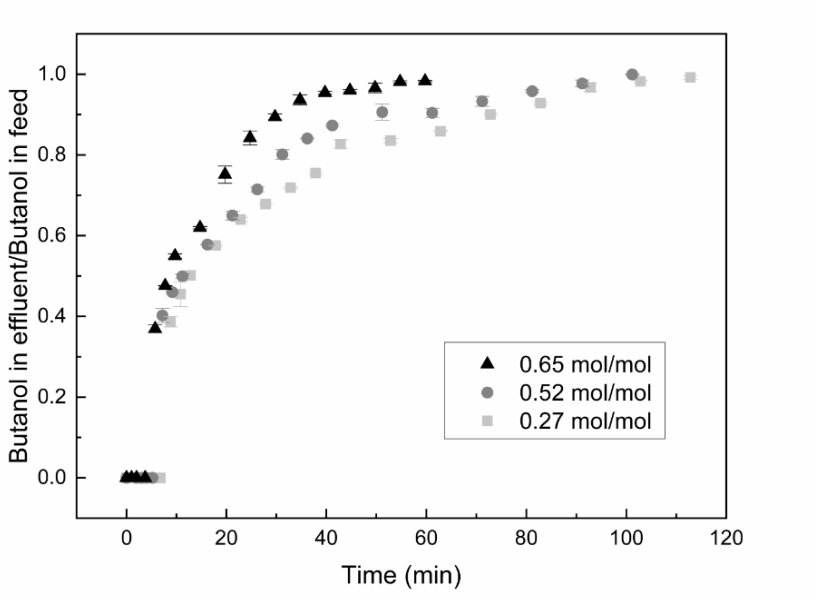

Figure 4.5. The breakthrough curve of butanol adsorption on the biosorbent at 392 K, 135 kPa at different feed concentrations

The equilibrium data for single component adsorption were obtained to analyze the affinity and capacity of adsorbates on biosorbents. The equilibrium adsorption capacity of biosorbent was calculated based on mass balance. The mass of adsorbed adsorbate was equal to adsorbate in feed minus adsorbate in effluent until equilibrium. The adsorption isotherms of water and butanol vapor on oat hulls at the same conditions were depicted in Fig. 4.6. The isotherm of water vapor adsorption shows the increase in water adsorption with the increase of water mole fraction. For butanol adsorption shown in Fig. 4.6, the increase in adsorption capacity was significant as the mole fraction was increased from 0.3 to 0.5. It can be concluded from the comparison of these two isotherms that the affinity of water for the biosorbent is stronger than that of butanol, and the water adsorption capacity of the biosorbent is also higher compared with butanol adsorption capacity. "It was observed that the achieved highest water adsorption capacity 0.132 g/g (equivalent to 0.132 cm^3/g) was much higher than the respective pore volume, 0.03 cm^3/g. This indicated that water adsorption occurs by penetration of water molecules into the adsorbent cellulosic matrix, in addition to adsorption on the pore surface." The above information may suggest that the oat hulls based biosorbent has great potential for butanol dehydration in the butanol-water binary system and the water adsorption on oat hulls could be much higher than butanol in a binary system when feed concentration is properly chosen.

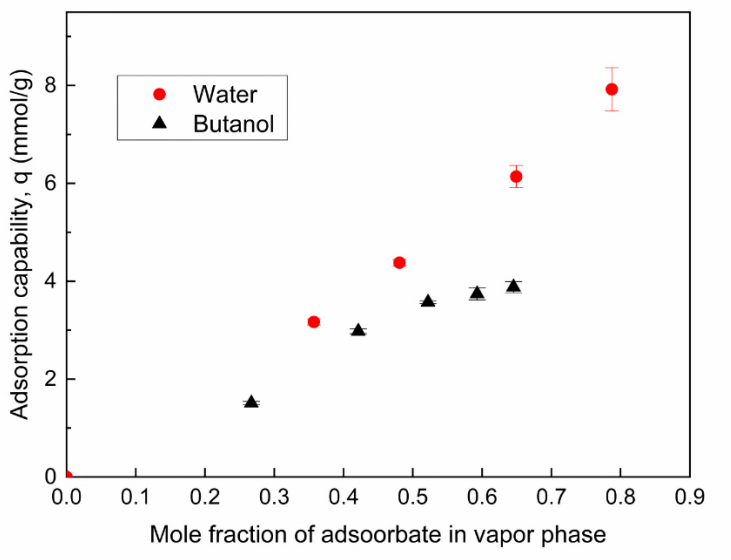

Figure 4.6. The adsorption isotherms of water and butanol on the biosorbent at 392 K, 135 kPa

4.3.3 Water/butanol adsorption on the biosorbent in the binary system

This study aimed to investigate whether oat hulls can be applied as a biosorbent for butanol dehydration. The enrichment of butanol from water/butanol azeotrope by adsorption was one of the focuses of this study as well. Thus, the water-butanol binary system experiments were carried out to obtain more information such as water selectivity over butanol, the situation of competitive adsorption, and the influence of different conditions. The water separation factor was calculated from Eq. (4.1). X_w and Y_w are the mass concentration of water in the biosorbent and vapor phases, respectively. X_b and Y_b are the mass concentration of butanol in the biosorbent and vapor phases, respectively. The higher water adsorption separation factors indicate that the water adsorption is more favorable.

$$\alpha = \frac{X_w/X_b}{Y_w/Y_b} \tag{4.1}$$

The adsorption capacity and separation factors with corresponding conditions were listed in Table 4.1. At the same temperature, the separation factors increased with the decrease of butanol concentration in the feed. The results in Table 4.1 also describe the competitive adsorption of water and butanol. With the increase in butanol content in the feed, the adsorption of water dropped sharply, while the adsorption of butanol was increased when the other conditions were same. This phenomenon was found at different temperatures. The competitive adsorption occurred when water and butanol were adsorbed on oat hulls. From the comparison of the adsorption capacity at 381 K, 386 K, 392 K, it was concluded that the water or butanol adsorption capacity decreased with the increase in temperature, indicating either water or butanol adsorption was exothermic. The temperature is an essential factor for water adsorption and butanol adsorption on oat hulls. The highest water adsorption capacity is 0.132 g/g obtained at 381 K when the butanol concentration in the feed is 57.6%.

Table 4.1 Adsorption characteristics of water and butanol on oat hulls and separation factors (135 kPa, 3 mL/min liquid feed rate)

Temperature (K)	Butanol concentration in feed (wt%)	Water adsorption capacity (g/g)	Butanol adsorption capacity (g/g)	Separation factor
381	57.6±0.3	0.132±0.002	0.061±0.002	2.88±0.01
381	69.1±0.3	0.089±0.003	0.090±0.004	2.28±0.05
381	79.7±0.6	0.067±0.001	0.181±0.009	1.50±0.03
381	90.3±0.7	0.034±0.005	0.300±0.006	1.06±0.07
386	61.9±0.1	0.098±0.007	0.078±0.006	1.94±0.15
386	79.8±0.6	0.047±0.002	0.150±0.004	1.22±0.10
386	91.3±0.2	0.023±0.003	0.241±0.010	0.98±0.09
392	56.5±0.1	0.061±0.001	0.026±0.001	3.09±0.07
392	79.3±0.1	0.037±0.000	0.050±0.002	2.75±0.01
392	85.3±0.1	0.027±0.001	0.071±0.001	2.19±0.05

The comparison of water adsorption capacity of different biosorbents was displayed in Table 4.2. The comparison shows that oat hulls based biosorbent has good water adsorption capacity and it is promising for butanol dehydration. The optimization of conditions for this process using the oat hulls based biosorbent is worth pursuing further.

The butanol breakthrough curves of the binary system at 381 K and various concentrations as a function of time are presented in Fig. 4.7. The concentration of effluent changed significantly within 60 min and then changed slowly when approaching equilibrium. It shows that the oat hulls were able to concentrate the lower grade butanol

and water mixture to butanol products of high purity. The highest butanol concentrations of effluent obtained from feed of various butanol content (57.6%, 69.1%, 79.7%, 90.3%) are 95.3%, 97.1%, 98.1% and 99.0%, respectively. The results demonstrate that the oat hulls can dehydrate the binary azeotrope of butanol and water, and even higher concentrated butanol mixtures. In comparison with canola meal reported in the literature for drying alcohols shown in Table 4.2, its water adsorption capacity is slightly lower than canola meal for drying lower grade butanol such as 55% butanol, but higher for drying higher grade butanol, 95%. It can be concluded that the oat hulls based biosorbent is an alternative for butanol dehydration.

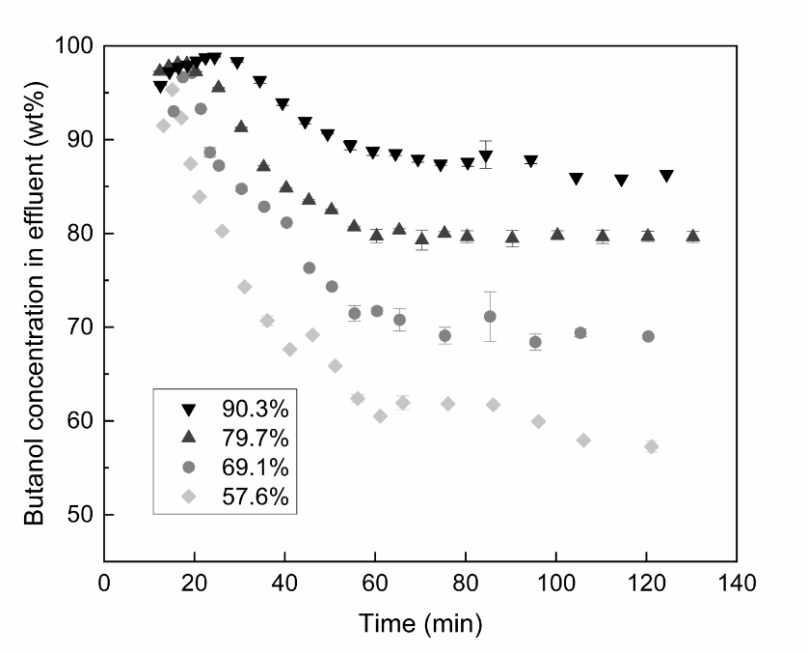

Figure 4.7. Breakthrough curves of butanol dehydration on the biosorbent at 381 K, 135 kPa and 3 mL/min liquid feed rate with different feeding concentrations

Table 4.2 Comparison of water adsorption capacity of different biosorbents

Adsorbent	Adsorbate	Butanol concentration in feed (wt%)	Water adsorption capacity (g/g)	Max alcohol concentration achieved (wt%)
Oat hulls (this work)	Butanol-water	57.6	0.132	95.3
Canola meal (Jayaprakash et al. 2017)	Butanol-water	55.0	0.480	98.8
Oat hulls (this work)	Butanol-water	90.3	0.034	99.0
Canola meal (Jayaprakash et al. 2017)	Butanol-water	95.0	0.016	99.0

4.3.4 Water adsorption equilibrium model simulation

The large pore Dubinin-Polanyi model model was used to successfully describe equilibrium water adsorption from binary ethanol-water, and butanol-water systems into natural materials such as canola meal and so on which contain large pores (Chang et al. 2006; Jayaprakash et al. 2017; Ranjbar et al. 2013).

The biosorbent used in this work is raw oat hull material, and the results of SEM and pore size distribution show the material mainly contains mesopores and macropores, basically large pores. Thus in this work, the large pore Dubinin-Polanyi model was chosen in comparison with the micropore Dubinin-Polanyi model to investigate their capability to simulate the equilibrium water adsorption from single water system, and binary water-butanol system.

The following Eq. (4.2) and Eq. (4.3) are Dubinin-Polanyi models for micropore and large pore materials respectively.

$$lnq = lnq_0 - \frac{\kappa_1}{\beta}\left[RTln\left(\frac{P^s}{P_i}\right)\right]^2 \quad (4.2)$$

$$lnq = lnq_0 - \frac{\kappa_2}{\beta}\left[RTln\left(\frac{P^s}{P_i}\right)\right] \quad (4.3)$$

q is equilibrium adsorption capacity of the adsorbate with the unit g adsorbed adsorbate/g adsorbent; q_0 is limiting mass for adsorption (g adsorbate/g adsorbent); κ_1 and κ_2 are pore constant for micropore and large pore materials; $ß$ is affinity coefficient. P_i is partial pressure of the adsorbate at adsorption temperature (kPa); P^s is saturated vapor pressure of the adsorbate at the same temperature (kPa).

According to the adsorption potential theory, the equilibrium data at different temperatures can be described in a single characteristic curve. One of the advantages of the Dubinin-Polanyi model is that the equilibrium data obtained at different temperatures can be represented in a single curve rather than in multiple curves.

$$\varepsilon = RTln(\frac{P^s}{P_i}) \quad (4.4)$$

The aforementioned Dubinin-Polanyi models were used to describe the water equilibrium data in the single system. Figures 8 and 9 demonstrate the experimental data for water adsorption in the single system and the fitting results of Dubinin-Polanyi model. The fitting results and isotherm parameters obtained from model fitting are listed in Table 4.3. The value of correlation coefficient (R^2=0.960) for large pore model is higher than that of micropore Dubinin-Polanyi model (R^2=0.853) and the residual sum of squares (RSS=0.0063) is smaller than that of micropore Dubinin-Polanyi model (RSS=0.0221). This indicates that the large pore Dubinin-Polanyi model described the water adsorption equilibrium data for single system better compared with the micropore Dubinin-Polanyi model. The value of the limiting mass for adsorption q_0 was estimated by model fitting as well.

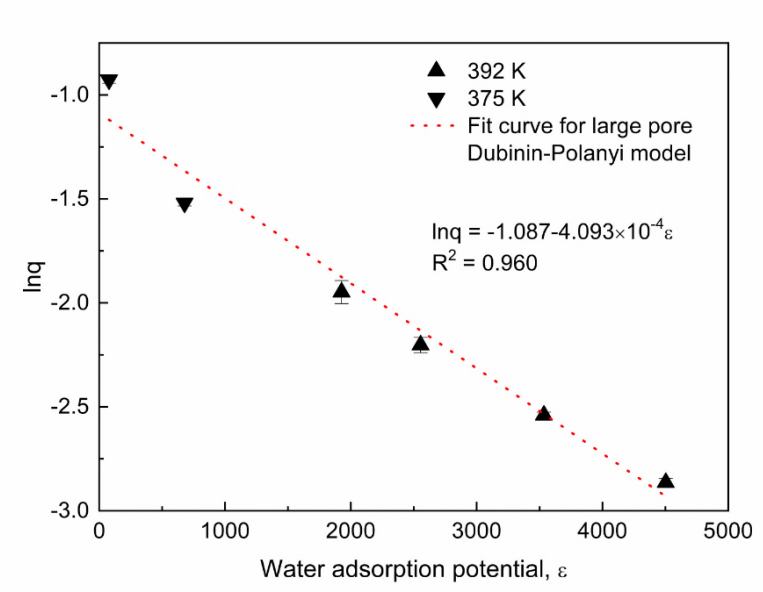

Figure 4.8. Equilibrium water adsorption data in the single system and fitting results of the large pore Dubinin-Polanyi model

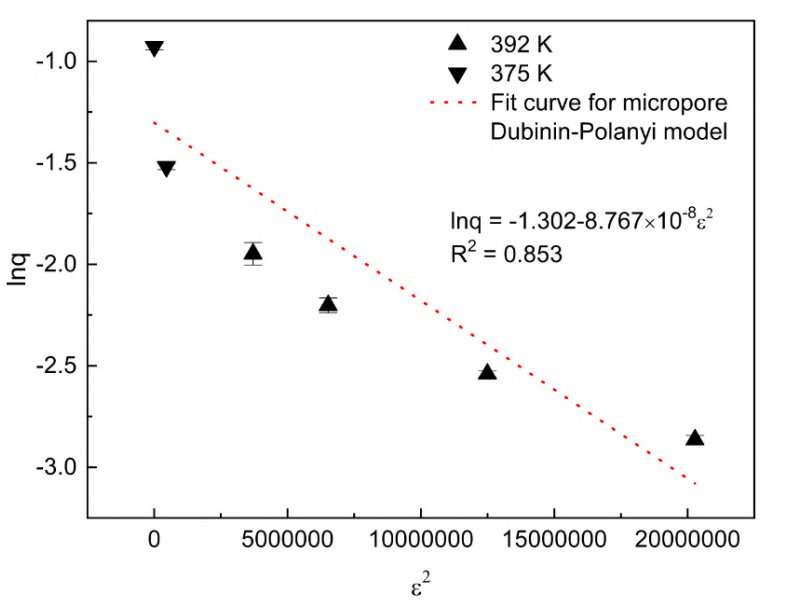

Figure 4.9. Equilibrium water adsorption data in the single system and fitting results of the micropore Dubinin-Polanyi model

The Dubinin-Polanyi models were also used to describe the water equilibrium data in the binary butanol-water system. The characteristic curve of Polanyi adsorption potential theory was demonstrated in Fig. 4.10. In this figure, the quantity of water adsorption

capacity q versus adsorption potential ε is plotted. It can be seen from Fig. 4.10 that nearly all the data points tend to compose one curve. This discovery indicates that the Polanyi adsorption potential theory has potential to be successfully applied in this case.

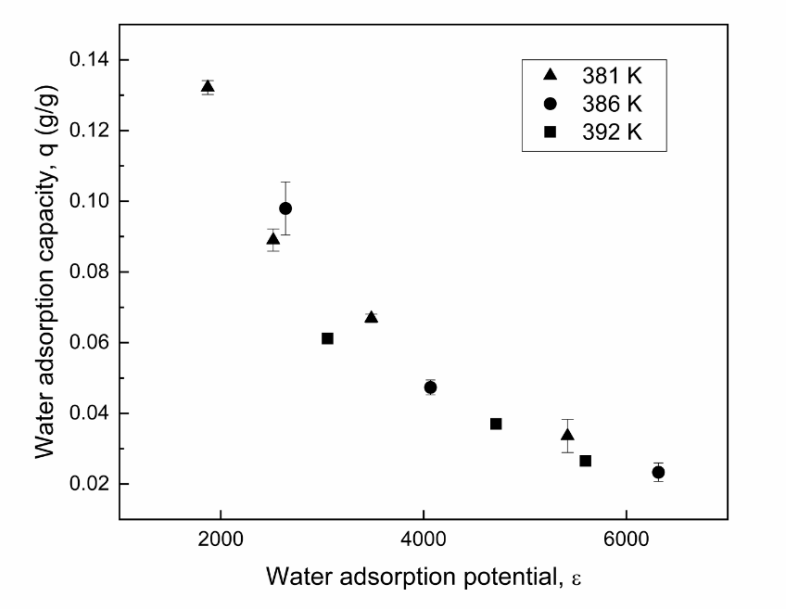

Figure 4.10. Water adsorption characteristic curve based on the Polanyi adsorption potential theory

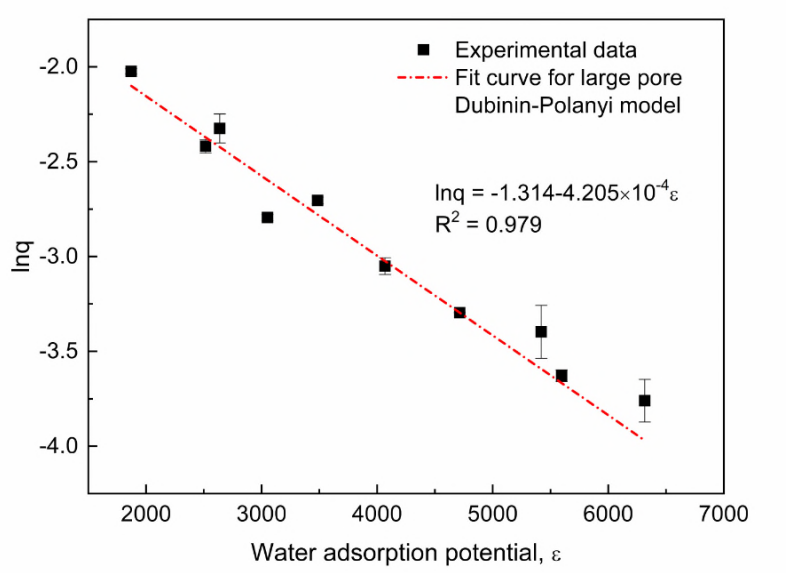

Figure 4.11. Equilibrium water adsorption data in the binary system and fitted large pore Dubinin-Polanyi model curve

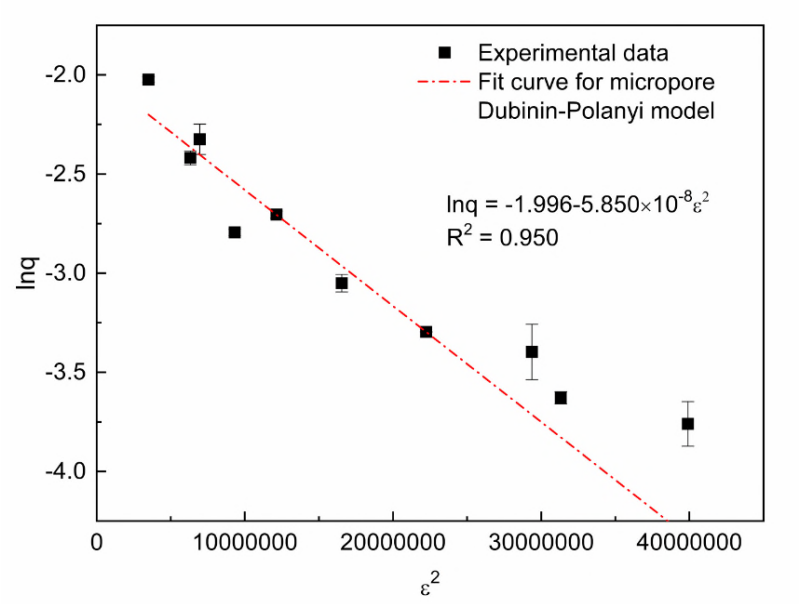

Figure 4.12. Equilibrium water adsorption data in the binary system and fitted micropore Dubinin-Polanyi model curve

The fitting curves of the Dubinin-Polanyi model are presented in Figs. 4.11 and 4.12. The isotherm parameters obtained from model fitting are also listed in Table 4.3. The P value of the large pore Dubinin-Polanyi model is far less than 0.05, which indicates that this model described the equilibrium data well. Again, the results show that the large pore model is better for representing the experimental water adsorption data in the water-butanol binary system due to the higher correlation coefficient (R^2) value and the lower residual sum of squares (RSS). This result is consistent with the results of water adsorption from Ranjbar's study on water adsorption from water-ethanol system (Ranjbar et al. 2013) and Jayaprakash's study of (Jayaprakash et al. 2017). The R^2 value of large pore Dubinin-Polanyi model in Ranjbar's study and Jayaprakash's study were 0.97 and 0.96, respectively, which are higher than that of the micropore Dubinin-Polanyi model. The results of these studies similarly indicate that the large pore model is better than the micropore Dubinin-Polanyi model to present the water adsorption in water-alcohol systems.

Table 4.3 Fitting results of the Dubinin-Polanyi models

	q_0 （g/g）	κ/β	R^2	RSS $((g/g)^2)$	P value
Single water system					
Large pore Dubinin-Polanyi model	0.337	4.093E-4	0.960	0.0063	3.80E-4
Micropore Dubinin-Polanyi model	0.272	8.767E-8	0.853	0.0221	0.00539
Binary water-butanol system					
Large pore Dubinin-Polanyi model	0.269	4.205E-4	0.979	0.0005	3.50E-8
Micropore Dubinin-Polanyi model	0.136	5.850E-8	0.950	0.0011	1.06E-6

Thus, the water adsorption equilibrium data in the single system or water/butanol binary system were both well described by the large pore Dubinin-Polanyi model. The better fitting results of the large pore Dubinin-Polanyi model indicated that water adsorption in this system is based on large pores, which are consistent to the results of SEM and pore size distribution that the oat hull material mainly contain large pores (mesopores and macropores). In addition, the modeling results of the large pore Dubinin-Polanyi model (Table 4.3) demonstrated that $q_{0,}$ limiting mass for adsorption (g adsorbate/g adsorbent) was decreased about 20% from 0.337 of the single water system to 0.269 of the binary system. This indicated that butanol molecules may compete for minor portion of the water adsorption sites.

4.3.5 Analysis of site energy distribution for water adsorption

Analysis of the site energy distribution is an effective method to describe the surface characteristics of adsorbent for a targeted adsorbate. Equation (4.5) defines the total adsorption (q_e) on the heterogeneous surface as the integral of homogeneous local isotherm (q_h) multiplied by a site energy frequency distribution (F(E)) over a range of energies. However, in most cases, the local isotherm is not clear and neither is the overall isotherm. It is difficult to obtain the exact distribution. The approximate site energy distribution proposed by Cerofolini (Cerofolini 1974) provides a widely-accepted solution. Based on the Cerofolini approximation the equilibrium pressure can be represented as a function of the site energy as can be seen in Eq. (4.6).

$$q_e(p) = \int_0^\infty q_h(E,p)F(E)dE \tag{4.5}$$

$$p = p^s exp\left(-\frac{E^*}{RT}\right) \tag{4.6}$$

By plugging Eq. (6) into isotherm expression Eq. (3), *q(p)* can be represented as $q(E^*)$. The site energy distribution can be obtained by differentiating theoretical isotherm expression with respect to E* based on Eq. (4.7).

$$F(E^*) = -\frac{dq(E^*)}{dE^*} \tag{4.7}$$

In this way, the approximate distribution function can be written in terms of parameters from an isotherm. In this work, the large pore Dubinin-Polanyi model for water adsorption was used because it provided better fitting to the equilibrium data. The site energy distribution function based on the large pore Dubinin-Polanyi isotherm model (Eq. (4.3)) is deducted in Eq. (4.8).

$$F(E^*) = \frac{\kappa_2}{\beta} \times \frac{q_0}{exp\left(\frac{\kappa_2 E^*}{\beta}\right)} \tag{4.8}$$

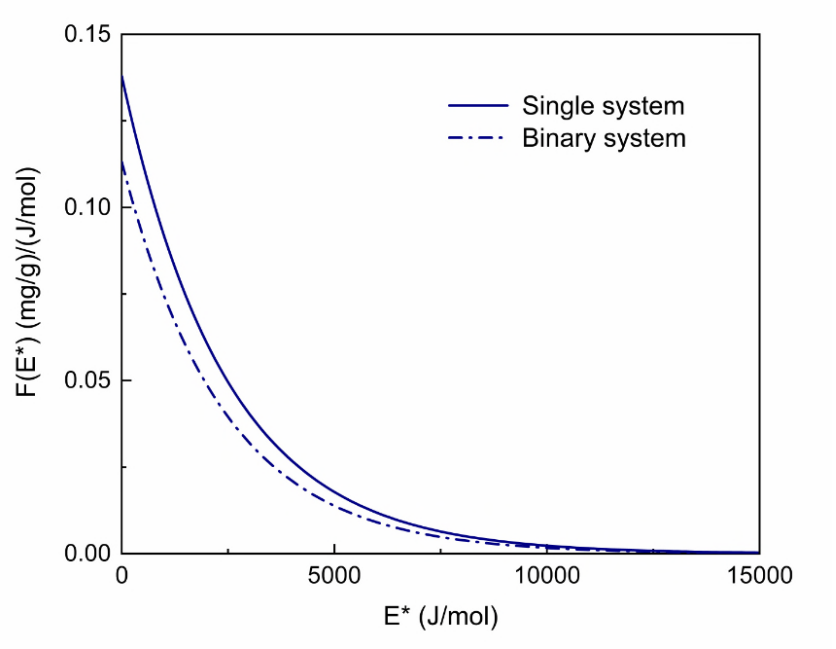

Figure 4.13. Site energy distribution of oat hulls for water adsorption according to the large pore Dubinin-Polanyi model

Figure 4.13 demonstrates the approximate site energy distribution curve of oat hulls for water adsorption in the single water system, and butanol/water binary system based on the Dubinin-Polanyi isotherm. The approximate distribution is not normalized, but it can provide the information about the heterogeneity of the biosorbent and water adsorption characteristics. For instance, the area under the site energy distribution curve can be interpreted as the maximum water adsorption capability. The distribution curve also shows the adsorption capacity within the different range of site energy. By comparison and analysis, it was found that the water adsorption capacity in the binary system was lower than that in the single system throughout the entire range of site energy. This difference describes the effect of butanol on water adsorption. Figure 4.13 suggests that almost all the water adsorption took place on the site with energy lower than 10,000 J/mol.

$$E_m = \frac{\int_0^{+\infty} E^* \times \mathrm{F}(E^*) dE^*}{\int_0^{+\infty} \mathrm{F}(E^*) dE^*} \tag{4.9}$$

$$E_m = \frac{\int_0^{+\infty} \frac{\kappa_2}{\beta} q_0 E^* exp\left(-\frac{\kappa_2 E^*}{\beta}\right) dE^*}{\int_0^{+\infty} \frac{\kappa_2}{\beta} q_0 exp\left(-\frac{\kappa_2 E^*}{\beta}\right) dE^*} \tag{4.10}$$

$$E_m = \frac{\beta}{\kappa_2} \tag{4.11}$$

The average site energy (E_m) was determined for water adsorption in this study. It is an indicator of the affinity of the adsorbate for the adsorbent surface, which can be calculated by Eq. (4.9). Plugging Eq. (4.8) in Eq. (4.9) and integrating led to Eqs. (4.10) and (4.11). In this study, the average site energy for water adsorption in the single water system, and the water-butanol binary system calculated based on the Dubinin-Polanyi model for large pores are 2443 J/mol and 2378 J/mol, respectively. The slightly higher average site energy indicates higher adsorption affinity. It is concluded that the affinity between water and the biosorbent in the single water system is a little higher than that in the water-butanol binary system. It may be because of the fact that in the binary system the butanol molecules compete with water molecules for a portion of the sites. The butanol adsorption capacity is much lower than that of water. Therefore the average site energy for the single system and the binary system are very close. The site energy distribution provides an approach to analyze the equilibrium data. It relates the changes in isotherm parameters to changes in the energy characteristics of sorbent surfaces.

4.4. SUMMARY

It is concluded from water and butanol isotherms that the affinity of water for oat hulls based biosorbent is stronger than that of butanol, and the water adsorption capacity of the biosorbent is also higher than butanol adsorption capacity. The highest water adsorption capacity is 0.132 g/g with a separation factor of 2.88 obtained at 381 K when the butanol concentration in the feed is 57.6%. At 381 K, the highest concentration of effluent obtained from feed of various butanol content (57.6%, 69.1%, 79.7%, 90.3%) are 95.3%, 97.1%, 98.1% and 99.0%, respectively, which indicates the oat hulls based biosorbent is able to dehydrate the water/butanol binary azeotrope and even at higher concentrated butanol solution.

The Dubinin-Polanyi model for large pore materials is slightly better for representing the experimental water adsorption data in both single water system and water-butanol binary system compared with the micropore Dubinin-Polanyi model. The fitting

results also suggest that the oat hulls based biosorbent are more likely to be a large pore material, which is consistent with the results from BET surface area analysis. The difference in limiting adsorption mass of single and binary system proves the competitive adsorption between water and butanol. The analysis of site energy distribution shows that in this case, most adsorption took place on the sites having energy lower than 10,000 J/mol. The calculated average site energy for water adsorption are 2443 J/mol and 2378 J/mol for the single and binary system. The site energy distribution method is transferrable to analyze the adsorption data of other heterogeneous materials.

4.5 ABBREVIATIONS

ABE	Acetone 1-butanol and ethanol
BET	Brunner-Emmet-Teller
FTIR	Fourier transform infrared spectroscopy
PSA	Pressure swing adsorption
RSS	Residual sum of squares
SEM	Scanning electron microscopy
TGA	Thermogravimetric analysis

4.6 NOMENCLATURE

E	Adsorption energy, J/mol
E_m	The average site energy, J/mol
E^*	Site energy, J/mol
$F(E)$	Site energy frequency distribution over a range of energies

$F(E^*)$	Site energy distribution over a range of energies, g·mol/(g·J)
P	Pressure, kPa
P_i	Partial pressure of the adsorbate, kPa
P^s	Saturated vapor pressure of the adsorbate, kPa
q	Mass adsorbed per unit mass of biosorbent, g/g adsorbent
q_0	Limiting mass for adsorption, g/g biosorbent
q_e	Equilibrium adsorption capacity, g/g biosorbent
q_h	Energetically homogeneous isotherm, g/g biosorbent
R	Universal gas constant, J/(mol·K)
R^2	Correlation coefficient
T	Temperature, K
X_b	Mass concentration of butanol in the biosorbent
X_w	Mass concentration of water in the biosorbent
Y_b	Mass concentration of butanol in vapor phase
Y_w	Mass concentration of water in vapor phase

Greek letters

α	Separation factor
$ß$	Affinity coefficient
ε	Adsorption potential, J/mol

κ_1 Constant for micropore materials, $(mol/J)^2$

κ_2 Constant for large pore materials, mol/J

4.7 REFERENCES

Banerjee, S., Sharma, G.C., Gautam, R.K., Chattopadhyaya, M.C., Upadhyay, S.N., Sharma, Y.C.: Removal of Malachite Green, a hazardous dye from aqueous solutions using Avena sativa (oat) hull as a potential adsorbent. J. Mol. Liq. 213, 162–172 (2016).

Beery, K.E., Ladisch, M.R.: Adsorption of Water from Liquid-Phase Ethanol-Water Mixtures atRoom Temperature Using Starch-Based Adsorbents. 40, 2112–2115 (2001).

Benson, T.J., George, C.E.: Cellulose based adsorbent materials for the dehydration of ethanol using thermal swing adsorption. Adsorption. 11, 697–701 (2005)

Boonfung, C., Rattanaphanee, P.: Pressure swing adsorption with cassava adsorbent for dehydration of ethanol vapor. World Acad. Sci. Eng. Technol. 71, (2010)

Carmo, M.J., Gubulin, J.C.: Ethanol-water adsorption on commercial 3a zeolites: kinetic and thermodynamic data. Brazilian J. Chem. Eng. 14, 0 (1997)

Cerofolini, G.F.: Localized adsorption on heterogeneous surfaces. Thin Solid Films. 23, 129–152 (1974).

Chang, H., Yuan, X.-G., Tian, H., Zeng, A.-W.: Experimental investigation and modeling of adsorption of water and ethanol on cornmeal in an ethanol-water binary vapor system. Chem Eng Technol. 29, 454–461 (2006).

Crawshaw, J.R., Hills, J.H.: Sorption of Ethanol and Water by Starch Materials. Ind. Eng. Chem. Res. 29, 307–309 (1990)

Davison, B.H., Thompson, J.E.: Continuous direct solvent extraction of butanol in a fermenting fluidized-bed bioreactor with immobilized Clostridium acetobutylicum. Appl. Biochem. Biotechnol. 39, 415–426 (1993).

Fahmi, A., Banat, F.A., Jumah, R.: Vapor-Liquid Equilibrium of Ethanol-Water System in

the Presence of Molecular Sieves. 34, 2355–2368 (1999)

Grande, C.A.: Advances in Pressure Swing Adsorption for Gas Separation. ISRN Chem. Eng. 2012, 13 (2012).

Groot, W.J., Soedjak, H.S., Donck, P.B., van der Lans, R.G.J.M., Luyben, K.C.A.M., Timmer, J.M.K.: Butanol recovery from fermentations by liquid-liquid extraction and membrane solvent extraction. Bioprocess Eng. 5, 203–216 (1990).

Groot, W.J., van der Lans, R.G.J.M., Luyben, K.C.A.M.: Batch and continuous butanol fermentations with free cells: integration with product recovery by gas-stripping. Appl. Microbiol. Biotechnol. 32, 305–308 (1989).

Jayaprakash, D., Dhabhai, R., Niu, C.H., Dalai, A.K.: Selective Water Removal by Sorption from Butanol-Water Vapor Mixtures: Analyses of Key Operating Parameters and Site Energy Distribution. Energy and Fuels. 31, 5193–5202 (2017).

Kim, Y., Hendrickson, R., Mosier, N., Hilaly, A., Ladisch, M.R.: Cassava starch pearls as a desiccant for drying ethanol. Ind. Eng. Chem. Res. 50, 8678–8685 (2011).

Kraemer, K., Harwardt, A., Bronneberg, R., Marquardt, W.: Separation of butanol from acetone–butanol–ethanol fermentation by a hybrid extraction–distillation process. Comput. Chem. Eng. 35, 949–963 (2011).

Ladisch, M.R., Dyck, K.K.: Dehydration of ethanol: new approach gives positive energy balance. Science (80-.). 205, 898 (1979)

Lin, X., Wu, J., Fan, J., Qian, W., Zhou, X., Qian, C., Jin, X., Wang, L., Bai, J., Ying, H.: Adsorption of butanol from aqueous solution onto a new type of macroporous adsorption resin: Studies of adsorption isotherms and kinetics simulation. J. Chem. Technol. Biotechnol. 87, 924–931 (2012)

Liu, F., Liu, L., Feng, X.: Separation of acetone–butanol–ethanol (ABE) from dilute aqueous solutions by pervaporation. Sep. Purif. Technol. 42, 273–282 (2005).

Luyben, L.W.: Control of the Heterogeneous Azeotropic n-Butanol/Water Distillation system. Energy & Fuels. 22, 4249–4258 (2008)

Maddox, I.S.: The Acetone-Butanol-Ethanol Fermentation: Recent Progress in Technology.

Biotechnol. Genet. Eng. Rev. 7, 189–220 (1989).

Oudshoorn, A., van der Wielen, L.A.M., Straathof, A.J.J.: Adsorption equilibria of bio-based butanol solutions using zeolite. Biochem. Eng. J. 48, 99–103 (2009).

Paschoal, G.B., Muller, C.M.O., Carvalho, G.M., Tischer, C.A., Mali, S.: Isolation and characterization of nanofibrillated cellulose from oat hulls. Quim. Nova. 38, 478–482 (2015)

Quintero, J.A., Cardona, C.A.: Ethanol dehydration by adsorption with starchy and cellulosic materials. Ind. Eng. Chem. Res. 48, 6783–6788 (2009)

Qureshi, N., Blaschek, H.P.: Butanol production using Clostridium beijerinckii BA101 hyper-butanol producing mutant strain and recovery by pervaporation. Appl. Biochem. Biotechnol. 84, 225–235 (2000).

Qureshi, N., Blaschek, H.P.: Recovery of butanol from fermentation broth by gas stripping. Renew. Energy. 22, 557–564 (2001). doi:http://dx.doi.org/10.1016/S0960-1481(00)00108-7

Qureshi, N., Hughes, S., Maddox, I.S., Cotta, M.A.: Energy-efficient recovery of butanol from model solutions and fermentation broth by adsorption. Bioprocess Biosyst Eng. 27, 215–222 (2005)

Rakshit, S.K., Ghosh, P., Bisaria, V.S.: Ethanol separation by selective adsorption of water. Bioprocess Eng. 8, 279–282 (1993).

Ranjbar, Z., Tajallipour, M., Niu, H.C., Dalai, A.: Water Removal from Ethanol Vapor by Adsorption on Canola Meal after Protein Extraction. Ind. Eng. Chem. Res. 52, 14429–14440 (2013)

Rebar, V., Fischbach, E.R., Apostolopoulos, D., Kokini, J.L.: Thermodynamics of Water and Ethanol Adsorption on Four Starches as Model Biomass Separation Systems. Biotechnol. Bioeng. 26, 513–517 (1984)

Saravanan, V., Waijers, D.A., Ziari, M., Noordermeer, M.A.: Recovery of 1-butanol from aqueous solutions using zeolite ZSM-5 with a high Si/Al ratio; suitability of a column process for industrial applications. Biochem. Eng. J. 49, 33–39 (2010).

Simo, M., Brown, C.J., Hlavacek, V.: Modeling of industrial PSA process for fuel ethanol production. In: AIChE Annual Meeting, Conference Proceedings (2006)

Vane, L.M.: Separation technologies for the recovery and dehydration of alcohols from fermentation broths. Biofuels, Bioprod. Biorefining. 2, 553–588 (2008).

Xue, C., Zhao, J.B., Chen, L.J., Bai, F.W., Yang, S.T., Sun, J.X.: Integrated butanol recovery for an advanced biofuel: current state and prospects. Appl Microbiol Biotechnol. 98, 3463–3474 (2014).

Yang, H., Yan, R., Chen, H., Lee, D.H., Zheng, C.: Characteristics of hemicellulose, cellulose and lignin pyrolysis. Fuel. 86, 1781–1788 (2007).

CHAPTER 5. ECONOMIC ANALYSIS

5.1 DRYING NATURAL GAS

5.1.1 INTRODUCTION

Several processes were applied in industry for natural gas dehydration including glycol systems, calcium chloride, and temperature swing adsorption (Kidnay, et al., 2011). Each process has its own advantages and drawbacks. To be more specific, glycol systems were recently banned due to contaminations and environmental issues (BETX), while temperature swing adsorption is energy intensive and produces a considerable amounts of greenhouse gases. In recent years, biosorbents have been widely used in wastewater treatment and gas/alcohol dehydration, and showed excellent performance. The authors used a biosorbent developed from flax shives in a pressure swing adsorption process in order to dehydrate natural gas. The biosorbents showed high performance in terms of adsorption capacity, selectivity, and regeneration properties. In this section, techno-economic analyses were performed on three different dehydration processes in order to investigate if pressure swing adsorption process using biosorbent would be feasible for drying natural gas.

5.1.2 DEHYDRATION IN A TETRAETHYL GLYCOL (TEG) PROCESS

5.1.2.1 Process Description

This process is comprised of an absorber column, a distillation column, a flash drum, and a series of heat exchangers, valves, and pumps (Kidnay, et al., 2011; Mokhatab and Poe, 2012). Firstly, liquid water is separated from natural gas in a knock-out drum; then, the wet natural gas is dried in an absorber column where the gas is brought in contact with TEG liquid stream. Next, any TEG impurities in the final product due to column flooding or TEG foaming is removed from natural gas, and the sales gas is sent into the pipelines. On the other hand, the rich or wet TEG is regenerated in a distillation column running on total reflux mode. The lean TEG stream is recycled back to the system once its pressure and temperature is adjusted. A makeup stream of TEG is necessary to compensate for the TEG losses in the system.

5.1.2.2 Simulation

The TEG dehydration process was simulated using ASPEN HYSYS process simulator. The HYSYS Glycol fluid package was selected for property calculations. Alberta natural gas conditions and composition were considered as an example for this simulation. The feed gas composition is shown in

Table 5.1. The feed gas to the dehydration unit is "Sweat Gas", which is the product of the acid removal unit in the natural gas processing plant (Mokhatab and Poe, 2012). In the Alberta plant, this sweat gas has a pressure and temperature of 60.05 bar and 29.44 °C.

Table 5.1. Composition of Alberta natural gas; sweat gas on dry basis (Kidnay, et al., 2011)

Component	Mole %
N2	3.16
CO2	1.68
H2S	3.26
CH4	76.10
Ethane	6.51
Propane	3.06
Butane	1.97
C5+	2.96
H2O	1.30

Figure 5.1 shows the process flowsheet of TEG dehydration unit simulated in ASPEN HYSYS. As can be noticed, a recovery of 99.99 % was achieved, and the water content of the sales gas is 2.37 lb/MMscf, which is within the range of pipeline quality gas (4-7 lb/MMscf) (Mokhatab and Poe, 2012).

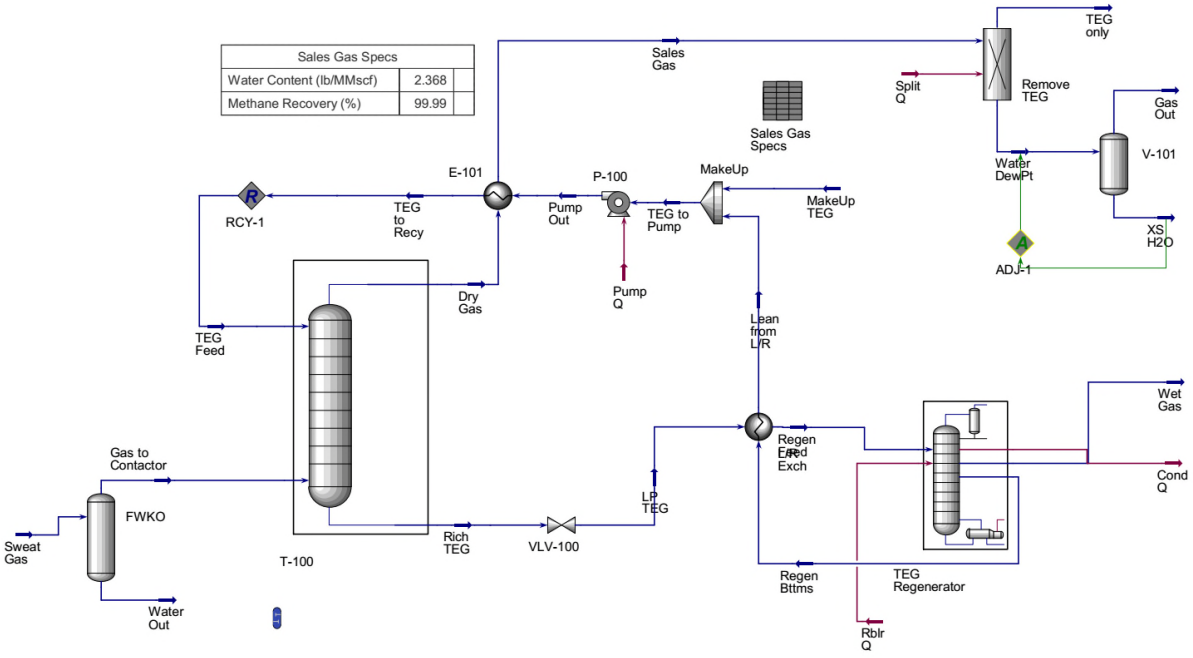

Figure 5.1. Process flowsheet of natural gas dehydration process using TEG simulated in ASPEN HYSYS.

5.1.2.3 Economic and Energy Analyses

ASPEN Economic Analyzer was used to perform an economic analysis on the simulated processes in this report. The capital cost and operating cost of the processes were estimated and compared. As can be seen in Table 5.2, a total capital cost of 30.7 million USD was estimated for the TEG dehydration process, 87.6 % of which is due to the raw material cost (mainly TEG).

Table 5.2. Summary of economic analysis; TEG dehydration process

Total Capital Cost [MUSD]	30.7
Total Operating Cost [USD/Year]	982,821
Total Raw Materials Cost [MUSD]	26.9
ETG Makeup cost [USD/Year]	315
Total Utilities Cost [USD/Year]	52,880.4
Equipment Cost [USD]	179,500
Total Installed Cost [USD]	755,600
Utilities	**USD/hour**
Electricity	5.5188
HP Steam	0.5138

Energy analysis was performed using ASPEN Energy Analyzer. The composite curve obtained from pinch analysis is shown in Figure 5.2. This figure suggests that further heat integration is possible; however, capital cost need to be considered at the same time. The pinch temperature is approximately 20 °C.

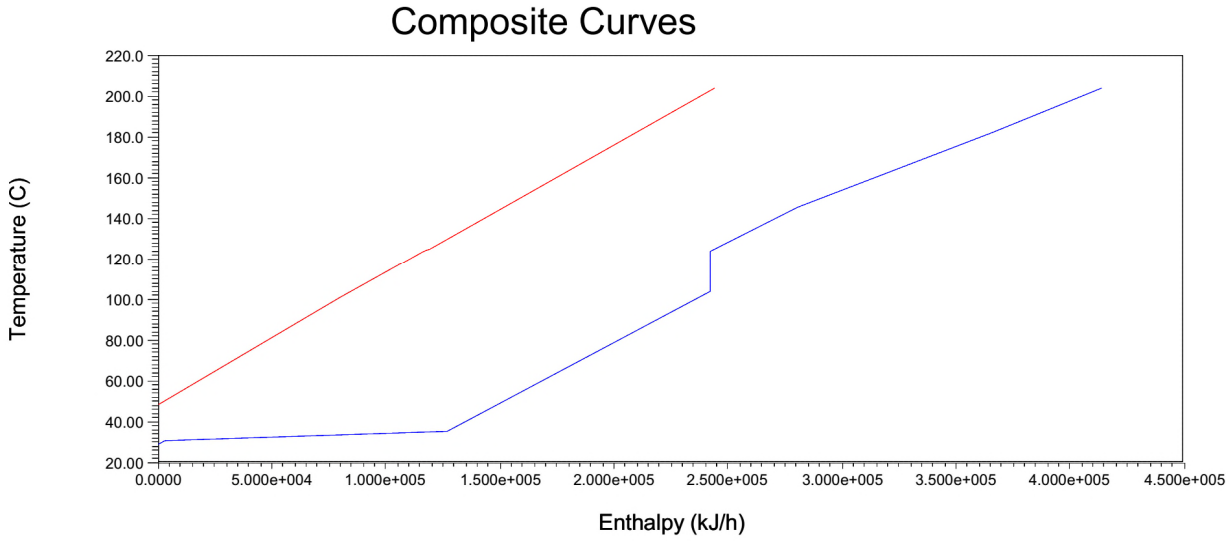

Figure 5.2. The composite curve obtained from pinch analysis on the TEG dehydration process.

Table 5.3 shows the heating and cooling utilities used in the TEG dehydration process. Carbon emissions are also estimated and compared to target values recommended by ASPEN for gas processing plants. The obtained values are close to the target values, except for cooling utilities. These results are also visually illustrated in Figure 5.3.

Table 5.3. Energy analysis results from ASPEN Energy Analyzer; the target values are recommended values by ASPEN for gas processing plants.

Property	Actual	Target	Available Savings	% of Actual
Total Utilities [kJ/h]	175,100	170,300	4805	2.75
Heating Utilities [kJ/h]	172,700	170,300	2,400	1.39
Cooling Utilities [kJ/h]	2,405	0	2,405	100
Carbon Emissions [kg/h]	9.785	9.517	0.2684	2.74

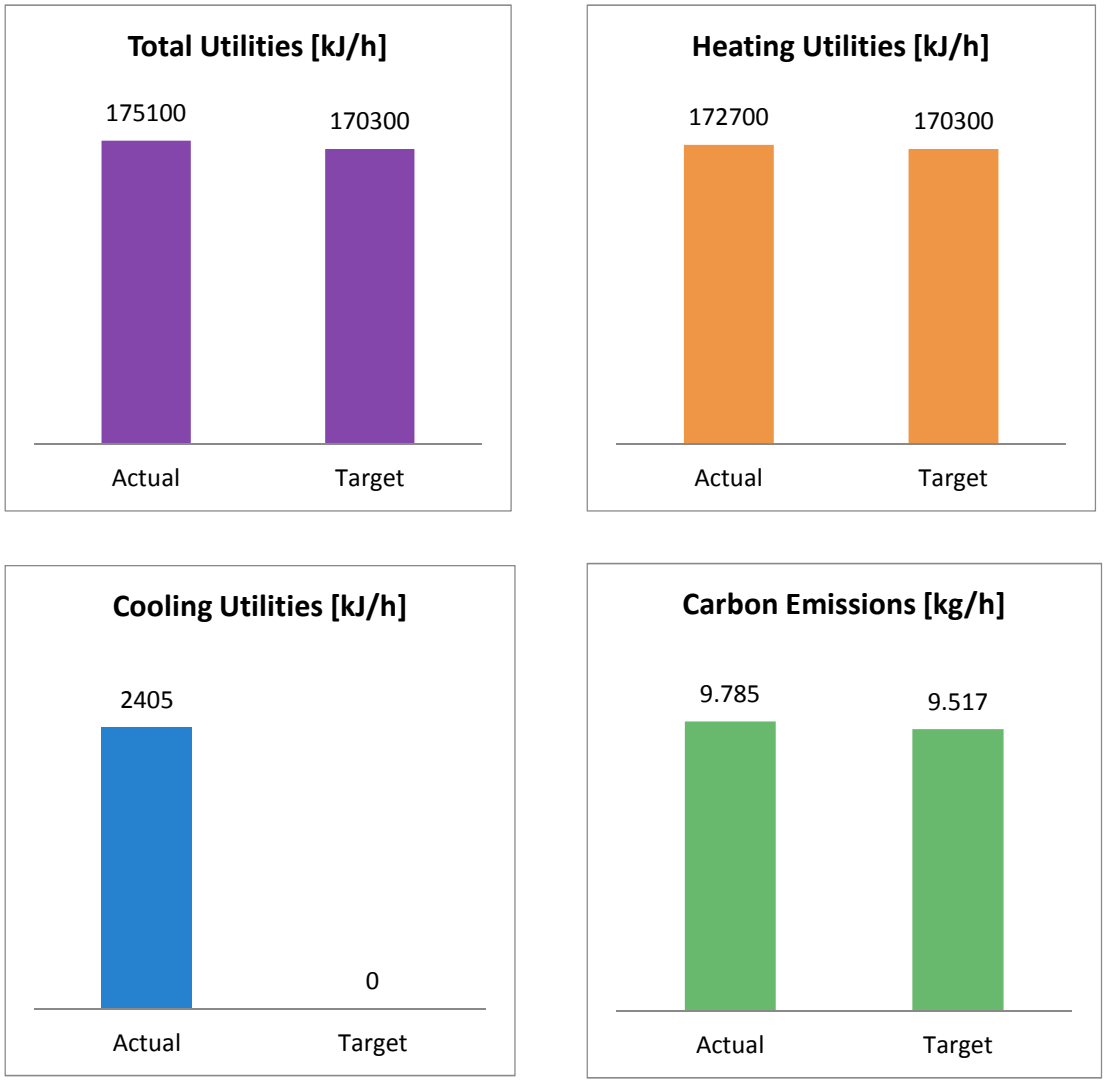

Figure 5.3. Energy analysis results from ASPEN Energy Analyzer; comparison of heating/cooling utilities and carbon emissions with target values recommended by ASPEN for gas processing plants.

5.1.3 DEHYDRATION IN A TEMPERATURE SWING ADSORPTION PROCESS

5.1.3.1 Process Description

In this process, two adsorption columns packed with molecular sieves were used in the temperature swing adsorption (TSA) process to dehydrate natural gas (Kidnay, et al., 2011; Mokhatab and Poe, 2012). While adsorption is taking place in one column at a relatively lower temperature, desorption takes place in the other column at higher temperature. These two columns

operate in a cyclic batch mode. Each column is switch from adsorption mode to desorption mode after a certain cycle time (a few minutes). A part of the dry product is sent into a furnace where it is heated to temperatures up to 300 °C. Then this gas is sent into one of the column as a carrier gas during the desorption step in the cycle. Water vapor is desorbed and carried with this hot gas stream, and the adsorbents are regenerated enough and ready for another adsorption cycle. Afterwards, this humid gas is cooled down, sent into a flash drum, compressed, and recycled back to feed in upstream.

5.1.3.2 Simulation

The TSA process was simulated in ASPEN HYSYS based on the adsorption capacities and selectivities reported for molecular sieves. NRTL-RK fluid package was used for property estimation. In order to simulate a dynamic cyclic batch process in a steady-state mode simulation in HYSYS, the feed was divided in half, and each stream is sent into an adsorption column separating water vapor from the natural gas. The total recovery of each column is specified as 99.9 % according to values reported in the handbook of natural gas processing (Mokhatab and Poe, 2012). A portion of the dried gas (S-110) is sent into a furnace, and heated to 300 °C, and mixed with the separated water streams in the adsorption columns (S-106 and S-107). The mixed gas is the humid gas exiting the adsorption columns during the desorption step. This stream is then cooled down using cooling water. Condensed water is separated in a flash drum, and the overhead gas is compressed in a compressor, and recycled back to the system. The standard L/D ratio of 2 was

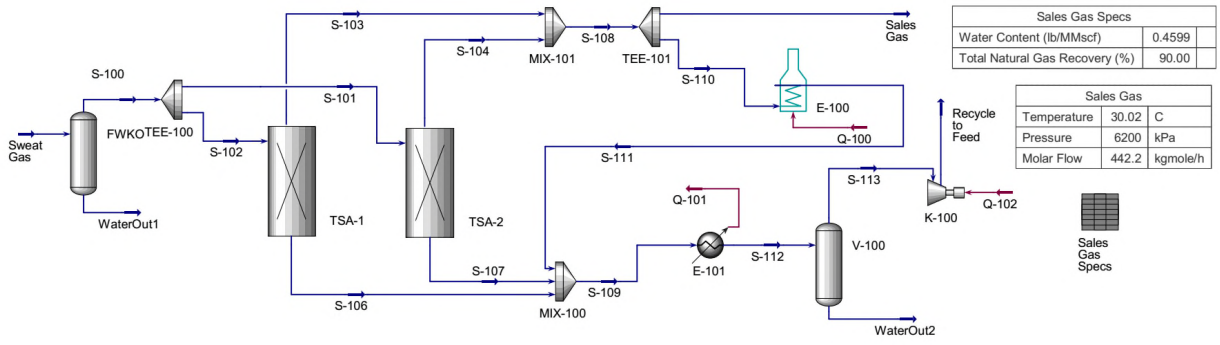

Figure 5.4. Process flowsheet of natural gas dehydration process in temperature swing adsorption simulated in ASPEN HYSYS.

considered for the adsorbent layer, and the required mass of adsorbent was calculated accordingly (Ruthven, 1984). The overall recovery of natural gas in this process was 90 %, and the water content of the sales gas is 0.46 lb/MMscf, which is way below the pipeline standards.

5.1.3.3 Economic Analysis

Similar to the TEG dehydration process, an economic analysis was performed on the TAS process. As can be seen in Table 5.4, a total capital cost of 4.44 million USD was estimated for the TSA process, which is much lower than the capital cost of the TEG dehydration process; however, the operating cost and utilities cost were slightly higher than those of the TEG dehydration process.

Table 5.4. Economic analysis results of the TSA process

Total Capital Cost [MUSD]	4.44
Total Operating Cost [MUSD/Year]	1.35
Total Adsorbent Cost [USD]	123,328.43
Total Utilities Cost [USD/Year]	59,580.6
Equipment Cost [USD]	74,7000
Total Installed Cost [USD]	1,303,800
Utilities	**USD/hour**
Electricity	3.1103
Cooling Water	0.1697
Furnace (natural gas)	3.5167

Energy analysis was similarly done and the results are shown in Figure 5.5 and Figure 5.6. A very low pinch temperature was obtained, which indicates that further heat integration is not worthy. Furthermore, the heating/cooling utilities, and gas emissions were much higher than the target values recommended by ASPEN. This is due to the furnace and sharp temperature fluctuations in the process. Natural gas is burnt in the furnace producing carbon dioxide and other pollutants. These results are also shown in

Table 5.5.

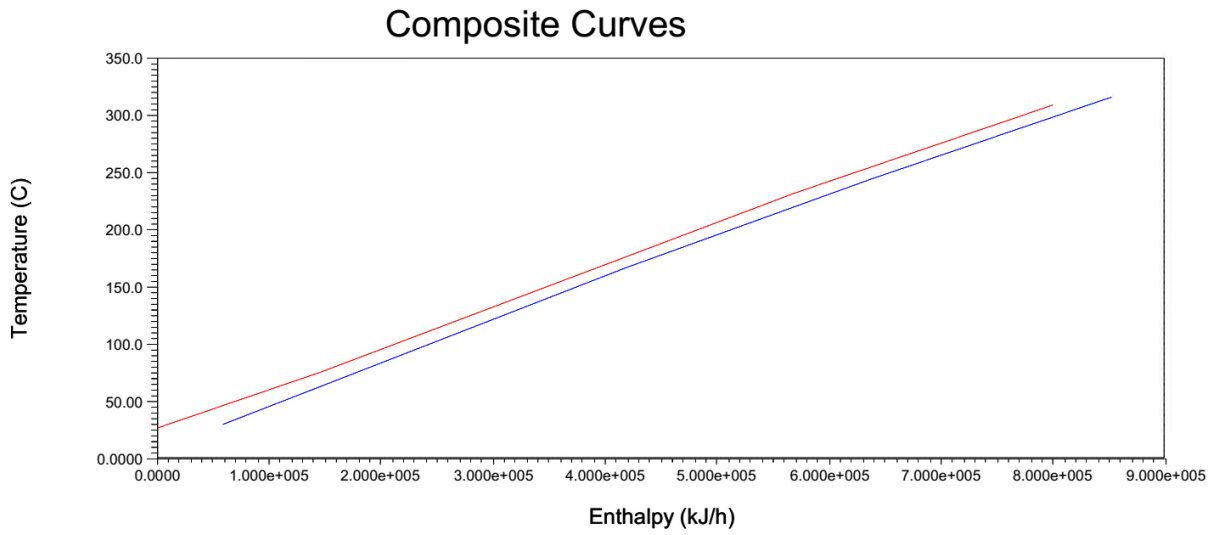

Figure 5.5. Pinch analysis results of the TSA process

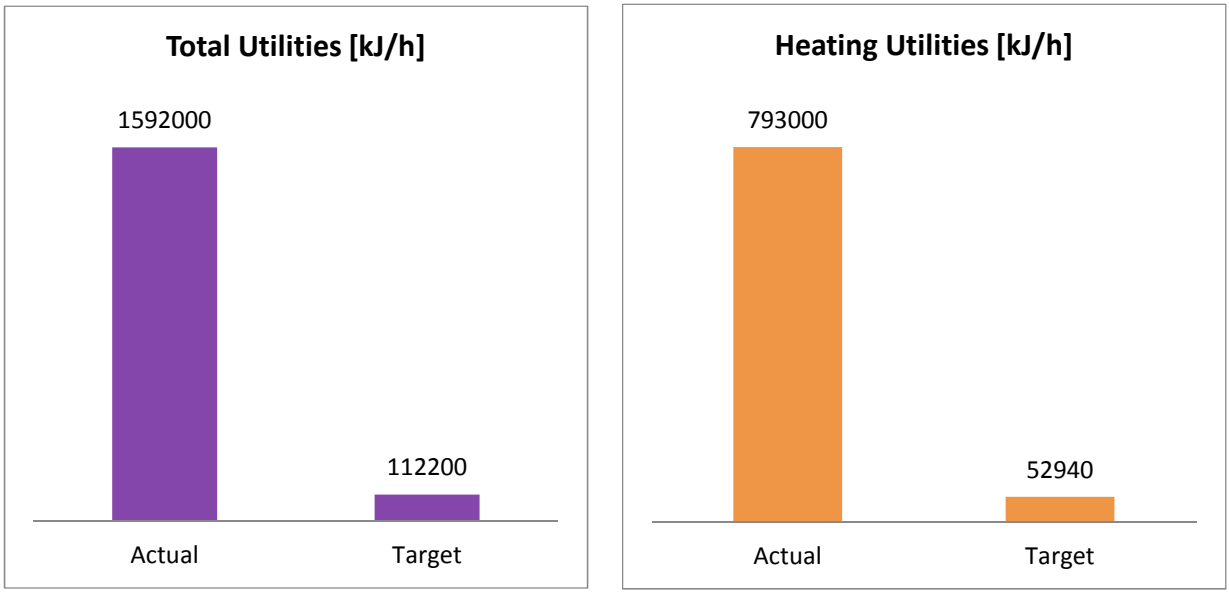

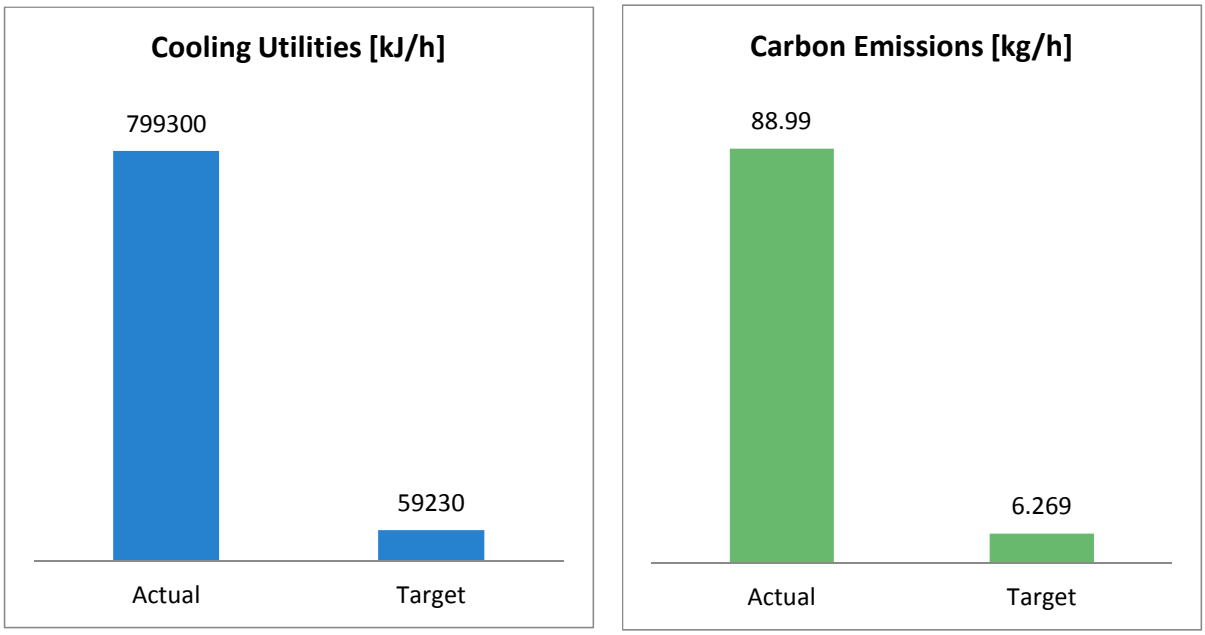

Figure 5.6. Comparison of heating/cooling utilities and gas emissions; TSA process.

Table 5.5. Energy analysis results for TSA process.

Property	Actual	Target	Available Savings	% of Actual
Total Utilities [kJ/h]	1,592,000	112,200	1,480,000	92.96
Heating Utilities [kJ/h]	793,000	52,940	740,100	93.32
Cooling Utilities [kJ/h]	799,300	59,230	740,100	92.59
Carbon Emissions [kg/h]	88.99	6.269	82.72	92.96

5.1.4 DEHYDRATION IN A PRESSURE SWING ADSORPTION PROCESS

5.1.4.1 Process Description

The pressure swing adsorption (PSA) process is very similar to the TSA process. The only difference is that the pressure is changed in the Skarstrom cycle where adsorption and desorption take place at high pressure and low pressure, respectively (Ruthven, 1984). The operating temperature is much lower than that of TSA, and it is slightly different during adsorption and desorption due to the heat of adsorption and the heat of desorption. The details of this cyclic

process is explained elsewhere (Ruthven, 1984; Ruthven, et al., 1994). In this process, a waste CO_2 stream from the upstream of natural gas processing unit is used as a carrier gas for the desorption step. This CO_2 stream is usually available in field site, especially for the plants that incorporate a CH_4-CO_2 PSA unit to produce 99.99 % purity methane for specific applications. Higher methane recovery was achieved using this stream for desorption in the PSA process.

5.1.4.2 Simulation

The PSA process was simulated using a User-defined model generated from our previous experimental data. Basically, the behavior of system at various temperatures, pressures, feed composition, and flow rate was predicted using property tables generated form the user model. The conditions of adsorption beds in terms of configuration, amounts of adsorbent, L/D ratio, etc. were the same as those in the TSA process. The main power consumption (utility) in this process, however, is the vacuum pump duty (Figure 5.7). A dual-stage pump with excess maximum capacity of 130% was sized and simulated, and its capital cost and power consumption was estimated using the manufacturer documentations (Kinney, KLRC 950 GPM 39). The methane (CH_4) purge stream is actually the gas holdup in the column during the pressure equalization step in the Skarstrom cycle, which was sent back to the upstream to be used as a utility (e.g. in a furnace or HP generation). A total methane recovery of 99.99 % was achieved as the amount of this purge stream was very small and the CO_2 stream was used as a carrier gas for desorption. Moreover, the water content of the sales gas was satisfactory for pipeline quality gas. The design process has an annual production of natural gas about 300 million gallons.

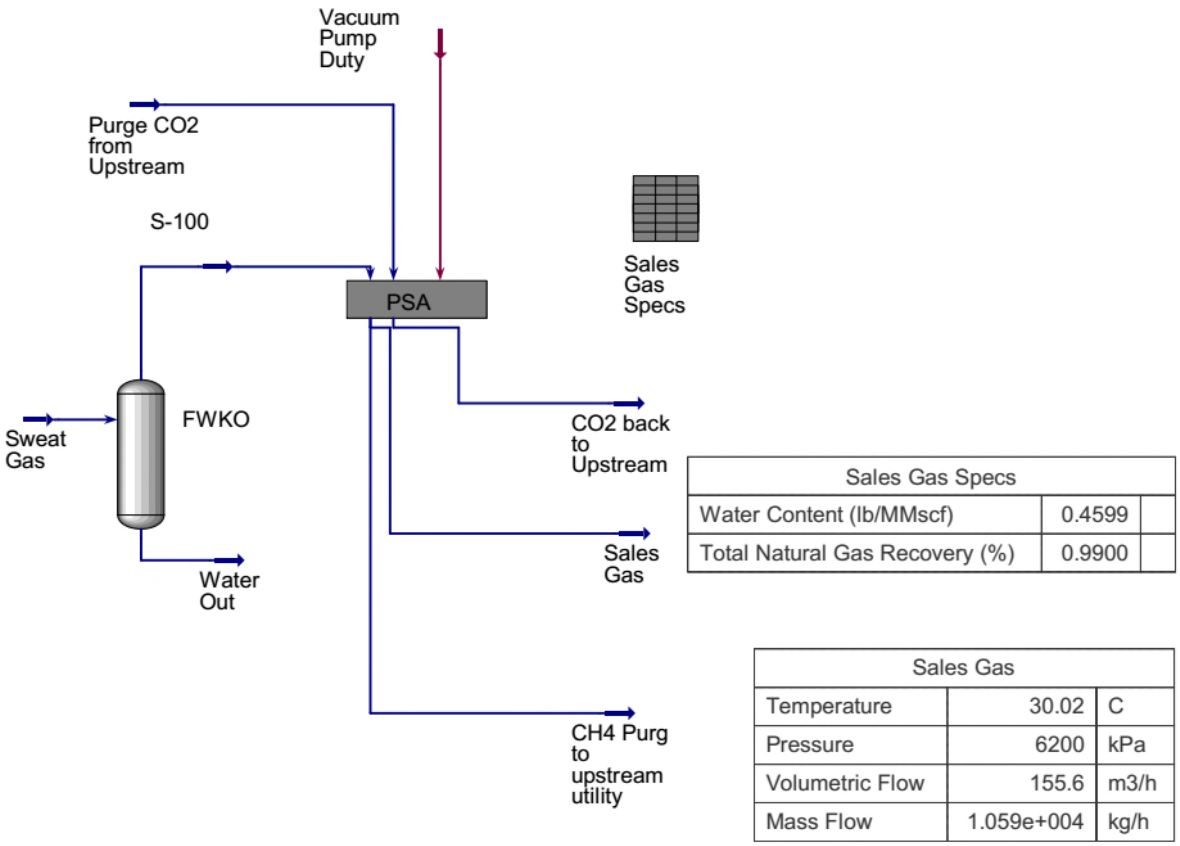

Sales Gas Specs		
Water Content (lb/MMscf)	0.4599	
Total Natural Gas Recovery (%)	0.9900	

Sales Gas		
Temperature	30.02	C
Pressure	6200	kPa
Volumetric Flow	155.6	m3/h
Mass Flow	1.059e+004	kg/h

Figure 5.7. Process flowsheet of PSA process for natural gas dehydration.

5.1.4.3 Economic Analysis

Similar to other two processes, an economic analysis was performed and the results are summarized in Table 5.6. A total capital cost of 2.45 million USD was estimated for this plant, where most of which was equipment cost. The total raw material cost is very low since biosorbent were supplied without any cost, and the only cost of the shipping and handling costs. About 1.67 ton of biosorbent was needed for two adsorption columns.

Table 5.6. Summary of economic analysis of the PSA process.

Total Capital Cost [MUSD]	2.45
Total Operating Cost [USD/Year]	955,753
Total Raw Materials Cost [USD]	53.2
Total Utilities Cost [USD/Year]	37,020.9
Equipment Cost [USD]	86,500
Total Installed Cost [USD]	323,800
Utility	**USD/hour**
Electricity	4.2232

Since electricity is the only utility used in this process, energy analysis is pointless. This process is highly environmental friendly as no heating utilities such as furnace that produces pollution was not used. The operating cost may be increased for large-capacity plants where a high gas flow need to be handled by multi-staged vacuum pumps.

The three drying methods were compared in Table 5.7. The results demonstrated that drying natural gas using flax shoves biosrbent in a pressure swing adsorption process is most economical and environmentally friendly.

Table 5.7. Comparison of natural gas dehydration processes.

Process	**Total Capital Cost (MUSD)**	**Annual Operating Cost (USD/year)**	**Gas Emissions (kg/h)**
TEG	30.7	982.821	9.78
TSA	4.44	1,350,851	88.99
PSA	2.45	955,753	<0.1

5.1.5 SUMMARY

In this section, three different natural gas dehydration process were simulated in ASPEN HYSYS and techno-economic analysis were performed to compare the capital and operating costs of these processes. The results show that the PSA process has the lowest capital cost, operating

cost, and gas emissions. The PSA process has fewer pieces of equipment, and is much easier to control. The cyclic system is automatically operated using computers. Due to lower operating temperatures, the operation is safer. The methane recovery and sales gas water content was within the pipeline quality gas standards. The PSA process using biosorbent seems to be promising for natural gas dehydration industry. However, more in depth economic analysis needs to be done for the biosorbent pellets suitable for large scale industrial application.

5.2 DRYING BUTANOL

5.2.1. Assumed conditions

Before the estimation, we have assumed the cost index based on the updated CHE cost index. All cost calculations were based on the chemical engineering plant cost index (CEPCI) of 628.2 (for 2017). The capital cost calculation is based on this value. The estimation does not take into consideration of war, natural disasters and other force majeure accident.

5.2.2. Pressure swing adsorption simulation by Aspen

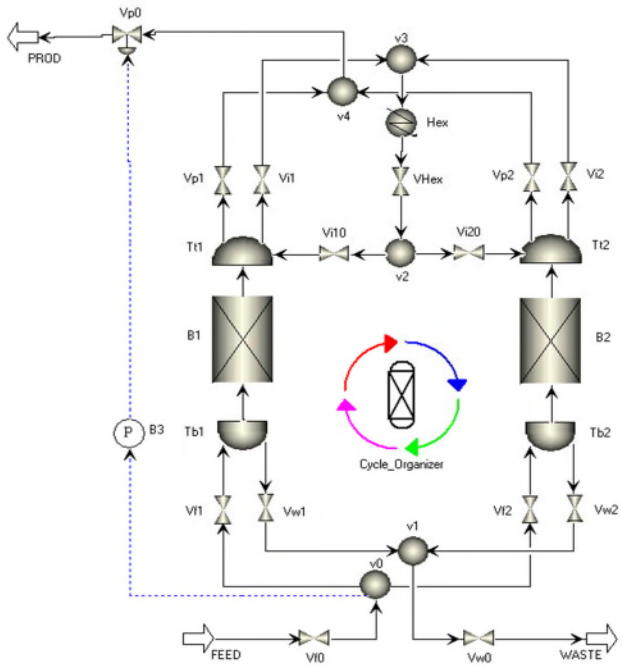

Figure 5.8. Adsorption stimulated in Aspen Adsorption

Aspen Adsorption was used to simulate the butanol drying in adsorption column using oat hulls based biosorbent. After simulation the stream information was applied in Aspen Hysys to simulate the dehydration process and calculate the cost.

The simulation in Aspen Adsorption aims to build adsorption simulation and to ensure that the simulation of the adsorption bed works effectively. It enables early testing of key model parameters and assumptions. The simulation based on the assumptions: Each adsorbent bed is identical (same adsorbent layers and model assumptions); only one bed is rigorously modeled; any number of interactions can be incorporated; material sent to an interacting bed (stored) is re-used (replayed) later in the cycle. The simulation is designed to produce 9800 ton butanol (99.5 wt%) product per year. The working days are 300 days per year. The butanol production scale obtained from simulation is 18.4 kmol/h. The calculated annual production scale is 9800 ton/yr. The canola meal, and oat hulls based biosorbents were used for the adsorption process. The feed butanol concentration was set to be 55% butanol to simulate the butanol vapor concentration generated directly from the preliminary distillation process in biobutanol industry, and 80% as a higher end for comparison.

According to the experiments conditions achieved from the lab scale experiments in this work, the adsorption was carried out at 110°C, and 135 kPa. The regeneration (desorption) was carried out in the same column after adsorption. Partial of the product was used to flash out the adsorbates. The depressurization was carried out at 105 °C, 20 kPa. The whole pressure swing adsorption process has been separated to 6 steps. The cycle information is listed below:

Step 1: 60 sec, feed / production (1) + depressurization (2)

Step 2: 360 sec, feed / production / purge out (1) + purge in (2)

Step 3: 30 sec, feed / production / repress out (1) + repress in (2)

Step 4: 60 sec, depressurization (1) + feed / production (2)

Step 5: 360 sec, purge in (1) + feed / production / purge out (2)

Step 6: 30 sec, repress in (1) + feed / production / repress out (2)

The feed stream was input to Aspen Hysys for equipment sizing and economic evaluations. Economic evaluations were carried out using Aspen Economic Evaluator.

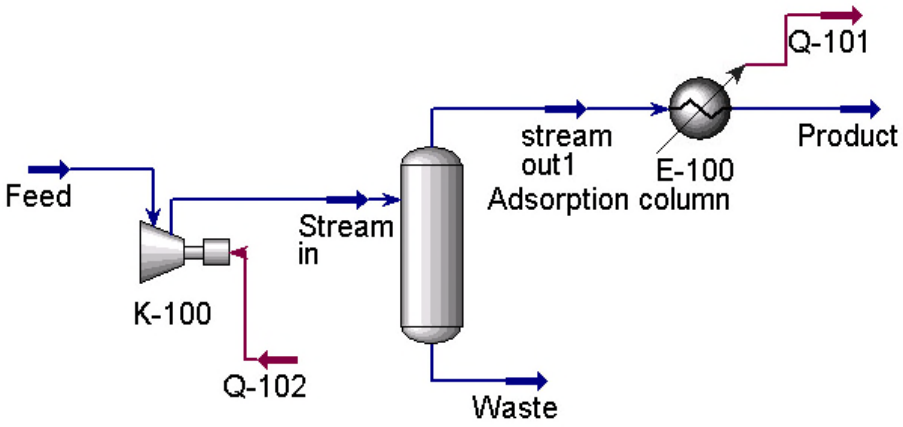

Figure 5.9. Butanol dehydration by adsorption stimulated in Aspen Hysys

5.2.2.1. Major equipment cost

Major instruments are compressor, adsorption column, condenser and pump. The purchase cost can be estimated by equipment parameters and specifications. The costs of equipment were demonstrated in Table 5.8.

Table 5.8. Equipment cost of adsorption process using different biosorbent

Oat hulls as biosorbent (55 v/v% butanol feed)			
Name of the equipment	No.	Equipment cost (USD)	Installed cost (USD)
Compressor	1	228,600	180,300
Adsorption column	2	15,600	103,300
Condenser	1	14,900	74,300
Pump	1	4,600	28,700
Continued			
Oat hulls as biosorbent (80 v/v% butanol feed)			

Name of the equipment	No.	Equipment cost (USD)	Installed cost (USD)
Compressor	1	228,600	180,300
Adsorption column	2	15,600	103,300
Condenser	1	14,900	74,300
Pump	1	4,600	28,700

Canola meal as biosorbent (55 v/v% butanol feed)

Name of the equipment	No.	Equipment cost (USD)	Installed cost (USD)
Compressor	1	228,600	180,300
Adsorption column	2	15,600	103,300
Condenser	1	11,000	61,600
Pump	1	4,600	28,700

Canola meal as biosorbent (80 v/v% butanol feed)

Name of the equipment	No.	Equipment cost (USD)	Installed cost (USD)
Compressor	1	228,600	180,300
Adsorption column	2	15,600	103,300
Condenser	1	11,000	61,600
Pump	1	4,600	28,700

The results show that the equipment costs required for drying butanol using canola meal or oat hulls are either comparable or slightly higher than canola meal because the latter has slightly higher water adsorption capacity.

5.2.2.2 Total capital cost and manufacturing cost estimation

The purchase cost for all the equipment are listed in Table 5.8. The cost of equipment and the installation will be used to calculate the fixed capital investment. Fixed capital investment was calculated using Aspen and CEPCI index that includes the components such as purchased equipment, setting of equipment, piping, civil, instrumentation, electrical fittings, insulation, administrative overheads, contingencies and escalations. The working capital is 15% of the fixed capital investment and the total capital investment is the sum of fixed capital investment and working capital. The total capital investment is about $2.05 million, and this value covered the investment before the plant can operate successfully and produce the desired product.

The expenses during the operating period include manufacturing expenses and general expenses. The direct manufacturing expenses include raw materials fees, utility fees and labor fees. The indirect manufacturing expenses include packing & storage cost, all insurance and local taxes. The manufacturing cost has been calculated according to the stimulation results and the assumption above. Table 5.9 shows the details of the operating cost and utility cost estimated by Aspen Economic Analyzer.

Table 5.9. Summary of economic analysis for butanol dehydration by adsorption

Oat hulls as biosorbent (55 v/v% butanol feed)	
Investment	**Cost**
Total capital investment (USD)	2,052,090
Total operating cost (USD/Year)	1070,300
Total utilities cost (USD/Year)	63,438
Total equipment cost (USD)	263,700
Total installed cost (USD)	386,600
Oat hulls as biosorbent (80 v/v% butanol feed)	

Investment	**Cost**
Total capital investment (USD)	2,034,140
Total operating cost (USD/Year)	959,126
Total utilities cost (USD/Year)	42,413
Total equipment cost (USD)	263,700
Total installed cost (USD)	386,600
Canola meal as biosorbent (55 v/v% butanol feed)	
Investment	**Cost**
Total capital investment (USD)	1,879,360
Total operating cost (USD/Year)	1,046,060
Total utilities cost (USD/Year)	63,438
Total equipment cost (USD)	259,800
Total installed cost (USD)	373,900
Canola meal as biosorbent (80 v/v% butanol feed)	
Investment	**Cost**
Total capital investment (USD)	1,879,360
Total operating cost (USD/Year)	953,759
Total utilities cost (USD/Year)	37,591
Total equipment cost (USD)	259,800

Total installed cost (USD)	373,900

The results show that using canola meal has lower costs in each of the categories than oat hulls in the process.

5.2.3. Economic analysis for butanol dehydration by distillation

Aspen Hysys was also applied to simulate the butanol dehydration process by distillation based the same production scale of adoption process. The feed of 80% butanol was used for comparison of the adsorption process and distillation. The major economic analysis results was summarized in Table 5.3.

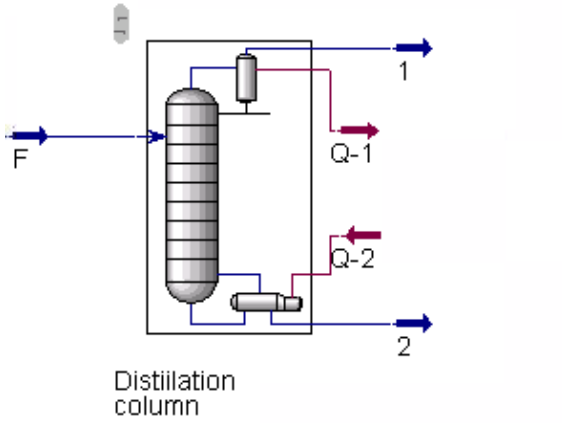

Figure 5.10. Butanol dehydration by distillation stimulated in Aspen Hysys

It can be seen in Table 5.3, the butanol dehydration process by pressure swing adsorption using oat hulls, or canola meal based biosorbents has lower capital cost, operating cost, and utilities cost than distillation.

Table 5.10. Summary of economic analysis for butanol dehydration by distillation

Investment	**Cost**		
	Distillation	**Ads by oat hulls**	**Ads by canola meal**
Total capital investment (USD)	2,642,710	2,034,140	1,879,360
Total operating cost (USD/Year)	1,132,150	959,126	953,759
Total utilities cost (USD/Year)	185,492	42,413	37,591
Total equipment cost (USD)	263,600	263,700	259,800
Total installed cost (USD)	493,500	386,600	373,900

5.2.4. SUMMARY

Pressure swing adsorption using biosorbents is an effective method for gas separation and purification for its low cost operation, high product recovery rates, and operational simplicity. It is a promising method for drying biobutanol in industry, as the biosorbents are cost effective, more available and environmentally friendly. The economic analysis shows that the capital cost and operating cost of the adsorption process are lower than those of distillation. Production of anhydrous biobutanol by pressure swing adsorption process using biosorbents seems economically feasible. However, more work needs to be done on the pilot scale adsorption process to verify the economic analysis.

5.3 REFERENCES

Kidnay, A. J.; Parrish, W. R.; McCartney, D. G., *Fundamentals of natural gas processing*. CRC Press: 2011; Vol. 218.

Mokhatab, S.; Poe, W. A., *Handbook of natural gas transmission and processing*. Gulf professional publishing: 2012.

Ruthven, D. M., *Principles of adsorption and adsorption processes*. John Wiley & Sons: 1984.

Ruthven, D. M.; Farooq, S.; Knaebel, K. S., *Pressure swing adsorption*. VCH publishers New York: 1994; Vol. 480.

CHAPTER 6. CONCLUSION AND RECOMMENDATION

The biosorbent particles developed from flax shives was able to effectively dehydrate natural gas (methane) with high selectivity for water adsorption. It demonstrated much higher water adsorption capacity (0.9 g/g) than most of the commercial adsorbents. Adsorption of methane, nitrogen and carbon dioxide was negligible. The water saturated biosorbent was regenerated at a fast rate at room temperature under vacuum, and had stable performance after 70 adsorption-desorption cycles. The biosorbent was also stable at temperatures up to 200 °C. The results show that the flax shive biosorbent is promising in the dehydration of methane (natural gas), and other non-polar gases in a pressure swing adsorption process.

The flax shvies based biosorbent has porous structure, and contains hydroxyl, carboxyl, and additional polar groups as evidenced by the SEM and XPS analyses, which are considered to play important roles for the high water adsorption capacity achieved in this work. The total pressure has the most significant effect on water adsorption capacity, followed by temperature. The interaction among temperature, pressure and feed water content are all significant. The water adsorption is exothermic, but mechanisms are different at lower (24^{o}C), and higher temperature (35-50^{o}C). The isotherm changed from type III isotherm at 24^{o}C to type I at 35-50^{o}C. The Redhead model provided satisfactory simulation for the isotherm obtained at 24^{o}C, and the F-G model for the isotherms at 35-50^{o}C. The surface area available for water adsorption was calculated to 1005 m^2/g based on the Redhead modeling results, which is significantly higher than that determined by the BET model via nitrogen adsorption. Selecting proper adsorbate for determination of surface area for adsorption is important. The F-G modeling results indicated that the adsorbed water molecules on the surface of the flax shive biosorbent were attractive to one another, however, the interaction force was very weak.

The length of mass transfer zone determined at various conditions showed that it increased with increase in the total gas flow rate, and decrease in temperature. Pressure did not have consistent effect at the tested conditions. More research in the regards is necessary.

It was demonstrated that canola meal (CM) has the capability to dry butanol from the azeotropic butanol concentration 55 v/v% to high purity butanol of 99 v/v%. Pressure again was found to be the most significant factor at the tested conditions, affecting butanol uptake, water selectivity, butanol recovery, and maximum effluent butanol concentration. The optimum conditions obtained from the statistical design resulted in a water separation factor of 5.4, butanol recovery of 90%, water uptake of 0.48 g/g-ads and fuel grade butanol of >99 v/v%. The Dubinin-Polanyi (D-P) model based on the adsorption potential theory for large pore materials gave a better fit to the water adsorption isotherms. The mean free energy indicated that water adsorption is predominantly physisorption. The approximate site energy distribution based on the D-P isotherm elucidated the uptake of water on the heterogeneous CM biosorbent. The high-energy sorption sites were first occupied at low concentration, followed by the low-energy sorption sites. Site energy distribution curve revealed that CM had negligible sorption sites with very high energy (e.g., >15,000 J/mol) in the tested range of parameters. The average site energy $\mu(E^*)$ was 3.33 kJ/mol, which again indicated physical nature of water adsorption, while the standard deviation σ_e^* of 2.36 kJ/mol indicated the heterogeneous nature of biosorbents. Saturated CM was regenerated at 110°C under vacuum and reused for more than 16 cycles.

The results also reveal that CM containing cellulose in this work has higher water uptake than starch-rich corn meal. It is also demonstrated that the water uptake and selectivity from the cellulose are much higher than those from protein, affirming that cellulose plays a more important role in the butanol dehydration of CM. However, the performance of pure cellulose is not as effective as that of the CM material. A synergetic effect of all components and physical properties and molecular structural makeup of CM may have attributed to the high water uptake and selectivity and thus it could serve as a promising material for butanol dehydration. However, further investigations are required in regards to the synergetic effect of CM.

It is concluded from water and butanol isotherms that the affinity of water for oat hulls based biosorbent is stronger than that of butanol, and the water adsorption capacity of the biosorbent is also higher than butanol adsorption capacity. The highest water adsorption capacity is 0.132 g/g with a separation factor of 2.88 obtained at 381 K when the butanol concentration in the feed is 57.6%. At 381 K, the highest concentration of effluent obtained from feed of various butanol content (57.6%, 69.1%, 79.7%, 90.3%) are 95.3%, 97.1%, 98.1% and 99.0%, respectively, which indicates the oat hulls based biosorbent is able to dehydrate the water/butanol binary

azeotrope and even at higher concentrated butanol solution. Oat hulls had slightly lower water adsorption capacity than canola meal when drying low grade butanol such as 55%.

The Dubinin-Polanyi model for large pore materials is slightly better for representing the experimental water adsorption data in both single water system and water-butanol binary system compared with the micropore Dubinin-Polanyi model. The fitting results also suggest that the oat hulls based biosorbent are more likely to be a large pore material, which is consistent with the results from BET surface area analysis. The difference in limiting adsorption mass of single and binary system proves the competitive adsorption between water and butanol. The analysis of site energy distribution shows that in this case, most adsorption took place on the sites having energy lower than 10,000 J/mol. The calculated average site energy for water adsorption are 2443 J/mol and 2378 J/mol for the single and binary system. The site energy distribution method is transferrable to analyze the adsorption data of other heterogeneous materials.

Three different natural gas dehydration processes including Glycol, temperature swing adsorption, and pressure swing adsorption were simulated in ASPEN HYSYS and techno-economic analysis were performed to compare the capital and operating costs of these processes. The results show that the pressure swing adsorption process using the flax shive based biosorbent has the lowest capital cost, operating cost, and gas emissions. The process has fewer pieces of equipment, and is much easier to control. The cyclic system is automatically operated using computers. Due to lower operating temperatures, the operation is safer. The methane recovery and sales gas water content was within the pipeline quality gas standards. The process using biosorbent seems to be promising for natural gas dehydration industry.

The economic analysis also shows that the pressure swing adsorption using canola meal or oat hulls biosorbents is also an effective method for drying biobutanol for its lower costs, high product recovery rates, and operational simplicity. It is a promising method for drying biobutanol in industry, as the biosorbents are cost effective, more available and environmentally friendly. The economic analysis shows that the capital cost and operating cost of the adsorption process are lower than those of distillation based on the comparison of treating same grade of butanol feed. Production of anhydrous biobutanol by pressure swing adsorption process using biosorbents seems feasible. However, more work needs to be done on the pilot scale adsorption process to verify the economic analysis.

CHAPTER 7. OUTCOMES AND ACKNOWLEDGEMENTS

7.1. NOVEL TECHNOLOGIES AND PRACTICAL IMPLICATIONS FOR PRODUCERS OR INDUSTRY

From this project, novel technologies have been developed which have impact by addressing energy, agriculture and environmental needs, and contribute to the fundamental knowledge of biosorption and adsorption, agricultural by-products, energy, and material science and engineering.

These novel technologies formulate biosorbents with enhanced adsorption performance, and establish biosorption processes with high efficiency and low cost for drying biofuel alcohols, and natural gas. The technologies are transferable to industries for drying additional industrial gases. This will reduce the costs of processing of renewal bioenergy, fossil energy and additional gases in the industry. Commercialization of agricultural byproducts such as oat hulls, flax shives, and canola meal after protein extraction for the regards would increase the revenue of the agriculture, and associated industries. Other agriculture by-products such as flax, barley, and wheat straw, and the like may also be applied for similar application. The new uses of the agriculture by-products can not only enhance the revenue, but also reduce the amounts of these by-products which have to be burnt in the field. Thus, the technologies generated from this project will benefit the environment of Saskatchewan, and Canada, and enhance the profitability of the above mentioned Saskatchewan, and Canadian industries. Furthermore, a number of students trained through this project have worked in and contributed to the aforementioned industries or related areas.

7.2. PATENTS/IP GENERATED/COMMERCIALIZED PRODUCTS

The results generated from drying natural gas using the flax shives based biosorbent were filed a part of US provisional patent application (Serial No. 62/575,137).

Additional improvement is expected to continue to enhance the stability of the biosorbents for drying application when they are made into pellets for ease of transportation and industrial application. The product of either natural gas (methane), or 99% butanol achieved in this project is in lab scale which is expected to enlarge to pilot scale and industrial scale production when

funding is available. We plan to continue to work with the Saskatchewan and Canadian agriculture, energy and related industries to advance the technologies toward industrial application.

7.3. LIST OF TECHNOLOGY TRANSFER ACTIVITIES

7.3.1 Journal publications

Q. Huang, C. H. Niu* and A. Dalai. 2018. Production of anhydrous biobutanol using a biosorbent developed from oat hulls. Submitted to Chemical Engineering Journal, under review.

S. Ghanbari, and C.H. Niu. 2018. Characterization of a High Performance Biosorbent for Natural Gas. Submitted to Energy and Fuels, under review.

R. Dhabhai, C.H. Niu* and A Dalai. 2018. Agricultural byproducts based biosorbents for purification of bio-alcohols: A review. Bioresources and Bioprocessing. 5:37. DOI: 10.1080/00986445.2017.1412307.

D. Jayaprakash, R. Dhabhai, C.H. Niu* and Ajay K. Dalai. 2017. Selective Water Removal by Sorption from Butanol–Water Vapor Mixtures: Analyses of Key Operating Parameters and Site Energy Distribution. *Energy and Fuels*, 31(5): 5193–5202. DOI: 10.1021/acs.energyfuels.7b00310.

R. Dhabhai, C.H. Niu* and A Dalai. 2018. Drying of non-polar gas in a pressure swing adsorption process using canola meal biosorbents. Asia-Pacific Journal of Chemical Engineering. DOI: 10.1002/apj.2232.

R. Dhabhai, C.H. Niu* and A Dalai. 2018. Selective Adsorption of Water from Aqueous Butanol Solution Using Canola Meal Based Biosorbents. *Chemical Engineering Communication*, 205(5): 637-646. DOI: 10.1080/00986445.2017.1412307.

B. Yan and C.H. Niu*. 2017. Pretreating Biosorbents for Purification of Bioethanol from Aqueous Solution. *International Journal of Green Energy*, 14(3):245-252. DOI:10.1080/15435075.2016.1254087.

7.3.2. Conferences presentation

S. Ghanbari and C.H. Niu*. 2017. Analysis of Pressure Swing Adsorption Process Using Biosorbents for Dehydration of Natural Gas. 68th Canadian Chemical Engineering Conference, Toronto, On, Canada, October 28-31.

A. Aghababaei, and C.H. Niu*. 2018. Adsorptive Removal of Carbamazepine from Aqueous Solution Using Hydrothermally Treated Agriculture Waste by Products. 68th Canadian Chemical Engineering Conference, Toronto, On, Canada, October 28-31.

Q. Huang, C.H. Niu* and A. Dalai. 2018. Dynamics and Simulation Studies of Water Adsorption on a Biosorbent. 68th Canadian Chemical Engineering Conference, Toronto, On, Canada, October 28-31.

S. Ghanbari and C.H. Niu*. 2017. Water Adsorption Properties of Flax Shives and Their Potential for Natural Gas Dehydration. 67th Canadian Chemical Engineering Conference, Edmonton, AB, Canada, October 22-25.

A. Aghababaei, R. Dhabhai, S. Ghanbari and C.H. Niu*. 2017. Drying Air Using Oat Hulls Based Adsorbents. 67th Canadian Chemical Engineering Conference, Edmonton, AB, Canada, October 22-25.

Q. Huang, C.H. Niu* and A. Dalai. 2017. Butanol/Water Adsorption on Oat Hulls and Site Energy Distribution Analysis. 67th Canadian Chemical Engineering Conference, Edmonton, AB, Canada, October 22-25.

J. Zhou, Q. Huang and C.H. Niu*. 2017. Pelletisation and Characterization of Biosorbents. 67th Canadian Chemical Engineering Conference, Edmonton, AB, Canada, October 22-25.

R. Dhabhai, M. Mahaninia, B. Yan, C.H. Niu* and Ajay K. Dalai. 2016. Drying of Nitrogen in a Pressure Swing Adsorption Process using Canola Meal Biosorbent. 66th Canadian Chemical Engineering Conference, Quebec, QC, Canada, October 17-19.

R. Dhabhai, C.H. Niu* and A. Dalai. 2015. Drying of Alcohols in Liquid Phase Batch Adsorption using Biomaterials. 65th Canadian Chemical Engineering Conference, Calgary, AB, Canada, October 4-7.

D. Jayaprakash, C.H. Niu* and A. Dalai. 2015. Bio-butanol Dehydration Using Bio-sorbents. 65th Canadian Chemical Engineering Conference, Calgary, AB, Canada, October 4-7.

D. Jayaprakash, R. Khandait, A. Dalai and C.H. Niu*. 2014. Drying Bio-alcohols Using Bio-adsorbents. 64th Canadian Chemical Engineering Conference, Niagara Falls, ON, Canada, October 20-23.

7.3.3. Patent application

S. Ghanbari and C.H. Niu*. 2017. Dehydration Using Biosorbents in Modified Pressure Swing Adsorption. Filed as a US Provisional Application, serial no. 62/575,137. November 21.

7.4. INDUSTRY CONTRIBUTIONS OR SUPPORT RECEIVED

We would like to give special thanks to the Spectrum Technologies Ltd, particularly, Mr. R. Tyagi, Chief Executive Officer, for providing advices and feedback to this project throughout the years of this project, and providing the tours of the industrial dehydration facility.

We also very much appreciate that Richardson Millings Ltd, Warman, SK, Canada, Bunge Global Innovation, White Plains, NY, USA, and SWM, Engineered for Tomorrow Inc., GA, USA provided free agricultural by-products samples such as oat hulls, canola meal after protein extraction, and flax shives for the experiments of this project.

Furthermore, we would like to thank Transgas Ltd for their support and interest to this project.

7.5. NECESSITY TO CONDUCT FOLLOW UP RESEARCH

This project demonstrated that the promising potential of agricultural byproducts in industrial applications of drying bioalcohols and natural gas, and additional gases.

The biosorbent particles developed from raw flax shives successfully dried natural gas (methane) in a lab-scale pressure swing adsorption (PSA) process. In addition, the biosorbent particles made from canola meal, and oat hulls have been used in PSA to successfully achieve over 99 wt% biofuel butanol from 55 – 95% butanol-water vapor mixtures. This results demonstrated

that the agriculture by-products and the like have the great potential for drying application in the industry.

However, the biosorbent cylindrical or spherical pellets were observed slightly deformed after contacting with water in a number of adsorption-desorption cycles though the biosorbent particles obtained directly from grinding performed very well. This affects the dehydration performance of the pellets in industrial drying applications. For this and ease of transportation, the biosorbents are preferred to make into pellets with higher density, and constant quality. In addition, the separation factor of water over butanol could be further enhanced. The selective water adsorption mechanism by the biosorbents need be further elucidated. The effect of other co-existing components in gas phase (e.g. in natural gas) on water adsorption needs to be investigated. This motivated to conduct the next step research with the following objectives:

Objective 1: Develop a methodology to formulate and characterize cost-effective novel biosorbent pellets with enhanced stability and reusability for adsorption of water vapor from gas phase;

Objective 2: Establish and optimize the pressure swing adsorption (PSA) process for drying bioalcohols, natural gas and additional industrial gases to enhance productivity, and reduce costs. Oat hulls, canola meal, and flax shives will be first used to develop the biosorbent pellets for this purpose. Other agriculture by products may be used; and

Objective 3: Scale up the drying processes optimized through objectives 2 and 3 to pilot scale and industrial scale, and conduct economic analysis.

When funding is available, the above mentioned research will be carried on.

7.6. ACKNOWLEDGEMENTS

We are very grateful to the financial support of the Saskatchewan Ministry of Agriculture and the Canada-Saskatchewan Growing Forward 2 bilateral agreement (Grant Number 20130220), Saskatchewan Canola Development Commission (Grant Number 20130220), Western Grains Research Foundation (Grant Number 20130220), Mitacs (Grant Number IT04850), Natural Science and Engineering Research Council of Canada (No. RGPIN 299061-2013), Canada Foundation for Innovation (No. 33172), and University of Saskatchewan through Deans

Scholarship, and Devolved Scholarships to this project. We also thank RLee Prokopishyn, Richard Blondin and Heli Eunike for their technical support.

Special thanks are given to the graduate and undergraduate students, and researchers of the Biosorption Research Group at the University of Saskatchewan for their great contributions to this work:

Postdoctoral research fellow: Ravi Dhabhai,

Graduate students (Ph.D. and Master students): Saeed Ghanbari, Dviya Jayaprakash, Sophie Huang Qian, Bei Yan, Jing Zhou, Aylin Aghababaei,

Research Assistant: Mohammad Mahaninia

Undergraduate students: Wei Cao, Kai Tang, Hao Liu, Rahul Khankait,

Their contributions are essential for successfully completing this project.